INVESTIGATIONS ON NON-INVASIVE FAULT DIAGNOSTIC TECHNIQUES FOR THREE-PHASE INDUCTION MOTOR WITH MIXED ECCENTRICITY

Thesis

Submitted in partial fulfillment of the requirements for the degree of

DOCTOR OF PHILOSOPHY

by

RAJALAKSHMI SAMAGA BL

DEPARTMENT OF ELECTRICAL AND ELECTRONICS ENGINEERING

NATIONAL INSTITUTE OF TECHNOLOGY

KARNATAKA, SURATHKAL, MANGALORE -575025

SEPTEMBER, 2013

D E C L A R A T I O N

by the Ph.D. Research Scholar

I hereby ***declare*** that the Research Thesis entitled **INVESTIGATIONS ON NON-INVASIVE FAULT DIAGNOSTIC TECHNIQUES FOR THREE-PHASE INDUCTION MOTOR WITH MIXED ECCENTRICITY** which is being submitted to the **National Institute of Technology Karnataka, Surathkal** in partial fulfillment of the requirements for the award of the Degree of **Doctor of Philosophy** in Power and Energy Systems, Department of Electrical and Electronics Engineering is a ***bonafide report of the research work carried out by me*.** The material contained in this Research Thesis/Synopsis has not been submitted to any University or Institution for the award of any degree.

082009EE08F04, **Rajalakshmi Samaga BL**

(Register Number, Name & Signature of the Research Scholar)

Department of Electrical and Electronics Engineering

Place: NITK-Surathkal

Date:

C E R T I F I C A T E

This is to *certify* that the Research Thesis entitled **"INVESTIGATIONS ON NON-INVASIVE FAULT DIAGNOSTIC TECHNIQUES FOR THREE-PHASE INDUCTION MOTOR WITH MIXED ECCENTRICITY"** submitted by Rajalakshmi Samaga BL, (Register Number: 082009EE08F04) as the record of the research work carried out by her, is *accepted as the Research Thesis submission* in partial fulfillment of the requirements for the award of degree of **Doctor of Philosophy**.

Dr.K.P.Vittal

Research Guide

Chairman - DRPC

(Signature with Date and Seal)

ACKNOWLEDGEMENT:

I consider it my privilege to express gratitude and respect to all those who guided and inspired me in the successful completion of my thesis.

First of all I would like to thank **GOD** who showered me with his blessings in my difficult times and was the guiding light throughout the research work.

It is with pleasure that I acknowledge my sincere thanks and deep sense of gratitude to my guide **Dr. K.P. Vittal**, Professor and Head, Department of Electrical and Electronics Engineering for his valuable guidance throughout the course of this work. His suggestions, directions and guidance have helped in smooth progress of the work.

I am deeply indebted to **NITK**, Surathkal for giving me an opportunity to carry out my research work in the institution and **MHRD** for the financial assistance for the work. I am grateful to **MIT**, Manipal for giving me three years of leave without pay.

I acknowledge my sincere gratitude to **Dr.Sriram**, Mysore for the help rendered in designing the eccentricity in the machine. I take this opportunity to thank the Principal and staff of **Hebich Technical Training Institute, Mangalore** for creating eccentricity in the machine. No words will be adequate to quantify their support and cooperation. I would like to acknowledge **Integrated Electric Co. Ltd**, Bengaluru, **Larsen and Toubro**, Bengaluru and **Darshan Switch Gears,** Mangalore for providing the machine with full details.

I sincerely thank **Dr.Ganagadharan,** Professor, Department of Mechanical Engineering and **Dr.Sripathi,** Professor, Department of Electronics and Communication Engineering for providing me the valuable suggestions as RPAC members.

I appreciate the help and cooperation rendered by all the **non teaching staff** of Machines lab, E & E Department. I take this opportunity to thank all the **teaching and non teaching staff** of Electrical & Electronics Department for their whole hearted help during the course of my work.

With very much love, I thank my father **Sri. Sooryanarayana Aithal K** and my mother **Late. Seethamma Aithal**, my husband **Dr. B.L.Samaga,** my children, **Master.Yashas Samaga** and **Master.Varun Samaga** and all my sisters for their unconditional support. My thanks to **Mrs.Prema** and **Miss. Reshma** who managed the house efficiently which helped me to carry out my work peacefully in the college.

There are many people who are responsible for the completion of this work. All of them have special place in my heart.

Rajalakshmi Samaga BL

ABSTRACT

Induction motors are extensively used in several industries such as oil, steel, petrochemical to name a few, and their failure may lead to the plant shut down resulting in the heavy financial losses. The motor operation management units are usually supported with protective gear which has the ability to detect the induction motor faults and stall the operation on detection. However, as a routine practice, it is essential to diagnose the defect in the motor by prognostic studies. There are various signature analysis techniques widely practiced in industries to detect nature and causes of failures in induction motor parts. Out of known causes of failures in these motors, 10 to 15% is attributed to the air gap eccentricity faults, thus demanding detection at the earliest. The major objective of this research work is to investigate the robust signatures to characterise the air gap eccentricity in the induction motor. To meet this objective, efficacy of various signatures that mark the presence of eccentricity are explored, and as an outcome it is found that d-q components of stator current can be used as the most suitable detector of machine failure due to mixed air gap eccentricity. Power signatures, Torque signatures and Power factor signatures were used for mixed eccentricity detection in the past by various researchers. These techniques use characteristic harmonics produced at the frequency signifying disturbances produced due to an air gap mixed eccentricity and used as signatures in air gap eccentricity diagnosis. In the present work it is shown that, the extracted d-q components of the stator currents contain characteristic harmonics signifying the presence of eccentricity and proposed as a better technique for performing the signature analysis. This technique is more advantageous and cost effective when compared to torque and power signatures analysis methods, since they are commonly used in controllers which are handling motor control.

The scope of research work is modularized into following four phases:

Phase 1: At this phase, mathematical expressions are derived for d-q components of stator currents in synchronous reference frame for the induction motor suffering from mixed air gap eccentricity. From the derived expressions, it is shown that they contain eccentricity specific harmonics in them.

Phase 2: Here, a dynamic model of squirrel cage induction motor suffering from air gap mixed eccentricity fault is developed. And this model is used in simulating

various mixed air gap eccentricity conditions and stored as a test data set. By systematic frequency signature analysis performed on the extracted d-q components of stator currents, it is shown that simulation results validate the mathematical expressions derived earlier.

Phase3: In this phase, observations made at the phases 1 and 2 are experimentally validated by conducting experiments on 3HP three phase induction motor suffering from mixed eccentricity. In addition a motor mounting frame having special provision for introducing eccentricity is specially fabricated to introduce various degrees of eccentricity.

Phase 4: To understand implications of supply voltage imbalances on eccentricity, detection technique is further investigated at this phase.

The d-q components of stator currents in synchronous reference frame are often used in controller as control variables, as these are found to be dc signals. But as a part of the research investigation it is also shown that d-q components of stator currents extracted from stator currents of an air gap eccentric machine in synchronous reference frame will contain DC component superimposed with ripple oscillations. This ripple is due to eccentricity and it can be characterized by harmonics frequency even when the machine is fed with 3 phase sinusoidal voltages and running under constant load.

As an outcome of all above work finally an integrated air gap eccentric condition monitoring unit and a controller unit for an induction motor has been proposed.

Key Words: Air gap eccentricity, d-q components of stator currents, Induction motor, Modeling and Simulation, Power Spectral Density Analysis.

CONTENTS

LIST OF FIGURES vi

LIST OF TABLES x

CHAPTER 1 1

1.0 INTRODUCTION 1

1.1 Types of faults 1

1.2 Air gap eccentricity faults 3

1.2.1 Types of air gap eccentricity 4

1.2.2 Effects of air gap eccentricity in the induction motor 7

1.2.3 Parameters affected by air gap eccentricity 8

1.2.4 Detection of eccentricity fault 9

1.3 Contribution from this research investigation 11

1.4 Methodology 12

1.5 Contents of this thesis 13

CHAPTER 2 15

2.0 LITERATURE SURVEY 15

2.1 Developments in the area of modeling of an induction motor for asymmetrical fault detection 15

2.1.1 Developments in the field of Winding Function Theory 17

2.1.2 Permeance calculation 21

2.2 Parameter identification to characterise the eccentricity fault and fault diagnostic techniques 21

2.2.1 Model based diagnosis 22

2.2.2 Fault diagnosis through signature analysis of machine quantity 22

2.3 Creation of mixed eccentricity artificially in the machine 26

CHAPTER 3 30

3.0 MODELING OF INDUCTION MOTOR HAVING MIXED AIR GAP ECCENTRICITY 30

3.1 Dynamic model of induction motor by Multiple Coupled Circuit Approach for balanced supply 30

3.1.1 Stator model *31*

3.1.2 Stator system voltage equations *31*

3.1.3 Rotor model *32*

3.1.4 Rotor system voltage equations *33*

3.1.5 Torque equations *35*

3.1.6 Calculation of inductances *35*

3.1.7 Permeance calculation for air gap eccentric machine *39*

3.2 Mathematical expressions for d-q components of stator currents 41

3.2.1 Mathematical Expressions for d-q components of stator currents of an induction motor suffering from air gap eccentricity fault. 41

3.3 Block diagram of the developed model 44

CHAPTER 4 46

4.0 EVALUATION OF MOTOR MODEL 46

4.1 Permeance variation with circumferential length of rotor 46

4.2 Inductance variation with rotor position 49

4.3 Simulation of dynamic behavior of machine 55

4.3.1 Dynamic behaviour of healthy machine *55*

4.3.2 Dynamic behaviour of eccentric machine *58*

4.4 Signature analysis of simulated signals 61

4.4.1 Motor Current Signature Analysis (MCSA) *61*

4.4.2 Instantaneous Power Signature Analysis *73*

4.4.3 Instantaneous Power Factor Signature Analysis *74*

4.4.4 Instantaneous d-q current Signature Analysis..... *78*

CHAPTER 5 83

5.0 DEVELOPMENT OF MOTOR ECCENTRICITY DETECTION SCHEME 83

5.1 Creation of artificial eccentricity in the machine 83

5.1.1 Creation of static eccentricity..... *84*

5.1.2 Creation of dynamic eccentricity..... *85*

5.3 Data acquisition software 93

5.4 Development and performance evaluation of eccentricity detection schemes .. 94

5.4.1 Eccentricity fault detection by eccentricity characteristic harmonics in stator current and its d-q components..... *95*

5.4.2 Eigenvalue based fault severity detection *101*

5.4.3 Laboratory experiments to evaluate eccentricity detection techniques..... *103*

CHAPTER 6 108

6.0 INFLUENCE OF UNBALANCE IN SUPPLY ON DETECTION OF MIXED AIR GAP ECCENTRICITY 108

6.1 Introduction 108

6.2 Modeling of induction motor for unbalance supply input..... 110

6.3 Validation of proposed model through experimental verification 113

6.4 Experimental results and analysis..... 116

7.0 CONCLUSION..... 119

APPENDIX..... 126

BIO-DATA: 151

PUBLICATIONS AND PRIZES WON OUT OF RESEARCH WORK..... 152

LIST OF FIGURES

Figure 1.1 Percentage of failures 3
Figure 1.2 Static eccentric rotor 5
Figure 1.3 Dynamic eccentric rotor in 4 different positions 6
Figure 1.4 Effect of non uniform air gap upon distribution of flux 7
Figure 2.1 Principle of model based diagnosis 22
Figure 2.2 Test motor built by Randy et al. (2006) 26
Figure 2.3 Creation of eccentricity (a) healthy bearing (b) eccentric bearing 27
Figure 2.4 End bell and end bell with eccentric sleeve inserted 27
Figure 2.5 Eccentric Sleeve and rings used for creation of eccentricity 28
Figure 3.1 Stator circuit model 31
Figure 3.2 Elementary rotor loops and current definitions 32
Figure 3.3 Rotor cage equivalent circuit 33
Figure 3.4 Skewed rotor 36
Figure 3.5 Winding layout of the machine 37
Figure 3.6 (a) Stator phase A turn function (b) rotor loop 1 turn function 38
Figure 3.7 Turn function for a rotor loop1 for the rotor having skewing angle γ 38
Figure 3.8 Computation sequence in modeling 44
Figure 4.1 Variation of permeance for different mixed eccentricity conditions δ_s-static eccentricity index, δ_d-dynamic eccentricity index 46
Figure 4.2 Variation of permeance for different sections along the axial length of the rotor over the rotor circumferential angle 47
Figure 4.3 3Dimensional View of variation of permeance along the rotor length over the rotor circumferential angle 48
Figure 4.4 Variation of mutual inductance between stator phase A and rotor loop1 and its derivative: Fig (a) and (b) without skewing Fig (c) and (d) with skew (5°) 49
Figure 4.5 Mutual inductance between stator phase A and rotor bar 1 in the axial direction with skew=0^o, 5^o, 9^o 50
Figure 4.6 Variation of mutual inductance between stator phase A and rotor loop1 and its derivative: Fig (a) (b) uniform axial eccentricity Fig (c) (d) inclined eccentricity. 51

Figure 4.7 Variation of mutual inductance between rotor loop1 and rotor loop2 and its derivative: Fig (a) (b) uniform axial eccentricity Fig (c) (d) inclined eccentricity.....52
Figure 4.8 Self inductance of rotor loop1 Fig (a) uniform axial eccentricity condition Fig (b) inclined eccentricity condition.....53
Figure 4.9 Variation of mutual inductance between stator phase A and stator phase B and its derivative: Fig (a), (b) uniform axial eccentricity Fig (c), (d) inclined eccentricity.....54
Figure 4.10 Self inductance of stator phase A Fig (a) uniform axial eccentricity condition Fig (b) inclined eccentricity condition.....55
Figure 4.11 Speed and dynamic torque waveforms of the healthy machine Fig (a) speed vs time Fig (b) dynamic torque vs time.....56
Figure 4.12 Stator phase current and rotor loop current waveforms 56
Fig (a) I_s vs time Fig (b) I_r vs time 56
Figure 4.13 Stator phase flux linkage and rotor loop flux linkage waveforms of the healthy machine Fig (a) $\lambda_s$vs time Fig (b) λ_r vs time.....57
Figure 4.14 i_{qd0} components of stator phase current waveforms of the healthy machine Fig (a) i_{qs} vs time Fig (b) i_{ds} vs time Fig (c) i_{0s}vs time 57
Figure 4.15 Dynamic waveforms: speed vs time, dynamic torque vs time, stator phase currents vs time, rotor loop currents vs time, stator phase flux linkages vs time, rotor loop flux linkages vs time Fig (a) uniform axial eccentricity with δ_s=0.3 and δ_d=0.1 Fig (b) inclined axial eccentricity with δ_{s1}=0 , δ_{s2}=0.3 and δ_d=0.1.....59
Figure 4.16 i_{qd0} components of stator phase current waveforms of the eccentric machine under full load conditions Fig (a) i_{qs} vs time Fig (b) i_{ds} vs time Fig (c) i_{0s}vs time (uniform eccentricity condition) Fig (d) i_{qs} vs time Fig (e) i_{ds} vs time Fig (f) i_{0s}vs time (inclined eccentricity condition).....60
Figure 4.17 Stator phase A current spectra Fig (a) Healthy Fig (b) Uniform axial eccentricity (δ_s=0.3 and δ_d=0.1) Fig (c) Inclined axial eccentricity (δ_{s0}=0.0, δ_{s1}=0.3 and δ_d=0.1).....63
Figure 4.18 Variation of eccentricity severity factor with dynamic eccentricity 69
Fig (a) ESF1vs % Dynamic Eccentricity Fig (b) ESF2 vs Dynamic Eccentricity.....69
Figure 4.19 Variation of Eigenvalue with dynamic eccentricity index 70

Figure 4.20 Stator current spectra for eccentric condition (δ_d=0.05 and inclined static eccentricity with δ_{s1}=0.2 and δ_{s2}=0.35).....71
Figure 4.21 Instantaneous Power spectra for eccentric condition (δ_d=0.05 and inclined static eccentricity with δ_{s1}=0.2 and δ_{s2}=0.35).....73
Figure 4.22 Instantaneous Power factor spectra for δ_d=0.05 and inclined static eccentricity with δ_{s1}=0.2 and δ_{s2}=0.35.....75
Figure 4.23 Power factor severity factor vs dynamic eccentricity index.....77
Figure 4.24 Slope of power factor severity factor curve 77
Figure 4.25 Current spectra under healthy and uniform eccentricity conditions (δ_s=0.3,δ_d=0.1) 78
Figure 4.26 Current spectra under healthy and inclined eccentricity conditions (δ_{s0}=0, δ_{s1}=0.3, δ_d=0.1) 79
Fig (a) i_{qs} current spectra –Healthy.....79
Fig (b) i_{qs} current spectra – Eccentricity 79
Fig (c) i_{ds} current spectra –Healthy.....79
Fig (d) i_{ds} current spectra – Eccentricity 79
Figure 4.27 Current spectra Fig (a) i_{as} current spectra Fig (b) i_{qs} current spectra.....80
Fig (c) i_{ds} current spectra.....80
Figure 4.28 Variation of amplitudes of eccentricity characteristic harmonics 81
Fig (a) (f_1-f_r), (f_1+f_r) in i_{as} current spectrum with variation in slope of inclination 81
Figure 5.1 Sectional view of the machine with modifications.....84
Figure 5.2 Bracket with shaft seating arrangement and its dimensions.....84
Figure 5.3 Bushing to be placed inside the shaft seating arrangement.....85
Figure 5.4 Front and back view of the bracket 86
Figure 5.5 Modified machine (a) side view (b) top view 86
Figure 5.7 SCXI-1125 block diagram (courtesy: www.NI.com).....90
Figure 5.8 Block diagram of DAQ 6024E (courtesy: www.ni.com) 91
Figure 5.9 Data Acquisition System- block diagram.....92
Figure 5.10 Data acquisition experimental set up.....93
Figure 5.11 i_d and i_q components of stator current Fig (a) inclined static eccentricity of slope 0.8333 (k=2.3809*) Fig (b) inclined static eccentricity of slope of 1.5 (k=4.2857*).....95

Figure 5.12 i_a, i_q and i_d current spectra 96
Figure 5.13 Variation of amplitudes of eccentric characteristic harmonics 100
Figure 5.14 Variation of Eigenvalue with static eccentricity (experiment).....102
Figure 5.15 Variation of Eigenvalue with static eccentricity (simulation).....102
Figure 5.16 Stator phase A current spectra under no load, 72.7% and full load conditions.....103
Figure 5.17 d-axis component of stator phase currents spectra under no load condition, 72.7% load condition and full load condition.....104
Figure 5.18 q-axis components of stator phase currents spectra under no load condition, 72.7% load condition and full load condition.....105
Figure 5.19 Instantaneous power spectra under no load condition, 72.7% loaded condition and full load condition.....106
Figure 6.1 Line voltage triangle.....113
Figure 6.2 (a) stator phase A turn function (b) rotor loop1 turn function.....113
Figure 6.3 Stator phase A Current Spectra (a) Balance condition (b) Unbalance condition (2.03%). 114
Figure 6.4 Stator phase A Current Spectra (a) Balanced condition (b) Unbalanced condition (2.02%) 117
Figure II-1.1 Schematic representation of the static air gap eccentricity 127
Figure II-2.1 Schematic diagram of the dynamically eccentric rotor 129
Figure II-3.1 Depiction of static and dynamic eccentricities in stator coordinates ...131

LIST OF TABLES

Table 2.1 Eccentricity Fault Frequency Equations 24
Table 4.1 Type of Fault and Frequency related component detection equations 62
Table 4.2 Lower and upper side band frequency components in the simulated PSD..64
Table 4.3 Full load with 20% dynamic eccentricity 65
Table 4.4 53.7 % load with 20% dynamic eccentricity 65
Table 4.5 No load with 20% dynamic eccentricity.....65
Table 4.6 Full load with 40% static eccentricity.....66
Table 4.7 53.7% load with 40% static eccentricity.....67
Table 4.8 No load with 40% static eccentricity 67
Table 4.9: ESF1 and ESF2 values vs % Dynamic Eccentricity.....69
Table 4.10 Eccentricity related frequency components (f_1-f_r) and (f_1+f_r) and its amplitudes 72
Table 4.11 Eccentricity related frequency components, f_r, ($2f_1$-f_r) and ($2f_1$-$2f_r$) and its amplitudes 74
Table 4.12 f_r, ($2f_1$-f_r) and ($2f_1$-$2f_r$) frequency components and their amplitude in power factor spectra. 76
Table 5.1 Eccentricity related characteristic components in current spectra for the eccentric machine under no load condition 97
Table 5.2 Eccentricity related characteristic components in current spectra for the eccentric machine under 85% load condition 97
Table 5.3 Eccentricity related characteristic components in current spectra for the eccentric machine under full load condition.....97
Table 5.4 Eccentricity related characteristic components in i_q and i_d current spectra for no load condition.....98
Table 5.5 Eccentricity related characteristic components in i_q and i_d current spectra for 85% load condition 98
Table 5.6 Eccentricity related characteristic components in i_q and i_d current spectra for Full load condition 99
Table 6.1 Line voltage magnitude corresponding to 3% unbalance.....110
Table 6.2 Comparison of eccentricity related harmonics in stator phase A current ..114

Table 6.3 Variation in magnitude of air gap eccentricity related harmonics under Over voltage unbalance.....115
Table 6.4 Variation in magnitude of air gap eccentricity related harmonics under...115
Under voltage unbalance.....115
Table 6.5 Variation in magnitude of air gap eccentricity related harmonics under...116
Mixed voltage unbalance 116
Table 6.6 Comparison of eccentricity related harmonics in stator phase A current ..117
Table 6.7 Variation of magnitude of air gap eccentricity related harmonics under Over, Under, Mixed voltage unbalance 118

NOMENCLATURE

C_1	-center of stator bore
C_2	-center of the rotation of rotor
d_d	-distance between center of rotation and center of the rotor in m
d_s	-distance between C_1 and C_2 in m
f_1	-supply frequency in Hz
f_e	-air gap eccentricity characteristic frequency component in Hz
f_r	-frequency of the rotor speed in Hz
g_0	-air gap radius under healthy (symmetrical) condition in m
$g^{-1}(\theta_r, \phi)$	- inverse air gap function in m^{-1}
I_r	-rotor current vector
I_s	-stator phase current vector
i_a	-line A current in A
i_b	-line B current in A
i_c	-line C current in A
i_{as}	-stator phase A current in A
i_{bs}	-stator phase B current in A
i_{cs}	-stator phase C current in A
i_0	-zero sequence component of stator current in A
i_{ds}	-d axis component of stator currents in A
i_{qs}	-q axis component of stator currents in A
J	-moment of inertia in kg m^2
L_{aa}	-self inductances of stator phase A in H
L_{ab}	-mutual inductance between stator phases A and B in H
L_{ac}	-mutual inductance between stator phases A and C in H
L_{ar}	-mutual inductance between stator phase A and r^{th} rotor loop in H
L_{cr}	-mutual inductance vector between stator phase A and r^{th} rotor loop in H
L_b	-inductance of rotor bar in H
L_{ba}	-mutual inductance between stator phases B and A in H

L_{bb}	- self inductances of stator phase B in H
L_{bc}	-mutual inductance between stator phases B and C in H
L_{br}	-mutual inductance vector between stator phase A and r^{th} rotor loop in H
L_{ca}	-mutual inductance between stator phases C and A in H
L_{cb}	-mutual inductance between stator phases C and B in H
L_{cc}	-self inductances of stator phase C in H
L_e	-inductance of end ring segment in H
L_{ij}	-mutual inductance between winding *i* and *j* in h
L_{ls}	-leakage inductance of the stator winding in H
L_{mr}	-magnetizing inductance of rotor loops in H
L_{ms}	-magnetizing inductance of the stator winding in H
L_{rs}	-transpose of the matrix L_{sr}
L_{rr}	-rotor inductance matrix
L_{sr}	-mutual inductance between stator phase and rotor loop matrix
L_{ss}	-stator inductance matrix
ℓ	-length of the stack in m
N	-number of turns/phase
$N_j(\theta_r, \phi)$	-winding function of winding j
N_r	-rotor speed in rpm
n	-number of rotor bars
n_d	-dynamic eccentricity order
$n_i(\theta_r, \phi)$	-turn function of winding i
P	-permeance of air gap in m^{-1}
p	-number of pole pairs,
p_j	-number of coils of winding j
p_{phasor}	-average power in watts
q_i	-number of coils of winding i
R	-stator phase A resistance in Ω
R_b	-stator phase B resistance in Ω
R_c	-stator phase C resistance in Ω

R'_b	-rotor bar resistance in Ω
R_e	-end ring segment resistance in Ω
R_r	-rotor resistance matrix
R_s	-stator resistance matrix
R'_s	-radius of the stator in m
R'_r	-radius of the rotor in m
$r(\theta_r, \phi) = r$	-average radius of air gap in non symmetrical conditions in m
r_s	-stator winding resistance in Ω
s	-slip
T_e	-electromagnetic torque in Nm
T_L	-load torque in Nm
V_{ab}	-line voltage between A and B in V
V_{bc}	-line voltage between A and B in V
V_{ca}	-line voltage between C and A in V
V_r	-rotor voltage vector
V_s	-stator phase voltage vector
V_{sl}	-stator line voltage vector
v	-stator harmonics that are present in the power supply driving the motor
v_a	-stator phase A voltage in V
v_b	-stator phase B voltage in V
v_c	-stator phase C voltage in V
v_o	-zero sequence component of voltage in V
W_{co}	-stored magnetic energy in Joules
z	-a section along the axial length of rotor
δ	-mixed eccentricity index
δ_s	-static eccentricity index
δ_d	-dynamic eccentricity index
μ_0	-absolute permeability of the air gap
θ	-arbitrary angle
θ_r	-rotor angle in radians.

ϕ	-rotor circumferential angle in radians.
$\langle f \rangle$	-mean of function f over [0,2π] range
α_r	-angle between two rotor bars in radians
ω_r	-rotor speed in electrical radians/sec
ω_{rm}	-rotor speed in radians/sec
λ_a	-stator phase A flux linkage in Wb
λ_b	-stator phase B flux linkage in Wb
λ_c	-stator phase C flux linkage in Wb
λ_r	-rotor flux linkages in Wb
λ_s	-stator flux linkages in Wb
λ_{sl}	-stator line flux linkage vector
γ	-skewing angle in radians

CHAPTER 1

1.0 INTRODUCTION

Induction motors are the main workhorse of industrial prime movers because of their wider applications mainly due to their low cost, reasonably small size, ruggedness, low maintenance and operation with an easily available power supply. They are the critical components in many industrial processes and power plants.

Reliability, efficiency and performance of these machines are the concern of the industries. In spite of its high reliability, these machines fail to perform because of various operating conditions. Preventive maintenance of electric drive systems with induction motors involves monitoring them for detection of abnormal electrical and mechanical conditions that may lead to the catastrophic failure of the system. In recent years, condition monitoring of electrical machines has gained importance in industries. It is aimed to reduce the downtime of these machines which results in loss of production and loss of revenue. Thus condition monitoring is the fast emerging technology for online detection of incipient faults and it avoids unexpected failures and greatly improves the system reliability. The proposed research work aims at early detection of one of the mechanical faults i.e. air gap eccentricity fault in induction motors using non-invasive techniques.

1.1 Types of faults

The major asymmetrical faults in induction motors can be classified as [Nandi et al. 2005, Chetwani et al. 2005] follows:

(i) Stator faults

- Inter turn fault resulting in the opening or shorting of one or more circuits of a stator phase winding
- Abnormal connection of stator winding.

(ii) Rotor faults

- Broken rotor bar

- Cracked rotor end ring

(iii) Bearing faults

- Flaking or spalling of bearings
- Contamination and corrosion by pitting
- Improper lubrication
- Improper installation of bearing
- Indentations formed in the raceways (brinelling)

The majority of the electrical machines use ball or rolling element bearings. Even under normal operating conditions with balanced load and good alignment, fatigue failures may take place. These faults may lead to increased vibration and noise levels. Flaking or spalling of bearings may occur. Almost 40-50% of all major faults are bearing related faults. Sometimes bearing faults might manifest themselves as rotor asymmetry faults which are often referred as eccentricity related faults.

(iv) Eccentricity related faults:

-Static/ dynamic air-gap irregularities

-Defect in stator and rotor structure

-Bent shaft which can result in a rub between rotor and stator which can result in serious damage to the stator core and windings.

-weak bearing

-misalignment

Machine air gap eccentricity is due to unequal air gap between the stator and the rotor. Almost all the mechanical faults (approximately 80%) lead to this condition in the machine.

Approximately 30%-40% of faults in induction motors are stator faults, 40%-50% are bearing related faults and 5%-10% are due to rotor faults [Nandi et al. 2005] and 10%-15% are eccentricity faults. Chetwani et al. (2005), have categorized the machine faults as 41% bearing faults, 37% stator faults, 10% rotor faults and 12% eccentricity faults and are shown in Figure1.1.

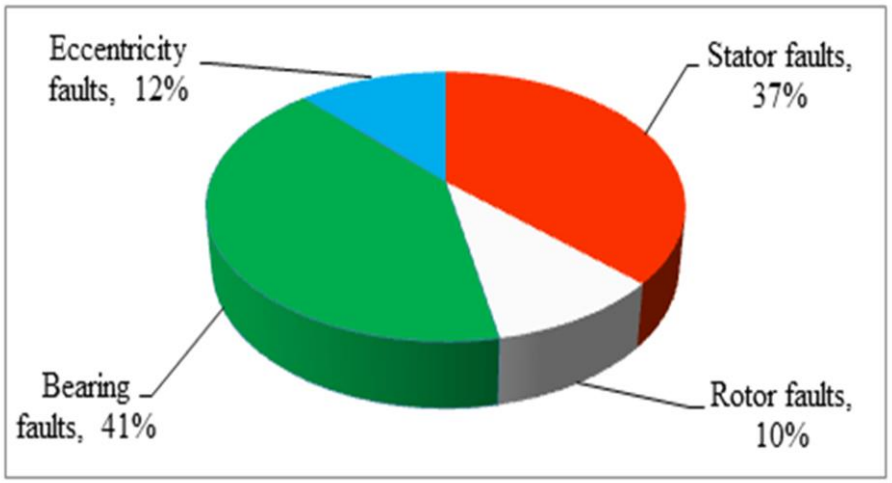

Figure 1.1 Percentage of failures [Chetwani et al. 2005]

Among the faults, bearing and eccentricity related faults are mechanical faults. Very often eccentricity related faults are misinterpreted as bearing faults.

1.2 Air gap eccentricity faults

Non uniform air gap between the stator and rotor is known as eccentricity. Due to mechanical reasons, certain amount of eccentricity is inherent in induction motors at the commissioning stage itself. The air gap should be as small as possible to obtain very good operating power factor. Due to mechanical issues, certain minimum air gap is maintained in the induction motor. The typical air gap is of the order 0.25mm to 3mm for a 4 pole machine. The air gap can be calculated using empirical formulae depending upon the required operating conditions such as power factor, efficiency and overall design. If the machine is expected to operate at high reliability, the air gap is usually kept more than that of calculated by empirical formulae. The air gap eccentricity may be caused by the following reasons [Nandi et al. 2005, Chetwani et al. 2005]:

- Ovality of the stator core
- Flexible stampings of the stator core
- Deformity in rotor structure
- Incorrect positioning of rotor and stator structure during assembly

- Incorrect positioning of the shaft in bearings
- Bent rotor shaft, bearing wear and tear
- Misalignment of bearings
- Mechanical resonance at critical speeds
- Unbalanced loads
- Broken rotor bars etc.

These eccentricities can occur at manufacturing stage, assembly stage or during major repair. Very often, the manufacturer wants to keep this eccentricity level below 10% in case of large machines. In small machines, if the shaft is small and rigid, eccentricity level up to 30% will not lead to machine failure [Nandi et al. 2005].

1.2.1 Types of air gap eccentricity

Eccentricity related faults are divided into circumferential unequal air gap and axial unequal air gap (inclined) [Cameron et al. 1986, Dorell et al. 1995, Faiz et al. 2003, Nandi et al. 2005, Chetwani et al. 2005, Xiaodong et al. 2007]. In circumferential air gap eccentricity, air gap eccentricity remains uniform throughout the axial length of the rotor, whereas inclined eccentricity occurs when the rotor's geometric axis is not parallel to that of the stator. Then along the rotor axial direction, the degree of eccentricity is not constant. Thus, axial or inclined eccentricity can also be treated as a variable circumferential eccentricity. Inclined eccentricity considers the air gap length as a function of the rotor angle and the position along the axial length of the rotor.

Further they are classified as

(i) Static air-gap eccentricity

Static eccentricity occurs, if the rotor is offset relative to the center of the stator bore, such that the air gap is less at one point and greater at the diametrically opposite point. This type of air gap eccentricity exists in the machine at the manufacturing stage itself. In this type of eccentricity, the position of minimal air gap length is fixed in space.

It may be caused by

- the ovality of the stator core

- incorrect positioning of the rotor or stator at the commissioning stage or during maintenance.

This occurs when the rotor rotates about the centerline of the stator bore, but this centerline does not coincide with that of the stator bore as shown in Figure 1.2. When machine suffers only from static air gap eccentricity, the center of the rotor does not coincide with that of the stator. This is measured in terms of static eccentricity index δ_s.

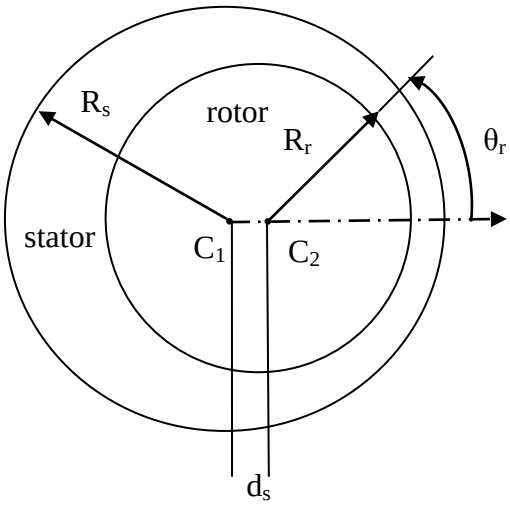

Figure 1.2 Static eccentric rotor

where C_1 is the center of stator bore

C_2 is the center of the rotation of rotor

R_s is the radius of the stator in m

R_r is the radius of the rotor in m

From Figure 1.2, Static eccentricity index (δ_s) is defined as

$$\delta_s = \frac{d_s}{g_0} \tag{1.1}$$

where d_s is the distance between C_1 and C_2 in m.

g_0 is the air gap radius under healthy condition (R_s-R_r) in m.

If the rotor-shaft assembly is sufficiently stiff, the level of static eccentricity does not change significantly over the period.

***(ii) Dynamic air-gap eccentricity**:*

If the rotor is eccentric with respect to the shaft, and the bearings are concentric with respect to the stator, then the center of the rotation changes when rotor rotates. This situation is known as the dynamic or rotating eccentricity. In this type of eccentricity, the center of the rotor is not at the center of rotation and the position of minimum air gap rotates with the rotor as shown in Figure1.3. This occurs when the rotor rotates about the centerline of the stator bore, but this centerline does not coincide with that of the rotor itself. This may be due to a bent rotor shaft, bearing wear or misalignment, mechanical resonance at critical speed etc.

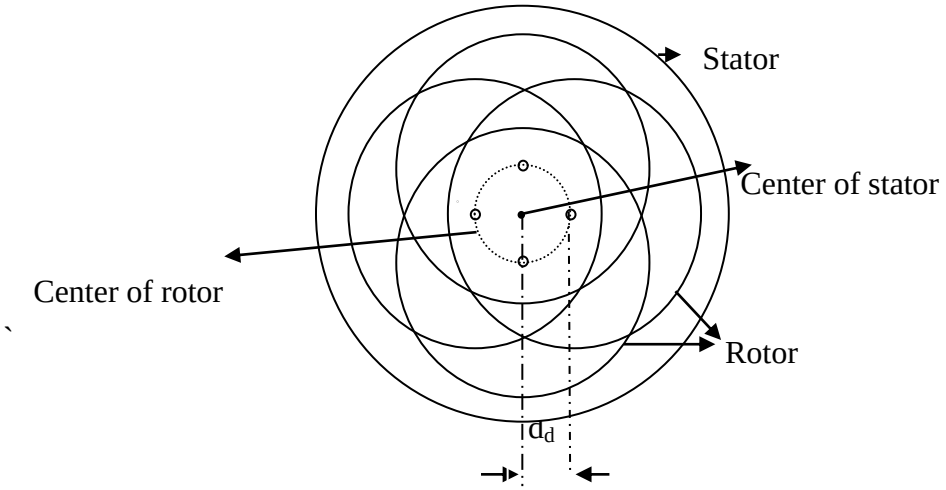

Figure 1.3 Dynamic eccentric rotor in 4 different positions

From Figure 1.3, dynamic eccentricity index (δ_d) can be defined as

$$\delta_d = \frac{d_d}{g_0} \tag{1.2}$$

where d_d is the distance between center of rotation and center of the rotor.

Dynamic eccentricity in a machine is controlled by the Total Indicated Reading (TIR) or "run-out" of the rotor.

(iii) Mixed air-gap eccentricity

Certain amount of static eccentricity will be present in the machine at the manufacturing stage. They give rise to dynamic eccentricity over a period of time. Both static and dynamic eccentricity co-exists in a machine. In this case, both rotor

symmetrical and mechanical rotation centerlines are displaced individually with respect to the stator symmetrical centerline.

1.2.2 Effects of air gap eccentricity in the induction motor

Many mechanical faults such as misalignment, rotor shaft bending and even worn bearing leads to various non-uniform air-gaps including stator and rotor eccentricity. The air gap length is of the order 2 mm to 6 mm for a 10 hp (7.45 kW) machine. Even a small percentage of eccentricity may produce non uniform distribution of the flux resulting in high amount of mechanical stresses on the rotor. Figure 1.4 shows the flux distribution of a simple winding in non uniform air gap.

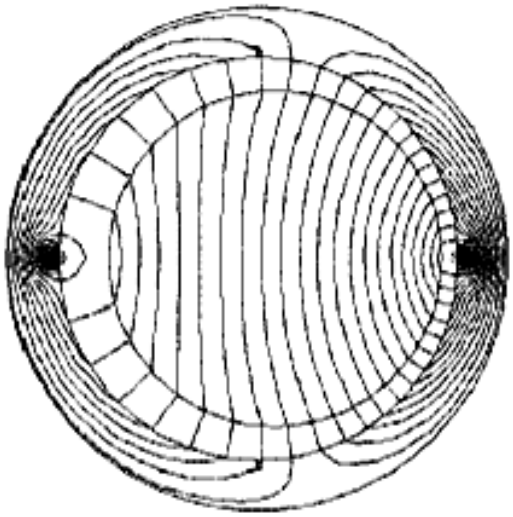

Figure 1.4 Effect of non uniform air gap upon distribution of flux [Faiz et al. 2002]

An inherent level of static eccentricity exists even in newly manufactured machines due to manufacturing and assembly method [Nandi et al. 2005]. Static eccentricity causes a force on the rotor which tries to pull the rotor further from stator bore center in one direction which is known as Unbalanced Magnetic Pull (UMP). Since UMP is inversely proportional to the square of the air gap length, the force is more where the air gap length is the least. UMP acting in one direction may lead to bent rotor shaft and bearing wear. This further increases the eccentricity level and produces some degree of dynamic eccentricity in the machine. Dynamic eccentricity also produces the unbalanced magnetic pull which acts on the rotor and rotates at

rotor speed. Presence of both static and dynamic eccentricity can cause excessive stressing of the machine, resulting in bearing wear and tear. This may lead to the insulation failure of the stator windings or breaking of rotor cage bars or end rings. This may even lead to rotor to stator rub, damaging the core, windings and rotor cage and hence failure of the machine. The radial magnetic force waves produced by eccentricity can also act on the stator core and hence stator windings get subjected to vibrations. Acoustic noise levels increase and rotor may whirl near critical speed.

Hence, eccentricity level in the machine should be kept as low as possible in order to reduce the unbalanced magnetic pull and to reduce vibration and noise.

1.2.3 Parameters affected by air gap eccentricity

Any form of eccentricity existing in the motor alters the normal flux distribution in the air gap. Therefore quantities such as torque developed, vibrations in the stator core, stator phase current, so on which are functions of air-gap flux also get altered. Air gap eccentricity in induction machines causes certain characteristic harmonic components in electrical, electromagnetic and mechanical quantities. Some of the parameters affected by the presence of eccentricity in the machine are discussed briefly below

(i) Magnetic flux: Non uniformity of the air gap in rotating electric machinery leads to a non uniform permeance of the air gap . In this case, air gap flux is also non uniform and unsymmetrical [Faiz et.al, 2002].

(ii) Vibration: The radial magnetic forces produced between the stator and rotor surfaces are proportional to the flux density squared and they result in stator core and winding vibration. Any change in air gap will result in a change in vibration spectrum. The vibration is usually sensed at the bearings and for each motor there is a different mechanical stiffness between the electromagnetic forces caused by air gap eccentricity and the position where vibration is sensed [Thomson 2009].

(iii) Stator Current: Current is the primary parameter in the induction motor to get affected by non uniform distribution of flux in the air gap. Eccentricity faults produce characteristic fault harmonics in the current. Vibration from the electromagnetic forces is a second order effect compared to current components directly induced from the specific rotating flux waves [Thomson 2009].

(iv) Air gap torque: The electromagnetic torque is produced in induction motor by the interaction of air-gap flux produced by three phase stator winding and the induced rotor currents. It is sensitive to unbalance created due to defects as well as unbalanced supply voltages. Eccentric specific harmonics present in the torque produces torque oscillations in the machine [Siddique et al. 2005].

(v) Power: The interaction of eccentricity characteristic harmonics with the mains sinusoidal supply voltage causes eccentricity specific harmonics in the power spectrum. It has definite advantage in comparison to current as a detection parameter because characteristic spectral component of the power appears directly at the frequency of the disturbance, independent of the synchronous speed of the motor [Drif et al. 2006].

(vi) Power factor: It is a characteristic quantity that is used in electrical machines to get affected by the presence of faults in the machine. The presence of eccentricity increases the mean value of the power factor. Eccentricity specific harmonics are present in the instantaneous power factor [Drif et al. 2008].

(vii) Noise: With the increase in the air gap eccentricity, vibrations induced in the machine also increases. As a result there will be an increase in the acoustic noise level in the machine [Siddique et al. 2005].

(vii) Others: Temperature, instantaneous angular speed, partial discharge are some of the other quantities getting affected by the air gap eccentricity in the machine [Siddique et al. 2005].

Hence, these quantities can be used to monitor the conditions of the motor.

1.2.4 Detection of eccentricity fault

Preventive maintenance of electric drive systems with induction motors involves monitoring them for detection of abnormal electrical and mechanical conditions (fault diagnosis) that may lead to the catastrophic failure of the system. In simple words, detection of fault in a machine which can lead to machine failure is known as fault diagnosis. There is a need to diagnose the type and severity of fault at its inception stage so that one can predict the time of major break-down. The problem of fault diagnosis consists in determining the type of fault and location of fault. Condition monitoring of machine can be offline or online. For example,

- a surge tester, a reliable and in many cases readily available off-line tool that can be employed for eccentricity detection, especially for routine and predictive maintenance [Xianghui et al. 2007].
- Search coils mounted inside the machine can be used for online detection.

Invasive and Non-invasive are the two methods used for online condition monitoring of the machines.

(i) Invasive methods: The sensors embedded inside the machine are used to detect the fault in the machine. Any distortion in the air-gap flux density due to air gap eccentricity can be sensed using search coils fitted around the shaft [Nandi et al. 2005]. The air gap flux can also be sensed by sensing the voltage across two properly located motor coils. Vibration sensors such as Micro Electro Mechanical Systems (MEMS) accelerometers [Krause et al. 1965], temperature sensors mounted on the winding or embedded in the insulation, speed sensors are also used to detect the fault in the machine.

(ii) Non-invasive methods: Physical sensors usually are objectionable due to factors such as fragility, cost, accuracy, mounting and reliability. Hence, sensor less technique is used for fault detection which is popularly known as non-invasive method. The fault detection using noninvasive methods demands in the detection of one of the following irregularities under faulty conditions [Nandi et al. 2005]:
   - Unbalanced air-gap voltages and line currents
   - Increased torque pulsations
   - Decreased average torque
   - Increased losses and reduction in efficiency
   - Increase in vibrations

To detect the eccentricity faults, many diagnostic methods are developed. Some of the developed non-invasive air gap eccentricities monitoring techniques are

- Motor Current Signature Analysis (MCSA)
- Vibration monitoring
- Instantaneous power spectral analysis
- Instantaneous power factor analysis
- Instantaneous Torque Spectral analysis

Vibration monitoring and motor current signature analysis are the two popular methods used in condition monitoring units in industrial drives.

1.3 Contribution from this research investigation

Induction motor is a critical component in many power plants, electric utility, petrochemical and chemical industries. Failure of induction motors increases the cost of production due to reduced output and emergency maintenance costs. Some time it may lead to plant shut down resulting in the loss of revenue to the tune of millions of dollars. A reliable fault predictor about the incipient faults can decrease the loss of revenue due to downtime. Condition monitoring is used to monitor the machine parameters for the purpose of detection, analysis and correction of the machine problems before the failure takes place. Very often machine failure is attributed to bearing faults. Most often machine failure may be due to eccentricity related faults which would have manifested as bearing faults. Motor Current Signature Analysis (MCSA) is the very popular eccentricity fault detection technique. This present study investigates various methods used in characterisation of the faults using MCSA and compares them and proposes new methods to detect the eccentricity related faults in three phase squirrel cage induction motor.

The following are the highlights of the current work:

- This study is a special study in that the parameters chosen for modeling and simulation are the same as the parameters of the experimental machine.
- A dynamic model of the machine is developed using multiple couple circuit approach and inductances are computed using 2 Dimensional Winding Function Theory which can be used to study the behaviour of the machine under both uniform and inclined eccentricity conditions.
- Fault severity factors using stator phase current signatures are proposed to predict the degree of the fault in the machine.
- It is shown that Eigenvalues computed by comparing eccentricity characteristic harmonics in the current with those of the installation condition can be used to predict the severity of the fault.

- Various signatures of other parameters such as instantaneous power, power factor and d-q components of stator current of the machine having mixed eccentricity are compared. All these methods have a unique advantage compared to stator current signature analysis as they produce an air gap eccentricity characteristic component at the frequency of rotational speed of the machine f_r.
- In this investigation, it is shown that instantaneous signature analysis of d-q components of stator currents is another method of eccentricity fault detection.
  The advantages of this method are
  - They also produce eccentricity characteristic component f_r
  - They are cost effective as they need only current sensors.
  - As d-q components are processed in controller unit, the same can be used for fault detection.
- By both modeling-simulation and experimental results, it is shown that the unbalance in supply voltage would affect the air gap eccentricity fault detection method by Motor Current Signature Analysis (MCSA) marginally.

1.4 Methodology

There is a need to study various signatures to characterise the eccentricity fault in the induction motor before a robust is adopted. To choose the proper parameter to characterise the air gap non uniformity in the machine, the investigations are conducted in three stages.

Stage 1: In this study, d-q component signature analysis is chosen to characterise the air gap eccentricity fault in the machine. Stator current expressions are obtained for an eccentric machine by substituting the eccentricity related harmonics in the stator current expressions of a healthy machine. Mathematical expressions for the d-q components of stator currents are derived from the abc-dq0 transformation.

Stage 2: A dynamic model of the squirrel cage induction motor suffering from both uniform and inclined mixed eccentricity condition is developed on a suitable platform. The model is simulated for various loading and eccentricity conditions and various signature analysis are explored and compared to characterise the fault. Signature analysis of d-q component is performed to identify the eccentricity related frequency components in them.

Stage 3: A machine is fabricated to include eccentricity fault in it. Various experiments are conducted on the machine for different eccentricity conditions of the machine under different loading conditions. d-q components of the stator currents are extracted and stored as test data for offline studies. Power Spectral Density (PSD) analysis is performed to validate the claim made by the mathematical expressions and modeling-simulation results.

1.5 Contents of this thesis

This thesis contains the details of the investigations conducted on a squirrel cage induction motor to characterise the eccentricity fault in the machine. It contains seven chapters including Chapter 1 which gives insight to the relevance of the investigation and the methodology adopted in this investigation.

In Chapter 2, Literature Survey conducted before and after defining the research problem is discussed. Discussion is presented in three phases

- Phase1: In this phase, various methods used by the researchers to model an air gap eccentric induction motor are explored.
- Phase2: Various parameters and methods adopted by the researchers to characterise the eccentricity fault in an induction machine are studied in this phase.
- Phase3: A survey is conducted to know the various ways by which the researchers have created air gap eccentricity in the machine artificially.

Chapter 3 gives complete insight into how the dynamic model of an induction motor suffering from eccentricity fault is developed in MATLAB/SIMULINK platform. Multiple coupled circuit approach is used to develop the model and 2D-Modified Winding Function Theory (2D-MWFT) is used to calculate the inductances between the windings. In the same Chapter, mathematical expressions are derived for the d-q components of stator currents of an air gap eccentric machine. Symbolic Math in MATLAB® is used for the derivation of these expressions.

Chapter 4 presents results and discussion on simulation studies carried out using developed motor models proposed in Chapter 3. In this Chapter various signature analysis to detect eccentricity fault harmonics are presented. Power Spectral Density (PSD) analysis is performed on the various extracted quantities such as motor

current and its d-q components, instantaneous power, instantaneous power factor and are compared.

To validate the mathematical expressions developed and the results obtained by modeling-simulation, experiments are conducted in the laboratory. The details of eccentricity creation in the machine, the Data Acquisition System (DAS) developed using NI hardware and LabVIEW® software are explained in Chapter 5. The experimental results are also presented in this chapter.

In Chapter 6, a brief report is presented on the investigation conducted on the induction motor to study the effect of unbalance in supply voltage on the mixed eccentricity detection method by MCSA. This chapter contains the details of changes that should be made in the model so that it accounts unbalance voltage supply. The results obtained by modeling and simulation and experiments are presented.

Conclusion and scope for future work is presented in Chapter 7.

CHAPTER 2

2.0 LITERATURE SURVEY

This research work is a prognostic study that aims at prediction of machine failure due to air gap eccentricity fault in the squirrel cage induction motor. The main objective is to identify the robust signature (may be multiple) to characterise the eccentricity fault in induction motor. For this purpose the research work is grouped in two phases.

Phase 1:

1.Develop a dynamic model of squirrel cage induction motor with air gap mixed eccentricity.

2.Characterisation of mixed eccentricity fault after exploring various signatures.

Phase 2:

Experimental validation of signatures on a specially fabricated three phase induction motor in which air gap eccentricity can be created artificially.

To achieve the objectives defined for the investigation, extensive literature survey is carried out in the following three fields:

- Development of a robust dynamic model that accommodates inclined air gap eccentricity in it.
- Parameters to characterise the air gap eccentricity fault in the machine and diagnostic methods.
- Creation of air gap eccentricity artificially in the machine.

2.1 Developments in the area of modeling of an induction motor for asymmetrical fault detection

Modeling and simulation of an induction motor help in studying the behavior of the machine under both healthy and unhealthy condition. It also helps in identifying the change in the machine parameters under fault conditions and characterisation of the fault in the machine. Hence, a robust model of an induction motor which can depict the behavior of the machine under faulty condition needs to be developed.

A dynamic model of induction motor can be developed in three ways. They are as follows:

(i) d-q model (abc-dqo model): The dynamic model of the induction motor is derived by using a two phase motor in direct and quadrature axes. This modeling technique converts vectors with fixed abc reference frame to d-q axis in any one of the following three rotating reference frame with speed ω_c defined with respect to fixed abc frame.

- Stator reference frame: $\omega_c=0$, the frame is fixed in stator
- Rotor reference frame: $\omega_c=\omega_r$, the frame is fixed in rotor
- Synchronous reference frame: $\omega_c=\omega_s$, the frame is fixed in synchronously rotating frame

Hence, the dynamic equations of induction machines are simplified to analogous to DC machine equations in synchronous reference frame [Krause et al. 1965].

Advantages:

- Transformation from abc to d-q axis
- Ideal for symmetrical operation.

Disadvantages:

- Harmonics of winding distribution are neglected.
- Asymmetric faults cannot be incorporated.

(ii) Finite Element Method: It uses the finite element method (FEM) associated with the state space models based on the Maxwell's equations by taking into account of machine geometry and the magnetic properties of materials [Thomson et al. 1998, Omar et al. 2005, Faiz et al. 2009].

Advantages:

- Considers magnetic saturation.
- It is flexible in modeling irregular geometry.
- Easy handling of sparse matrices.

Disadvantages:

- Necessity of expensive tools (high C.P.U cost).
- Large memory requirement
- Requires high computing time

- Gives little information about line of faults.

(iii) Multiple coupled circuit approach: This is based on Kirchof's laws. Machines are modeled as having m-stator circuits and n-rotor bars. Models are drawn for healthy machines (under normal working conditions), and then faults in the rotor by breaks of the rotor bars and/or a break in the end ring segment are simulated using mesh equations. Magnetic saturation is neglected [Hamid et al. 1995, 1996, Omar et al. 2005,]. Air gap non uniformity is accounted while calculating the inductances between the stator phase and rotor bars.

Advantages:

- Simple Kirchof's laws are used.
- Asymmetrical faults can be incorporated.

Disadvantages:

- Neglects magnetic saturation.
- Neglects eddy current losses.

Model-based diagnosis requires the availability of some type of "model" of the process being diagnosed. The model must be accurate, though not too complicated. Present research work demands a machine model in which machine asymmetries can be incorporated. Modeling by abc-dq frame conversion method cannot be used because of its inability to model the machine air gap eccentricity. Coupled magnetic theory i.e Finite Element Method (FEM) or Multiple Coupled Circuit Approach are the methods suitable for the work. FEM demands an expensive tool to model the machine whereas Multiple Coupled Circuit Approach can be used to develop the model in easily available platform such as MATLAB. Hence Multiple Coupled Circuit Approach is chosen for modeling the machine.

.

2.1.1 Developments in the field of Winding Function Theory

In multiple coupled circuit method of modeling the machine, stator phases and rotor bars are represented as simple electric circuits consisting of inductances and resistances. Resistances are obtained by conducting suitable tests on the induction motor whereas inductances are calculated by using Winding Function Theory (WFT).

Hamid et al. (1995), Hamid et al. (1996), Nandi et al. (1998), Alfredo et

al.(1999) , Gojko et al. (2000), Faiz et al. (2003), have made use of WFT Equation(2.1) to calculate the inductances between two windings 'i' and 'j'.

$$L_{ij}(\theta_r) = \mu_0 \ell \int_0^{2\pi} r(\theta_r, \phi)\ g^{-1}(\theta_r, \phi)\ n_i(\theta_r, \phi)\ N_j(\theta_r, \phi)\ d\phi \qquad (2.1)$$

where μ_0 = Absolute permeability of the air gap

ℓ = Length of the stack in m

θ_r = Rotor angle in radians.

ϕ = Rotor circumferential angle in radians.

$r(\theta_r, \phi)$ = Average radius of air gap in non symmetrical conditions in m.

$g^{-1}(\theta_r, \phi)$ = Inverse air gap function in m^{-1}.

$n_i(\theta_r, \phi)$ = turn function of winding i

$N_j(\theta_r, \phi)$ =winding function of winding j and represents in effect the magneto motive flux distribution along the air gap for a unit current flowing in winding j.

Equation (2.1) makes use of both turn and winding functions of the windings. For non symmetrical air gap conditions prevailing in the machine, it is found that $L_{ij} \neq L_{ji}$.

In 1998, Nabil et al. have used a model for synchronous machine with dynamic eccentricity using Modified Winding Function Theory (MWFT). The main advantage of MWFT is that it makes use of only turn functions of the windings. The mutual inductance between the windings 'i' and 'j' is calculated using Equation (2.2).

$$L_{ij}(\theta_r) = \mu_0 \ell \int_0^{2\pi} r(\theta_r, \phi)\ g^{-1}(\theta_r, \phi)\ n_i(\theta_r, \phi)\ n_j(\theta_r, \phi)\ d\phi \qquad (2.2)$$

where

$$n_j(\theta_r, \phi) = N_j((\theta_r, \phi) - \frac{1}{2\pi\left\langle g^{-1}(\theta_r, \phi)\right\rangle} \int_0^{2\pi} N_j((\theta_r, \phi)\, g^{-1}(\theta_r, \phi)\, d\phi \qquad (2.3)$$

In 2002, Nandi et al. have made use of MWFT to calculate mutual inductance between two windings in induction motor and have proved that mutual inductance between two windings i,j and j,i are equal (i.e. $L_{ij}=L_{ji}$). These hold good for non-uniform air gap machines as long as the magnetic circuit is linear. Many researchers have made use of MWFT in their work as it can accommodate space harmonics, stator

and rotor slot harmonics [Nasiri et al. 2004, Nandi 2004, Hamidi et al. 2004].

In 2002, Faiz et al. have simplified the Equation (2.2) to calculate the inductance between two windings 'i' and 'j' and is given as

$$L_{ij} = 2\pi\mu_0 r\ell \left[\left\langle Pn_i n_j \right\rangle - \frac{\left\langle Pn_i \right\rangle \left\langle Pn_j \right\rangle}{\left\langle P \right\rangle} \right] \tag{2.4}$$

where $\left\langle f \right\rangle = \frac{1}{2\pi} \int_0^{2\pi} f(\theta)\, d\theta$ is the mean of function 'f 'over [0,2π] range.

P= Permeance of air gap in m^{-1}.

The author reports in the same paper, that the above equation has cumulative property i.e. $L_{ij}=L_{ji}$ and this property exists in linear magnetic circuits.

In most of the above mentioned works, the machine analysis is carried out assuming air gap uniformity down the axial length of the motor with skewing of the slots in the machine being ignored [Faiz et.al 2002,2003, Hamidi et al 2004]. Joksimovic et al. (1999), have considered the effect of skewing with the assumption that in any radial section of the machine, the mutual inductance per unit length is constant. i.e. the stator coil and a rotor loop has the same shape, but is displaced in space. In 2007, Xiadong et al. have accounted the effect of skewing in the rotor bars by incorporating a multiplying factor sin (hγ/2) where h=1,2,3……. in the turn function equations of the rotor loops. Ahmadian et al. (2007) have modeled the skew effect by simply considering each skewed bar into *n* (8) direct bars of equal length (rotor length/n) and each of these n parts are shifted by α_r/n . The turn function for i^{th} rotor bar defined by them is given as

$$\begin{aligned} n_j(\phi) &= \left(\frac{1}{\alpha_r} \right)\phi + (i-1) \qquad (i-1)\alpha_r < \phi < i\alpha_r \\ &= \left(-\frac{1}{\alpha_r} \right)\phi + (i+1) \qquad i\alpha_r < \phi < (i+1)\alpha_r \end{aligned} \tag{2.5}$$

where $\alpha_r=2\pi/n$, the angle between two rotor bars in radians, *n* is the number of rotor bars, ϕ is the circumferential angle of the rotor .

They have shown that skew reduces ripples in derivative of inductance and as a result in the electromagnetic torque as well.

Recently, focus is on the development of machine models which can take into account of the effect produced by the axial air-gap non-uniformity. In 2002,

Guillermo et al. have developed a 2-Dimensional model of induction motor, in which MWFT equation has been extended to the axial direction (z). The mutual inductance between two windings '*i*' and '*j*' for any rotor position θ_r and along the axial length *z* is calculated using 2D Modified Winding Function Theory (2D-MWFT) by the equation

$$L_{ij}(\theta_r) = \mu_0 \; r \int_0^{2\pi} \int_0^{\ell} n_i(\phi, z, \theta_r)\, N_j(\phi, z, \theta_r)\; g^{-1}(\phi, z, \theta_r)\, dz\, d\phi \tag{2.6}$$

where

$$n_j(\phi, z, \theta_r) = N_j(\phi,\ z, \theta_r) - \frac{1}{2\pi\ell \left\langle g^{-1}(\phi, z, \theta_r) \right\rangle} \int_0^{2\pi} \int_0^{\ell} N_j(\phi, z, \theta_r)\; g^{-1}\{\phi, z, \theta_r)\, dz\, d\phi \tag{2.7}$$

Main advantage of calculating inductance by 2D-MWFT is that it accounts both the effects of skewing of rotor bars and inclined eccentricity. In the year 2006, Ghoggal. et al. have made use of Equation (2.4) with some modifications which reduces the computational requirements significantly. The inductance is calculated as a function of $x_r (= r\,\theta_r)$ where *r* is the mean air gap radius and is given as

$$L_{ij}(x_r\} = 2\pi\, r\, \ell \mu_0 \left[\left[\sum_{x=1}^{qi} \sum_{y=1}^{pj} \left\langle Pn_{ix}\, n_{jy} \right\rangle \right] - \frac{\left\langle Pn_x \right\rangle \left\langle Pn_y \right\rangle}{\left\langle P \right\rangle} \right] \tag{2.8}$$

where 'qi' and 'pj' are the number of coils of winding '*i*' and '*j*' respectively.

In the model developed by them, average radius of the air-gap does not vary even in the presence of eccentricity. Good knowledge of coil distribution of stator phases is needed to develop the model. It is observed that there is no change in the mutual inductance magnitude between stator phase and rotor bar with or without skewing. However, its shape is smooth in presence of skew, mainly in region where inductance varies. It is also observed that shape of the derivative (with respect to rotor position) of mutual inductance waveform changes with skewing [Guillermo et al. 2002, Ghoggal et al. 2005, 2006].

As the air gap is non-uniform over the circumferential length of the rotor and also along the axial length of the rotor, permeance needs to be calculated for different rotor positions of the rotor along the axial length of the rotor to estimate the mutual inductance between rotor bar and stator phase. The permeance calculation for both healthy and eccentric machines is discussed in the next section.

2.1.2 Permeance calculation

For a healthy machine (without air gap eccentricity), permeance *P* is a constant and is given by

$$P = \frac{1}{g_0} \tag{2.9}$$

where g_0 is the air gap length under symmetrical conditions.

If the machine suffers from static rotor eccentricity, the effective air-gap function is [Toliyat et al. 1996]

$$P = g_0\left(1 - \delta_s \cos(\phi)\right) \tag{2.10}$$

In case of dynamic eccentricity, the effective air gap function is a function of rotor position θ_r also and is given as [Toliyat et al. 1996]

$$P = g_0\left(1 - \delta_d \cos(\phi - \theta_r)\right) \tag{2.11}$$

If both static eccentricity and dynamic eccentricity (mixed) are present, then effective air gap is defined as [Cameron et al. 1986]

$$P = g_0\left(1 - \delta_s \cos(\phi) - \delta_d \cos(\phi - \theta_r)\right) \tag{2.12}$$

Permeance is the inverse air gap function and can be obtained from the reciprocal of effective air gap. These equations are further modified to accommodate the air gap eccentricity in the axial direction.

2.2 Parameter identification to characterise the eccentricity fault and fault diagnostic techniques

Some of the machine quantities which get affected by the air gap non uniformity in the machine are air gap flux, stator current, vibrations, air gap torque, instantaneous power, instantaneous power factor, negative sequence current, and temperature. Condition monitoring units are used in the industrial drives to assess the health of the machine by continuously monitoring any one of these quantities. The variation or any change in these quantities from healthy condition to unhealthy condition can be used for fault detection. There are broadly two class of on line fault detection methods [Toliyat et al. 1996]:

(i) Model based fault diagnosis

(ii) Fault diagnosis through signature analysis of machine quantity.

In the following sections, both the methods are explained.

2.2.1 Model based diagnosis

By modeling and simulation methods, it is easier to identify the parameter to characterise any type of faults in the machine. It is also a cost effective and non-distructive method. Now days, model based behavioural studies for fault diagnosis are becoming popular. It has a two step procedure [Toliyat et al. 1996]

Step1: The actual behavior of the system, as manifested by the measured operating variables, is compared against the behavior by a model of the system, and residuals are generated which reflect the impact of faults.

Step2: The residuals are evaluated, and through a model-based inversion process, the faults that cause the observed behavior are identified.

Another method is to make use of the model to compare the parameter observed from the faulty machine with that of the parameter estimated from the healthy machine model. It can be represented as shown in the block diagram (Figure 2.1)

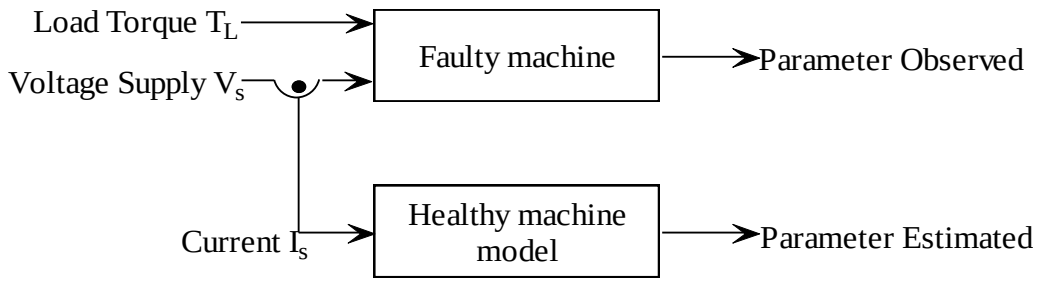

Figure 2.1 Principle of model based diagnosis

In 1992, Pattern et al. proposed this method to detect the fault in the machine. Thomas et al. (2003) have made use of similar method to detect rotor bar fault in the machine by observing air gap torque as the parameter. Torque is the parameter observed and estimated by them.

2.2.2 Fault diagnosis through signature analysis of machine quantity

Dorrell et al. 1995, Joksimovic et al. 2000, Nandi 2004, Ghoggal et al. 2006, Xiaodong et al. 2007, Thomson et al. 2009, Faiz et al. 2009, have used Motor Current Signature Analysis (MCSA) to detect either static eccentricity or dynamic eccentricity or both. The extensive study conducted by Nandi et al. on various asymmetrical fault

detection methods is published in the form as a review paper in 2005. Their findings in the area of MCSA based air gap eccentricity detection method are given below:

The air gap eccentricity characteristic frequency components f_e can be found by using Equation (2.13)

$$f_e = f_1\left[(kR \pm n_d)\frac{(1-s)}{p} \pm v\right] \tag{2.13}$$

where n_d=0 in case of static eccentricity and n_d=1,2,3…….in case of dynamic eccentricity (n_d is known as eccentric order), *R* is the number of rotor slots, *s* is the slip, *p* is the number of pole pairs, *k* is any integer and *v* is the stator harmonics that are present in the power supply driving the motor (v=±1,±3,±5), f_1 is the supply frequency in Hz.

Principal slot harmonics (PSH) can be seen only when *p* and *R* are related by Equation (2.14)

$$R = 2p[3(m \pm q) \pm r] \tag{2.14}$$

where m,q qnd r are constants and can be defined as m ± q = 0,1,2,3,…, r=0 or 1

Only a particular combination of machine pole pairs and rotor slot number will give rise to significant only static and only dynamic eccentricity related components and is given by

$$R = 2p[3(m \pm q) \pm r] \pm k \tag{2.15}$$

where, m±q=0,1,2,3,4…. and r=0 or 1

Although Equation (2.14) is valid for the most motors, Equation (2.15) is valid only for motors generating principal slot harmonics (PSH). The difference is because the additional pole pair rotor Magneto Motive Force (MMF) harmonics, which are produced by the MMF acting on the air gap between the stator and the rotor are different between the two types of motors.

If both static and dynamic eccentricities exist together in the machine, they produce low frequency components (also known as side band frequency components) near the fundamental given by Equation (2.16).

$$f_e = \left| f_1 \pm m f_r \right|, \qquad m = 1,2,3..... \tag{2.16}$$

where f_r is the rotor rotational frequency (rotor speed frequency) and is given as

$$f_r = N_r/60 = f_1((1-s)/p) \quad (2.17)$$

where N_r is the rotor speed in rpm, s is the slip and p is the number of pole pairs.

Equation (2.16) is valid for all combinations of pole pairs and rotor bars of the machine. These low frequency components also give rise to high frequency components as given by Equation (2.13). However, these components are strong for only those combinations of pole pairs p and rotor slot numbers R given by Equation (2.14) and Equation (2.15) with k=1.

Recently, multiple signature analysis is used for eccentricity detection. Xianodang et al. (2007) have analysed the performance of a 3 phase induction machine with inclined static eccentricity by both MCSA and vibration monitoring. Since MCSA did not produce strong signatures for faults that are substantial near the bearings but low on the average, they have made use of an accelerometer to detect the eccentricity in the machine. Randy et al. (2006) have also made use of multiple signatures to investigate static eccentricity in induction motors. They have used flux signal analysis, MCSA and vibration analysis to detect the static eccentricity fault in the machine and studied the effect of loading on the detection procedure. The characteristic eccentricity fault frequency component in the vibration signal can be found from using the equations listed in Table 2.1.

Table 2.1 Eccentricity Fault Frequency Equations [Randy et al. 2006]

Eccentricity Fault frequencies	**Eccentricity Types**	**Equation number**
$f_e = 2f_1 \pm f_r$	Dynamic, Static	(2.18)
$f_e = \text{vibration}_{rms}$	Dynamic, Static	(2.19)
$f_e = f_r$	Dynamic	(2.20)
$f_e = 2(f_1 \pm f_r)$	Dynamic	(2.21)
$f_e = 3f_r$	Static	(2.22)
$f_e = 2f_1$	Static	(2.23)

Other fault diagnostic methods used for air gap eccentricity detection include Instantaneous Power Signature Analysis [Drif et al. 2006], Instantaneous Power

Factor Signature Analysis [Drif et al. 2008], Torque Spectral Analysis [Kral et al. 2001]. Their spectrum contains eccentricity specific harmonic which appear at the following disturbance frequency

$$f_e = m f_r \quad \text{for} \quad m = 1 \tag{2.24}$$

The main advantage is that these spectra contain an air gap eccentricity specific harmonic which is far apart from the other harmonic components present in the spectrum and also provide simultaneous information about the current and voltage. Unlike MCSA, they produce an air gap characteristic harmonic at f_r independent of synchronous speed.

Fast Fourier Transforms (FFT) or Power Spectral Density (PSD) analysis is commonly used for frequency analysis to extract fault specific harmonics from the signals. FFT and PSD are the most commonly adopted frequency analysis tools for eccentricity detection by MCSA as stator current is considered to be stationary [Nandi et al. 1998, 2005, Joksimovie et al. 2000, Kral et al. 2001, Nandi 2004, Nandi et al. 2005, Chetwani et al. 2005, Ghoggal et al. 2005, 2006, Randy et al. 2006, Drif et al. 2006, 2008, Thomson et al. 2009, Faiz et al. 2009]. However in reality, stator current signals turn out to be non stationary as they are affected by power supply changes and load fluctuations. Hence, many researchers have introduced new techniques such as Short Time Fourier Transform (STFT), Wavelet Transform (WT), Wavelet Packet Transform (WPT) etc. to identify the eccentricity related frequency components in the stator currents [Hamidi et al. 2004, Antonino et al. 2006, 2007, Jordi et al. 2008, Gang et al. 2008, Guang-Ming et al. 2009]. Recently artificial intelligence methods such as Neural Networks, Fuzzy Logic and Genetic Algorithms are also used for asymmetrical fault detection in the machine [Siddique et al. 2005, Tian et al. 2005, Tan et al. 2007, Yaguo et al. 2007].

As the increase in the non uniformity of air gap is a very slow process, time information from the current signal is not of great concern in the asymmetrical fault detection process. As this study is conducted for the machine running under constant load conditions, investigation is restricted only to the fault diagnosis by Power Spectral Analysis (PSD analysis).

2.3 Creation of mixed eccentricity artificially in the machine

For experimental validation of the results obtained by the modeling and simulation, there is a need to create mixed eccentricity fault in the induction motor. Hence, extensive literature survey is conducted to study the various methods by which the researchers have artificially created air gap eccentricity in the induction motor.

Nandi et al. (1998), have introduced static eccentricity in the machine by machining the bearing housings of machine and the end bells. In the year 2002, Nandi et al. have created static eccentricity artificially in the machine by placing eccentric sleeves in the bearing housings of the end bells. Dynamic eccentricity is introduced by first building up on the shaft under bearings and then machining eccentrically. By displacing only one bearing with respect to stator geometric axis, inclined static eccentricity in the machine is created artificially by Guillermo et al. (2002). Static eccentricity is introduced in the machine by Long et al. (2005) by first machining the bearing housing of the end bell eccentrically and then placing a shim of 0.015" in the end bell to offset the rotor. By replacing the rotor bearings by a set of faulty bearings, a small level of eccentricity is created by Ghoggal et al. (2006).

Randy et al. (2006), have built a test motor as shown in Figure 2.2, which consists of custom built motor end plates which contain adjustable bearing housing. While conducting experimental investigations, the graduated screws in the air gap allow us to introduce static eccentricity.

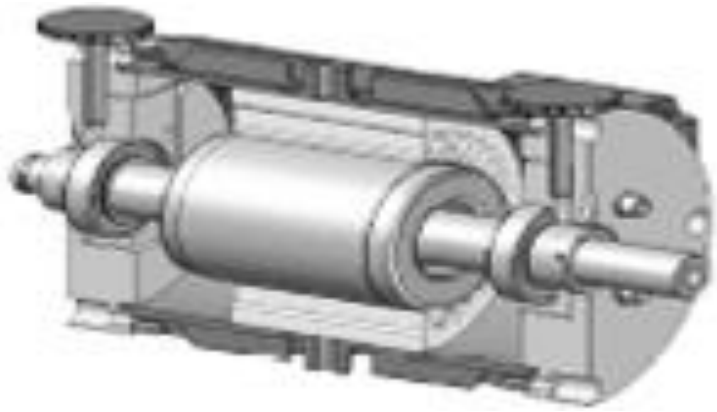

Figure 2.2 Test motor built by Randy et al. (2006)

Guillermo et al. (2006), have replaced one bearing by another of bigger interior diameter and of equal external diameter plus an eccentric bushing made of steel adopts the shaft diameter to the internal bearing diameter as shown in Figure 2.3.

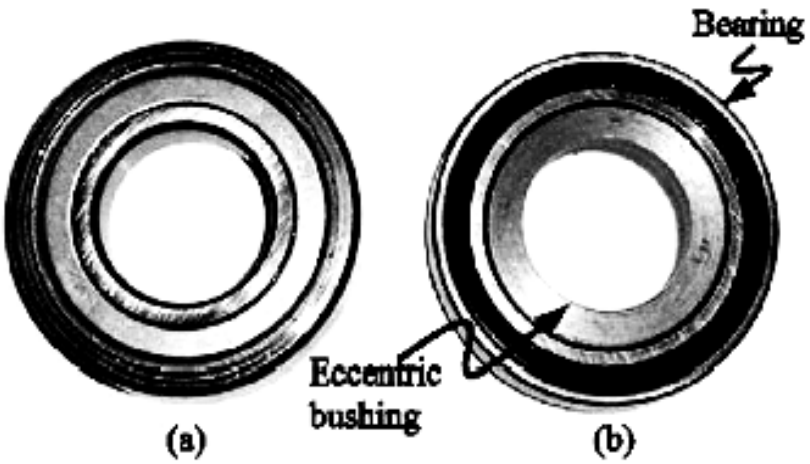

Figure 2.3 Creation of eccentricity (a) healthy bearing (b) eccentric bearing [Guillermo et al. 2006]

Xiaodong et al. (2007), have created eccentricity in the machine by placing eccentric sleeves with maximum eccentricity points marked on them. In order to create an inclined static eccentricity, they were put into the bearing housing with these points located diametrically opposite to one another.

Nandi et al. (2009) have created static eccentricity by using press fit eccentric cut sleeves in the end bells as shown in Figure 2.4.

Figure 2.4 End bell and end bell with eccentric sleeve inserted [Nandi et al. 2009]

Dynamic eccentricity is introduced by using eccentric cut rings between the bearing and the shaft. Eccentric cut rings and sleeves are as shown in Figure 2.5.

Figure 2.5 Eccentric Sleeve and rings used for creation of eccentricity [Nandi et al. 2009]

From the literature survey, it can be inferred that majority of the researchers have created eccentricity in the machine by altering the bearing structure.

The highlights of the literature survey are the following:

- Current is the primary quantity to get affected by the non uniformity of the air gap and many researchers have made use of it to characterise eccentricity fault in the machine.
- Even today motor current signature analysis is a very popular method used for eccentricity fault detection in the machine. They contain air gap eccentricity characteristic harmonics at ($f_1 \pm mf_r$) for m=1,2….
- Other signatures such as instantaneous power, power factor and torque signatures produce an air gap eccentric harmonic at f_r which is independent of synchronous speed.
- Multiple coupled circuit approach is a popular method used to model air gap eccentricity in the machine.
- The advantage of 2D-MWFT is that the motor can be modeled with inclined eccentricity (axial non uniformity).
- Air gap eccentricity can be created artificially in the machine by modifying either by the bearing structure or end bell structure.

From these inferences drawn from the literature survey, following research objectives were set forth:

- To investigate the feasibility of considering d-q components of stator currents as the parameter to diagnose the eccentricity in the machine as

– these components are flux and torque producing components in dq0 frame.

– its signature analysis can produce eccentricity characteristic component f_r in it.

– it makes use of only current transducers unlike other signature analysis which make use of both current and voltage transducers (power) or torque transducers (torque).

– it is cost effective.

– these components are already in use in motor control circuits

- A dynamic model of induction motor is to be developed using multiple couple circuit approach and 2D-modified winding function theory.
- Fabrication of an eccentric machine to validate the modeling-simulation results experimentally by adjusting the shaft alignment at the either ends of the motor.

In the next chapter, the details of development of the dynamic model of an induction motor using multiple coupled circuit approach are presented.

CHAPTER 3

3.0 MODELING OF INDUCTION MOTOR HAVING MIXED AIR GAP ECCENTRICITY

Model based behavioural studies of induction motor under faulted conditions help in characterising the faults by their unique signature. These studies help in characterisation of faults, as the parameter signatures of the healthy machine can be compared with those of an unhealthy machine. It also help in estimating certain parameters such as speed, torque etc in both healthy and unhealthy machines. In order to characterise the air gap eccentricity fault in the machine by modeling-simulation method, a robust dynamic model of induction motor is necessary which can accommodate the rotor eccentricity in it. Two popular approaches presently used for behavioural study are finite elements and equivalent circuit based asymmetrical machine modeling and simulation. In this chapter, the details of development of a dynamic model of an induction motor by equivalent circuit based asymmetrical machine modeling method is presented.

3.1 Dynamic model of induction motor by Multiple Coupled Circuit Approach for balanced supply

Multiple coupled circuit approach is very simple and it makes use of simple Kirchoffs laws. The following assumptions are made

Assumptions:

- Negligible saturation
- *m* identical stator windings with axes of symmetry
- *n* uniformly distributed cage bars or identical rotor windings with axes of symmetry such that even harmonics of the resulting spatial winding distributions are zero
- iron of infinite permeability which would facilitate the inclusion of MMF drop across the iron
- eddy current, friction, and windage losses are neglected
- insulated rotor bar

3.1.1 Stator model

The stator is viewed as having identical m (=3) circuits as shown in Figure 3.1.

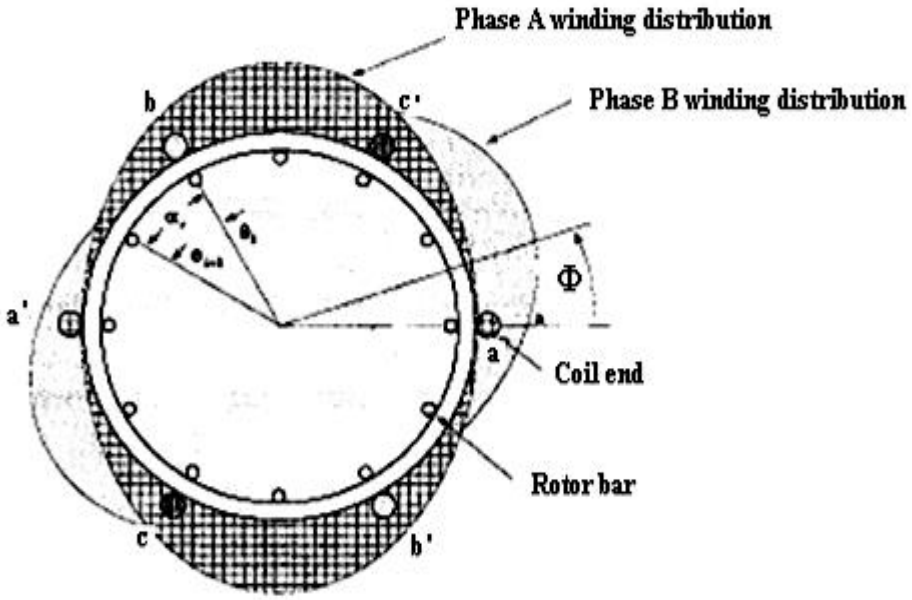

Figure 3.1 Stator circuit model [Alfredo et al. 1999]

Each phase is represented by its resistance and inductance.

3.1.2 Stator system voltage equations

The voltage equations for the stator loops can be written as, [Toliyat et al. 1995]

$$V_s = R_s I_s + \frac{d\lambda_s}{dt} \tag{3.1}$$

where the stator flux linkages λ_s, can be written as,

$$\lambda_s = L_{ss} I_s + L_{sr} I_r \tag{3.2}$$

where L_{ss} is a symmetric *m x m* stator inductance matrix given as

$$L_{ss} = \begin{bmatrix} L_{ls} + L_{ms} & -\frac{L_{ms}}{2} & -\frac{L_{ms}}{2} \\ -\frac{L_{ms}}{2} & L_{ls} + L_{ms} & -\frac{L_{ms}}{2} \\ -\frac{L_{ms}}{2} & -\frac{L_{ms}}{2} & L_{ls} + L_{ms} \end{bmatrix}$$

where L_{ls}= leakage inductance of the stator windings

L_{ms}= magnetizing inductance of the stator windings

The mutual inductance matrix L_{sr} is an *m x (n+1)* matrix comprised of the mutual inductances between the stator coils and the rotor loops.

Stator and rotor current vectors are defined as

$$I_s = [i_1^s \; i_2^s \; i_3^s \; .....i_m^s]^t$$

$$I_r = [i_1^r \; i_2^r \; i_3^r \; .....i_n^r \; i_e]^t$$

Stator voltage vector V_s is defined as

$$V_s = [v_a^s \; v_b^s \; v_c^s]^t$$

The stator resistance matrix R_s is a diagonal *m x m* matrix consists of resistances of each coil and is defined as

$$R_s = \begin{bmatrix} r_{s1} & 0 & 0 \\ 0 & r_{s2} & 0 \\ 0 & 0 & r_{sm} \end{bmatrix}$$

where r_{s1}, r_{s2}……r_{sm} are stator winding resistances.

3.1.3 Rotor model

The squirrel cage rotor can be viewed as n identical and equally spaced rotor loops as shown in Figure 3.2.

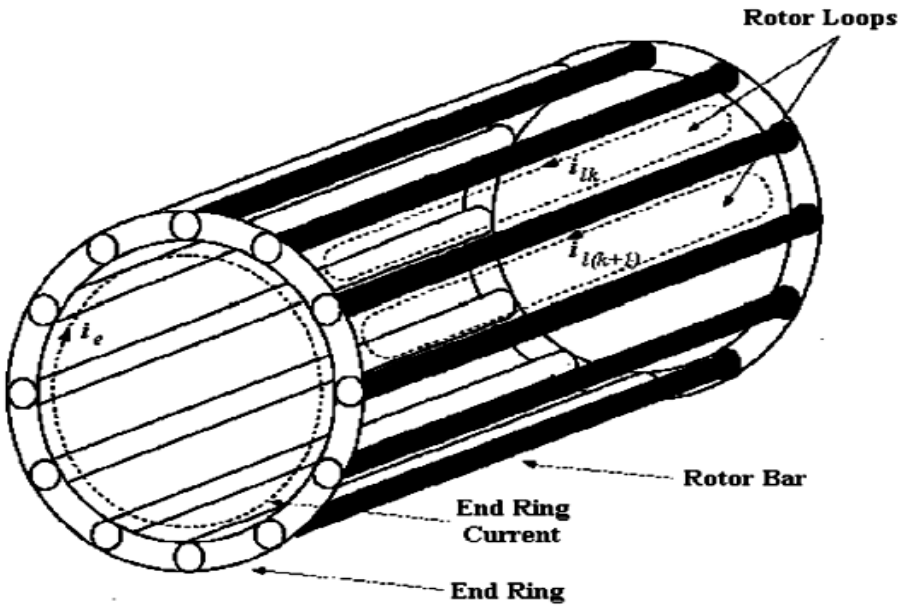

Figure 3.2 Elementary rotor loops and current definitions [Alfredo et al. 1999]

The rotor cage equivalent circuit is as shown in Figure 3.3.

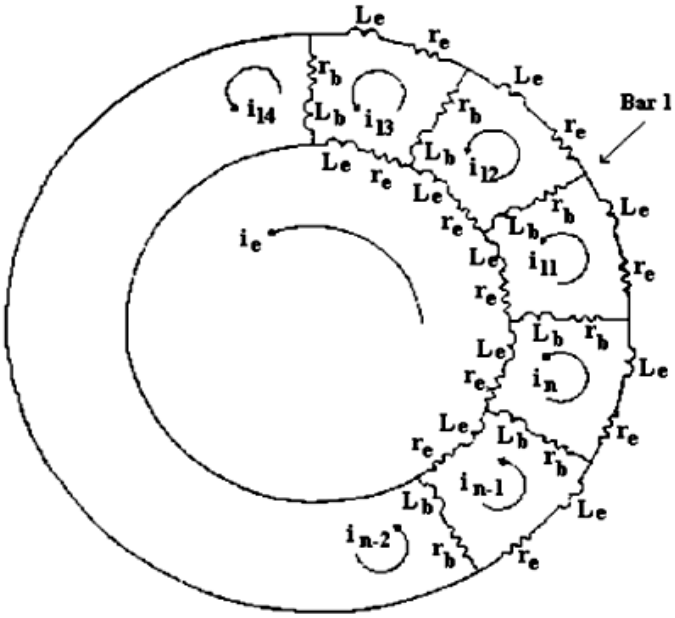

Figure 3.3 Rotor cage equivalent circuit [Toliyat et al. 1995, 1996]

The cage rotor can be viewed as *n* identical and equally spaced rotor loops. For a cage having *n* bars, there are *2n* nodes and *3n* branches. Therefore, the current distribution can be specified in terms of *n+1* independent rotor currents. These currents comprise of the *n* rotor loop currents and a circulating current in one of the end rings**.** Obviously, in a motor with complete end rings would be equal zero. The rotor loop currents are coupled to each other and to the stator winding, through the mutual inductances. However, the end ring loop current does not couple with the stator windings, and couples with the rotor loops currents only through the end ring leakage inductance and the end ring resistance.

3.1.4 Rotor system voltage equations

From Figure 3.3, the voltage equations [Toliyat et al. 1995] for the rotor loops are

$$V_r = R_r I_r + \frac{d\lambda_r}{dt} \tag{3.3}$$

where rotor voltage vector is defined as

$V_r = [0\ 0\ .....0]^t$, for a squirrel cage rotor

The rotor flux linkages λ_r, can be written as,

$$\lambda_r = L_{rs} I_s + L_{rr} I_r \tag{3.4}$$

where the matrix L_{rs} is the transpose of the matrix L_{sr} and represents the mutual inductance between rotor loops and stator windings.

The rotor inductance matrix L_{rr} is the *(n+l)* x *(n+l)* symmetric matrix and is given as

$$L_{rr} = \begin{bmatrix} L_{mr}+2(L_b+L_e) & L_{r1r2}-L_b & \ldots\ldots\ldots & L_{r1rn}-L_b & -L_e \\ L_{r2r1}-L_b & L_{mr}+2(L_b+L_e) & \ldots\ldots\ldots & L_{r2rn} & -L_e \\ . & . & & . & . \\ . & . & & . & . \\ . & . & & . & . \\ L_{r(n-1)r1} & L_{r(n-1)r2.} & \ldots\ldots\ldots & L_{r(n-1)rn}-L_b & -L_e \\ L_{rnr1}-L_b & L_{rnr2.} & \ldots\ldots\ldots & L_{mr}+2(L_b+L_e) & -L_e \\ -L_e & -L_e & \ldots\ldots\ldots & -L_e & nL_e \end{bmatrix}$$

where L_{mr}=magnetizing inductance of rotor loops

L_b=inductance of rotor bar

L_e=inductance of end ring segment

The rotor resistance matrix R_r is *(n+1)* x *(n+ 1)* symmetric matrix and given as

$$R_r = \begin{bmatrix} 2(R_b^{'}+R_e) & -R_b^{'} & 0 & \ldots\ldots\ldots & 0 & -R_b^{'} & -R_e \\ -R_b^{'} & 2(R_b^{'}+R_e) & -R_b^{'} & \ldots\ldots\ldots & 0 & 0 & -R_e \\ . & . & . & . & . & . & \\ . & . & . & . & . & . & \\ . & . & . & . & . & . & \\ 0 & 0 & 0 & \ldots\ldots\ldots & 2(R_b^{'}+R_e) & -R_b^{'} & -R_e \\ -R_b^{'} & 0 & 0 & \ldots\ldots\ldots & -R_b^{'} & 2(R_b^{'}+R_e) & -R_e \\ -R_e & -R_e & -R_e & \ldots\ldots\ldots & -R_e & -R_e & nR_e \end{bmatrix}$$

where R_e is the end ring segment resistance and $R_b^{'}$ is the rotor bar resistance.

3.1.5 Torque equations

The mechanical equation of motion is simply,

$$J\frac{d^2\theta_{rm}}{dt^2} + T_L = T_e \tag{3.5}$$

where T_L is the load torque in N-m, J is the moment of inertia in kg-m^2 and Te is the electromagnetic torque produced by the machine and is given by the expression

$$T_e = \left[\frac{\partial W_{co}}{\partial \theta_m}\right]_{(I_s, I_r \text{ constant})} \tag{3.6}$$

where W_{co} is the stored magnetic energy given as

$$W_{co} = \frac{1}{2}I_s^t L_{ss} I_s + \frac{1}{2}I_s^t L_{sr} I_r + \frac{1}{2}I_r^t L_{rs} I_s + \frac{1}{2}I_r^t L_{rr} I_r \tag{3.7}$$

θ_m is the rotor displacement in mechanical angle and the rotor mechanical speed is defined as,

$$\omega_m = \frac{d\theta_m}{dt} \tag{3.8}$$

where ω_{rm} is the rotor speed in radians/second.

θ_r is the rotor displacement in electrical radians and is given by

$\theta_r = p \times \theta_{rm.}$

Equations (3.1) to (3.8) are used to develop the dynamic model of the machine. These equations make use of stator phase resistances, rotor bar resistances, end ring resistances, stator phase leakage inductances, stator phase magnetizing inductances, rotor bar inductances, rotor end ring inductances and machine moment of inertia which are provided by the manufacturer of the machine. The mutual inductances between the stator phases, rotor bars and between stator phase and rotor bar needs to be calculated, the details of which are presented in the section to follow.

3.1.6 Calculation of inductances

Two Dimensional Modified Winding Function Theory (2D-MWFT) is used to calculate the inductance along the axial length of the rotor. In an air gap inclined eccentric machine, the inductance value varies along axial length of the rotor for different rotor positions. Skewing of rotor bars also can be considered while defining the turn function for the rotor bars. Hence 2D-MWFT equation is used in this research work to calculate inductance between stator phase and rotor bars, between rotor bars,

and between stator phases. The inductances computed are as functions of rotor position (θ_r), rotor circumferential angle (ϕ) and rotor axial length (z).

Consider the skewed rotor as shown in Figure 3.4

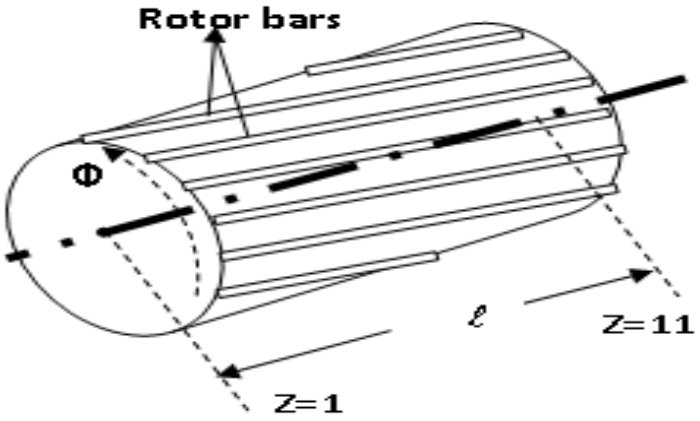

Figure 3.4 Skewed rotor

Basic 2D-MWFT equation to calculate the mutual inductance between windings 'i' and 'j' is given by Equation (3.9) [Guillermo et al. 2002]

$$L_{ij}(\theta_r) = \mu_0 r \int_0^{\ell} \left[\int_0^{2\pi} n_i(\phi, z, \theta_r)\, n_j(\phi, z, \theta_r)\, g^{-1}(\phi, z, \theta_r)\, d\phi \right] dz \qquad (3.9)$$

where θ_r - angular position of the rotor with respect to some reference

Φ - particular position along the stator inner surface

$g^{-1}(\Phi,,z,\theta_r)$, P - inverse effective air-gap function, permeance,

$P=1/g_0$ a constant for uniform air-gap

l - length of the stack

r - average radius of the air-gap

$n_i(\Phi,,z,\theta_r)$ - winding distribution of winding i, turn function

$n_j(\Phi,z,\theta_r)$- winding distribution of winding j, turn function

Numerical integration method is used to calculate the inductances between two windings. The air gap between the rotor and stator along the axial length ℓ of the

motor is divided into 10 sections of equal length (11 points). For each section (z), the inductances are calculated for a given rotor position (θ_r) over the circumferential length of the stator (Φ) using Equation (3.10).

$$L_{ij}(\theta_r, z) = 2\pi\mu_0 r\left[\left\langle Pn_i n_j\right\rangle - \frac{\left\langle Pn_i\right\rangle\left\langle Pn_j\right\rangle}{\left\langle P\right\rangle}\right] \text{ x } \frac{\ell}{10} \tag{3.10}$$

The sum of all the section's inductance for a given value of rotor position 'θ_r' gives the mutual inductance between the two windings (say rotor loop and stator phase) and calculated as

$$L_{ij}(\theta_r) = \sum_{z=1}^{z=11} L_{ij}(\theta_r, z) \tag{3.11}$$

The winding layout of the machine is as shown in Figure 3.5. The machine selected for analysis has a single layer, 24 slot stator winding.

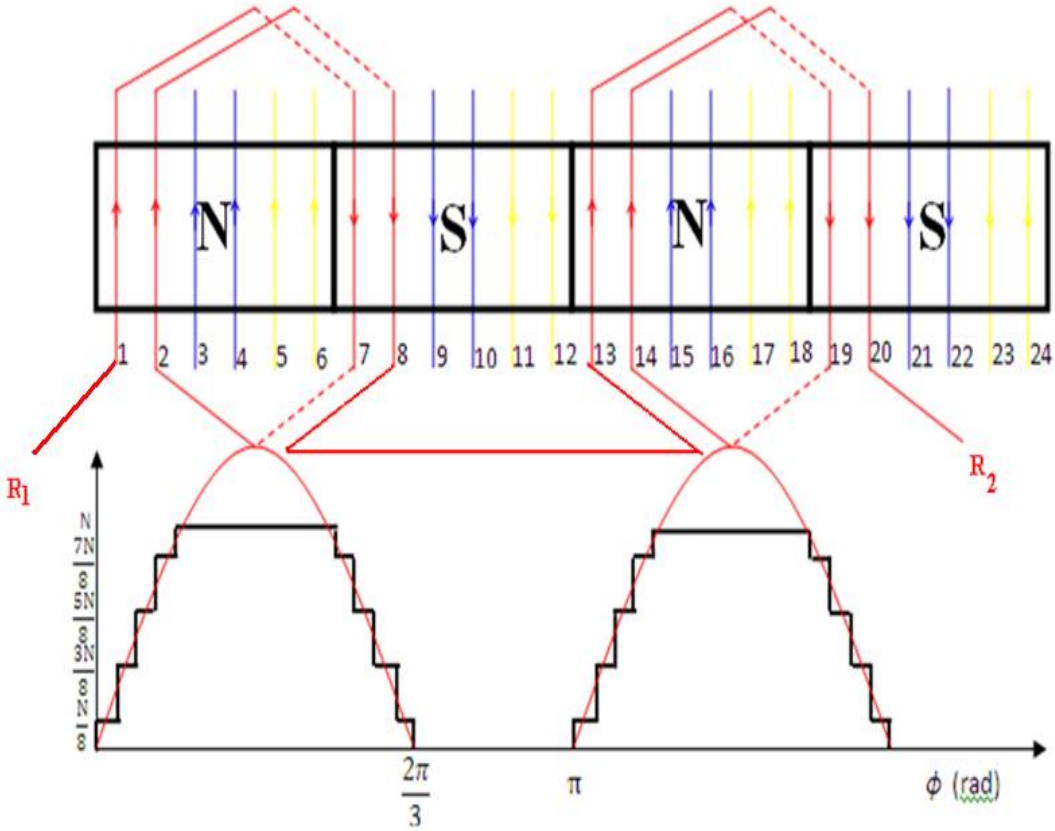

Figure 3.5 Winding layout of the machine

where N is the number of turns/coil

The stator phase ‘A’ turn function and rotor loop1 turn function are defined as given in Figure 3.6.

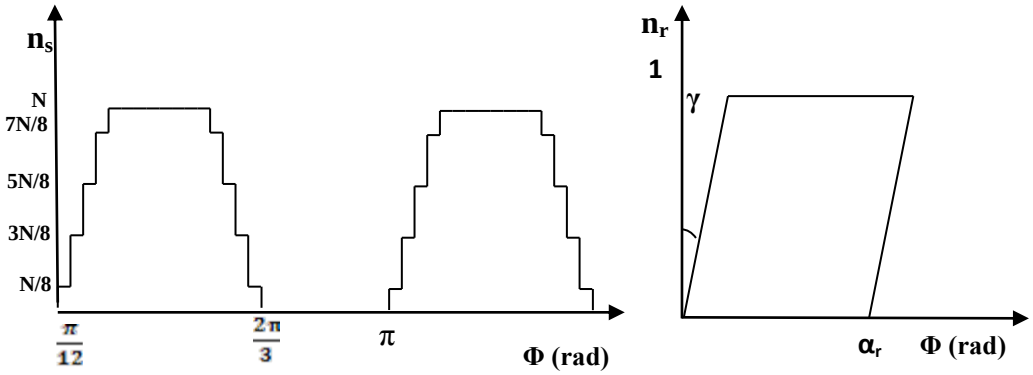

Fig 3.6 (a) Fig 3.6 (b)

Figure 3.6 (a) Stator phase A turn function (b) rotor loop 1 turn function

The turn function for rotor loop1 is defined by an equation which can account for the skewing of rotor bars. Consider the rotor loop1 turn function which is divided into three regions R_1, R_2 and R_3 as shown in the Figure 3.7.

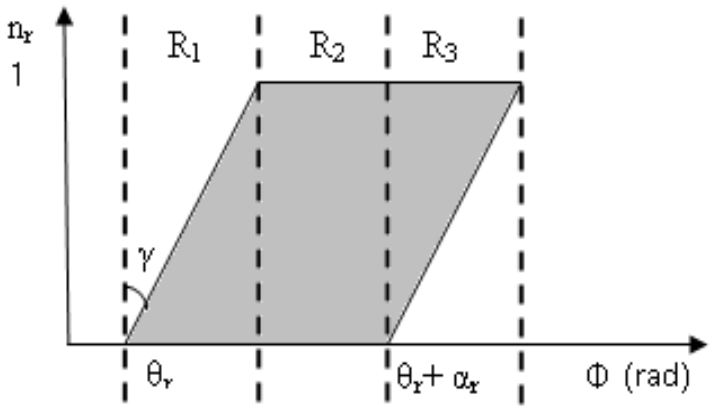

Figure 3.7 Turn function for a rotor loop1 for the rotor having skewing angle γ

Skewing angle of rotor bars γ in the model is accounted by defining the turn function of the rotor loop1 by the Equation 3.12.

For Region R_1, $0 \le \phi \le \ell \tan(\gamma)$

$$n(\phi, z, \theta_r) = 1 \qquad 0 \le z \le \left(\frac{\phi}{\tan(\gamma)}\right) r$$

$$= 0 \qquad \left(\frac{\phi}{\tan(\gamma)}\right) r \le z \le \ell$$

For Region R_2, $\ell \tan(\gamma\gamma \le \varphi \le \alpha_r$

$$n(\phi, z, \theta_r) = 1 \qquad (3.12)$$

For Region R_3, $\alpha_r \le \phi \le \alpha_r + \ell \tan(\gamma)$

$$n(\phi, z, \theta_r) = 0 \qquad 0 \le z \le \left(\frac{\phi - \alpha_r}{\tan(\gamma)}\right) r$$

$$= 1 \qquad \left(\frac{\phi - \alpha_r}{\tan(\gamma)}\right) r \le z \le \ell$$

The stator turn functions for the other two phases B and C are obtained by shifting the stator turn function by 60° and 120° degrees respectively. The turn functions for other rotor loops are obtained by shifting the turn function of rotor loop1 by $\alpha_r i$ where i=1,2,….n, where $\alpha_r = 2\pi/n$.

To calculate the mutual inductances, the permeance of the air gap for every rotor position needs to be calculated. The following section gives details about the permeance calculation along the axial length of the rotor for different rotor positions.

3.1.7 Permeance calculation for air gap eccentric machine

Non uniform air gap gives rise to air gap eccentricity. Air gap eccentricity results in non uniform distribution of flux in the air gap and can be accounted by modifying the permeance equation. The permeance *P* is calculated using the Equation 3.13 [Ghoggal et al. 2006].

$$P(\phi, z, \theta_r) = P_0(z) + P_1(z)\cos(\phi - \rho(z)) + P_2(z)\cos(2\phi - 2\rho(z)) \ldots\ldots\ldots\ldots \qquad (3.13)$$

where P_0, P_1, P_2 and ρ are given by

$$P_0(z) = \frac{1}{g_0}$$

$$P_1(z) = 2\left[\frac{1}{g_0\sqrt{1-\delta^2(z))}}\right]\left[\frac{(1-\sqrt{1-\delta^2(z)}}{\delta(z)}\right]$$

$$P_2(z) = 2\left[\frac{1}{g_0\sqrt{1-\delta^2(z))}}\right]\left[\frac{(1-\sqrt{1-\delta^2(z)}}{\delta(z)}\right]^2$$

$$\rho(z) = \tan^{-1}\left(\frac{\delta_d(z)\sin(\theta_r)}{\delta_s(z)+\delta_d(z)\cos(\theta_r)}\right)$$

$$\delta(z) = \sqrt{\delta_s^2(z)+\delta_d^2(z)+2\delta_s(z)\delta_d(z)\cos(\theta_r)}$$

For derivation of permeance equation, refer Appendix II.

In case of inclined static eccentricity condition, static eccentricity level will not remain constant along the rotor axial length. Its variation along the rotor axial length is given by the expression [Guillermo et al. 2002]

$$\delta_s(z) = \delta_{s0} + k\,z \tag{3.14}$$

where δ_{s0}= the static eccentricity index at one end of the machine.

k = the slope with which the rotor is inclined.

Thus the developed dynamic model of the machine has the following features

(i) Skewing of the rotor bar can be accounted

(ii) Asymmetrical faults can be accounted.

(iii) Both uniform and inclined static eccentricity can be incorporated.

(iv) Mixed eccentricity fault can be considered.

Non uniform air gap in the machine leads to non uniform distribution of the flux in the air gap. The stator current is the primary quantity to get affected by this non uniform flux in the air gap. Non uniform distribution of flux introduces harmonics in the stator currents. As d-q components are extracted from the stator currents, they also will contain eccentricity characteristic harmonics in them. In the next section mathematical expressions are derived for d-q components of stator currents to find the air gap eccentricity specific frequency components in them.

3.2 Mathematical expressions for d-q components of stator currents

Induction motor is used as a variable speed drive in many industrial applications. Recent advances in power electronic fields and the DSP technology have helped to design fast, reliable and cost effective controllers for induction motors. One can get the control characteristic similar to that of separately excited DC machine, by modeling the machine in a synchronously rotating reference frame. The main advantage is that all the sinusoidal variables appear as DC quantities. The added advantage of conversion to synchronous reference d-q frame is that all the harmonics present in the current due to inverter and the load are transformed into oscillations. In this section, it is shown that the presence of both static and dynamic (mixed) air gap eccentricity prevailing in the machine can also cause oscillations in the d-q components of stator currents.

3.2.1 Mathematical Expressions for d-q components of stator currents of an induction motor suffering from air gap eccentricity fault.

A dynamic model for the three phase induction motor can be derived from the two phase machine based on the equality of the MMF produced in the two phase and three phase windings and equal current magnitudes. Alfredo et al. (1999), have exploited the theory that the sinusoidal coupling between the stator and rotor circuits can be eliminated by referring all the equations to a common reference frame and have presented an equivalent circuit based on arbitrary d-q reference frame rotating at angular speed ω. The required d-q variables in this common reference frame are defined by the vector transformations as

$$i_{qds} = 2/3 e^{-j\theta} i_s \tag{3.15}$$

where $i_{qds}=[i_{qs}\ i_{ds}\ i_{0s}]^t$, where i_{qs}, i_{ds} and i_{0s} are q-axis, d-axis and zero sequence components of stator currents, $i_s=[i_{as}\ i_{bs}\ i_{cs}]^t$ where i_{as}, i_{bs} and i_{cs} are stator phase currents and θ is an arbitrary angle.

If $\theta=\omega_s t$ (in synchronously rotating reference frame and $\omega_s=2\pi f_1$ where f_1 is the fundamental frequency), then i_{qs} and i_{ds} are defined as

$$i_{qs} = 2/3\,[\cos(\omega_s t)\, i_{as} + \cos(\omega_s t - 2\pi/3)\, i_{bs} + \cos(\omega_s t + 2\pi/3)\, i_{cs}] \quad (3.16)$$

$$i_{ds} = 2/3\,[\sin(\omega_s t)\, i_{as} + \sin(\omega_s t - 2\pi/3)\, i_{bs} + \sin(\omega_s t + 2\pi/3)\, i_{cs}] \quad (3.17)$$

The presence of both static and dynamic eccentricity (mixed) in the machine can be detected by the presence of side band frequency components around base frequency (f_1) using Motor Current Signature Analysis (MCSA) [Nandi et al. 2005]. The equation to extract the side band frequency components from current is given by

$$f_e = |f_1 \pm m f_r|, \qquad m = 1,2,3..... \quad (3.18)$$

where f_r is the rotor frequency and is given as

$$f_r = N_r/60 = f_1\,((1-s)/p) \quad (3.19)$$

where N_r is the rotor speed in rpm, s is the slip and p is the number of pole pairs.

These low frequency components can give rise to high frequency components and can be detected by using (3.20) [Nandi et al. 2005].

$$f_e = f_1\left[(kR \pm n_d)\frac{(1-s)}{p} \pm v\right] \quad (3.20)$$

where n_d=0 in case of static eccentricity and n_d=1,2,3…….in case of dynamic eccentricity (n_d is known as eccentric order, R is the number of rotor slots, s is the slip, p is the number of pole pairs, k is any integer and v is the stator harmonics that are present in the power supply driving the motor (v=±1,±3,±5).

However, these components are strong only for machines whose pole pairs p and rotor slot numbers R are related by Equations (3.21) and (3.22)

$$R = 2p[3(m \pm q) \pm r] \pm k \quad (3.21)$$

$$R = 2p[3(m \pm q) \pm r] \quad (3.22)$$

where, m±q=0,1,2,3,4…. and r=0 or 1, k=1 .

It is been reported in the literature that with k=2, these components are found to be very weak and noticeable only under light load conditions [Nandi et al. 2005].

For the machine (whose parameters are defined in Appendix I) chosen for the analysis has number of rotor bars, R=30, pole pairs p=2

$$R = 30 = 2\,x\;2\left[3x3-1\right]-2 \qquad \text{with } (m \pm q) = 3$$
$$R = 30 = 2\,x\;2\left[3x2+1\right]+2 \qquad \text{with } (m \pm q) = 2$$

Since Equation (3.21) is valid only for k=2, the high frequency components in the current signature will be very weak and noticeable only under light load conditions. Hence, only low frequency components defined by the Equation (3.18) is considered for further analysis.

Assuming m=1,2,3 in Equation (3.18), with all higher eccentricity related characteristic harmonic components being neglected, three phase currents i_{abc} are defined by taking i_{as} as reference.

$$\begin{aligned} i_{as} &= I_1\sin(2\pi f_1 t - \phi_1) + I_2\sin[2\pi(f_1 - f_r)t - \phi_2] + I_3\sin[2\pi(f_1 + f_r)t - \phi_3] + \\ &\quad I_4\sin[2\pi(f_1 - 2f_r)t - \phi_4] + I_5\sin[2\pi(f_1 + 2f_r)t - \phi_5] + I_6\sin[2\pi(f_1 - 3f_r)t - \phi_6] + \\ &\quad I_7\sin[2\pi(f_1 + 3f_r)t - \phi_7] \end{aligned}$$

$$\begin{aligned} i_{bs} &= I_1\sin[(2\pi f_1 t) - 2\pi/3 - \phi_1] + I_2\sin[2\pi(f_1 - f_r)t - 2\pi/3 - \phi_2] + \\ &\quad I_3\sin[2\pi(f_1 + f_r)t - 2\pi/3 - \phi_3] + I_4\sin[2\pi(f_1 - 2f_r)t - 2\pi/3 - \phi_4] + \\ &\quad I_5\sin[2\pi(f_1 + 2f_r)t - 2\pi/3 - \phi_5] + I_6\sin[2\pi(f_1 - 3f_r)t - 2\pi/3 - \phi_6] + \\ &\quad I_7\sin[2\pi(f_1 + 3f_r) - 2\pi/3 - \phi_7] \end{aligned} \qquad (3.23)$$

$$\begin{aligned} i_{cs} &= I_1\sin[(2\pi f_1 t) + 2\pi/3 - \phi_1] + I_2\sin[2\pi(f_1 - f_r)t + 2\pi/3 - \phi_2] + \\ &\quad I_3\sin[2\pi(f_1 + f_r)t + 2\pi/3 - \phi_3] + I_4\sin[2\pi(f_1 - 2f_r)t + 2\pi/3 - \phi_4] + \\ &\quad I_5\sin[2\pi(f_1 + 2f_r)t + 2\pi/3 - \phi_5] + I_6\sin[2\pi(f_1 - 3f_r)t + 2\pi/3 - \phi_6] + \\ &\quad I_7\sin[2\pi(f_1 + 3f_r)t + 2\pi/3 - \phi_7] \end{aligned}$$

where I_1, I_2, I_3, I_4, I_5, I_6, I_7 being the peak magnitude of currents and Φ_1 , Φ_2 , Φ_3 , Φ_4 , Φ_5, Φ_6, Φ_7 being the phase angles corresponding to frequencies f_1, f_1-f_r, f_1+f_r , ,f_1-$2f_r$, f_1+$2f_r$, f_1-$3f_r$ and f_1+$3f_r$ respectively.

Currents in three phase form i_{abc} are transformed into two phase form i_{qd0} in Synchronous Reference Frame ($\omega_s=2\pi f_1$) using Equations (3.16) and (3.17)**.** The expressions for i_{qs} and i_{ds} are given by the Equations (3.24) and (3.25) respectively.

$$i_{qs} = -I_1\sin(\phi_1) + I_2\sin(2\pi f_r t - \phi_2) - I_3\sin(2\pi f_r t + \phi_3) + I_4\sin(4\pi f_r t - \phi_4) - I_5\sin(4\pi f_r t + \phi_5) + I_6\sin(6\pi f_r t - \phi_6) - I_7\sin(6\pi f_r t + \phi_7) + \ldots\ldots \quad (3.24)$$

$$i_{ds} = I_1\cos(\phi_1) + I_2\cos(2\pi f_r t - \phi_2) + I_3\cos(2\pi f_r t + \phi_3) + I_4\cos(4\pi f_r t - \phi_4) + I_5\cos(4\pi f_r t + \phi_5) + I_6\cos(6\pi f_r t - \phi_6) + I_7\cos(6\pi f_r t + \phi_7) + \ldots\ldots \quad (3.25)$$

From (3.24) and (3.25), it is inferred that both i_{qs} and i_{ds} currents contain eccentricity related characteristic components mf_r where m=1,2,3…..

In case of a machine suffering from mixed air gap eccentricity, they no longer remain as pure DC quantities; they contain harmonics due to air gap eccentricity. In the presence of air gap eccentricity induced harmonics, the currents i_{qs} and i_{ds} appear as DC components but superimposed with oscillations. The presence of these harmonics in d-q components of currents can be exploited to detect the severity of air gap eccentricity in the machine.

3.3 Block diagram of the developed model

Using the equations given in this chapter, the dynamic model of an eccentric machine is developed. The overall block diagram of the machine model is as shown in Figure 3.8.

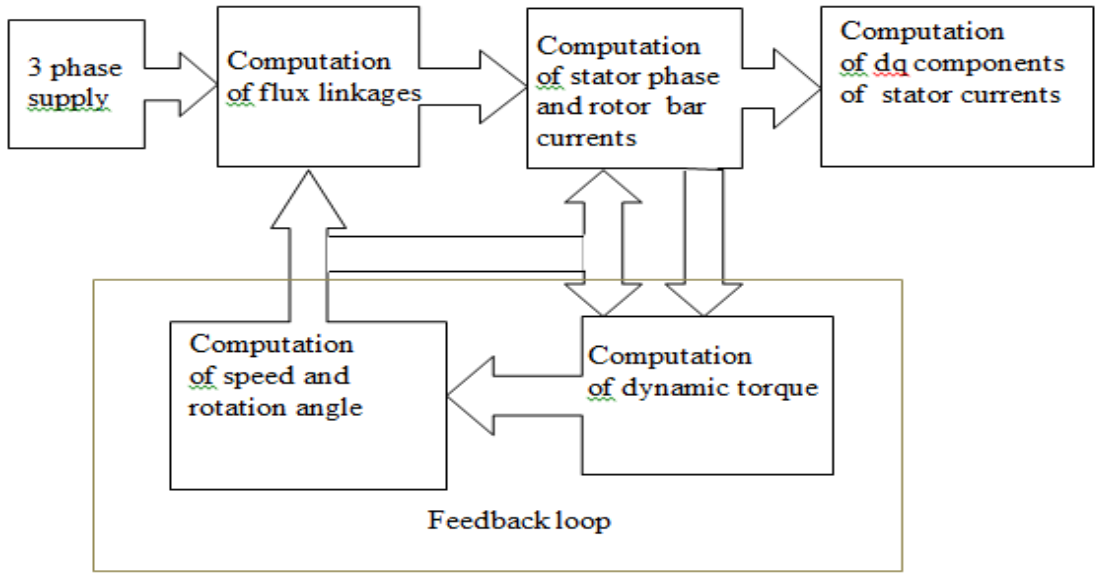

Figure 3.8 Computation sequence in modeling

The model is developed in SIMULINK / MATLAB and block diagrams are given in Appendix III.

In this chapter, the details of development of machine model are presented. The mathematical expressions are derived for d-q components of stator currents drawn from an induction motor suffering from mixed eccentricity condition. From the derived expressions, it is concluded that they contain harmonics which are multiples of rotor speed frequency. The developed machine model is simulated for different operating conditions and obtained results are discussed in the following chapter.

CHAPTER 4

4.0 EVALUATION OF MOTOR MODEL

The dynamic model of the induction motor developed in Chapter 3 has the ability to simulate both uniform axial eccentricity and inclined eccentricity conditions. The developed model is simulated for different conditions of the air gap using the machine parameters as given in Appendix I. This Chapter presents the simulation results obtained from simulating the dynamic machine model developed for different eccentricity conditions.

4.1 Permeance variation with circumferential length of rotor

The non uniformity in the air gap is taken into account in the model by using Equation (3.13). For uniform axial eccentricity, the mixed eccentricity level does not change along axial length of the rotor. The permeance is calculated for uniform axial eccentricity conditions for different mixed eccentricity conditions and is compared with that of healthy condition. The variation of permeance over different circumferential angles for different eccentric conditions is as shown in Figure 4.1.

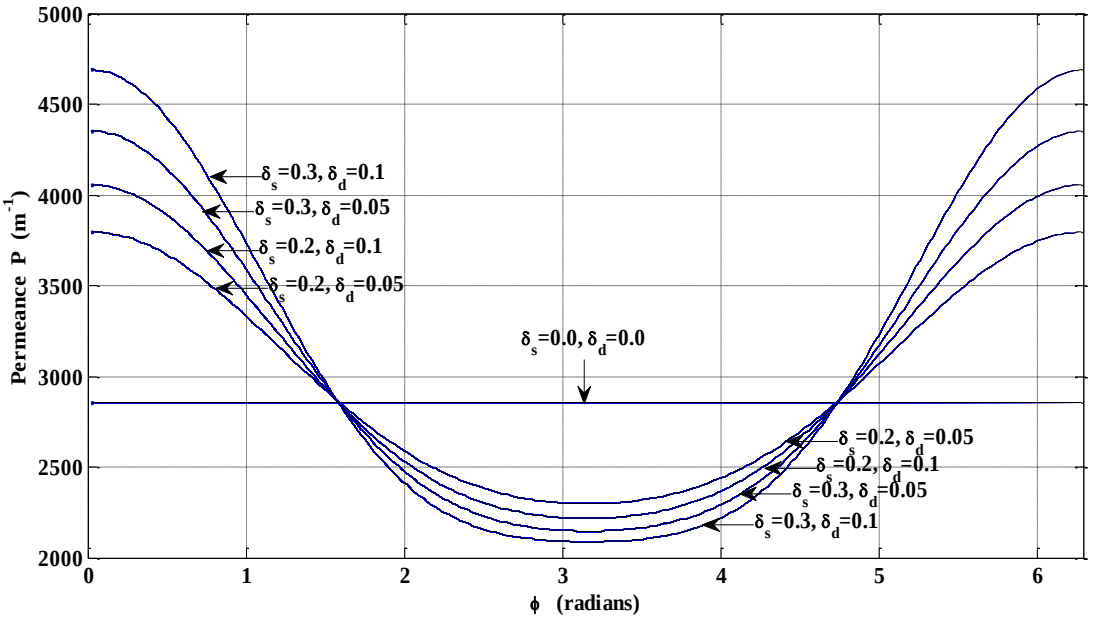

Figure 4.1 Variation of permeance for different mixed eccentricity conditions δ_s-static eccentricity index, δ_d-dynamic eccentricity index

*Refer Sections 3.1.6 and 3.1.7 for equation for calculation of Permeance.

From Figure 4.1, following observations are made

- Permeance remains constant for healthy machine at $1/g_0$.
- All the permeance curves meet at $\phi=\pi/2$ and $\phi= 2\pi-\pi/2$.
- The permeance increases with the increase in the mixed eccentricity level for rotor circumferential angle positions $0 <\phi<\pi/2$ and $\phi > (2\pi- \pi/2)$.
- It decreases with the increase in mixed eccentricity level for the rotor circumferential angle positions $\pi/2 <\phi< 2\pi-\pi/2$.

The permeance variation waveforms obtained is similar to those reported by Faiz et al. (2003).

In case of inclined eccentricity, mixed eccentricity level changes because the static eccentricity varies along the axial length of the rotor as described by the Equation (3.14). In the model, rotor axial length is divided into 11 sections and for each section permeance is calculated. Variation of permeance along rotor length over the rotor circumferential angle for the machine suffering from inclined eccentricity condition of static eccentricity of 0% at one rotor end ($\delta_{s0}=0$) and 30% on the other end ($\delta_{s1}=0.3$) is shown in Figure 4.2. The machine also suffers from 10% dynamic eccentricity ($\delta_d=0.1$).

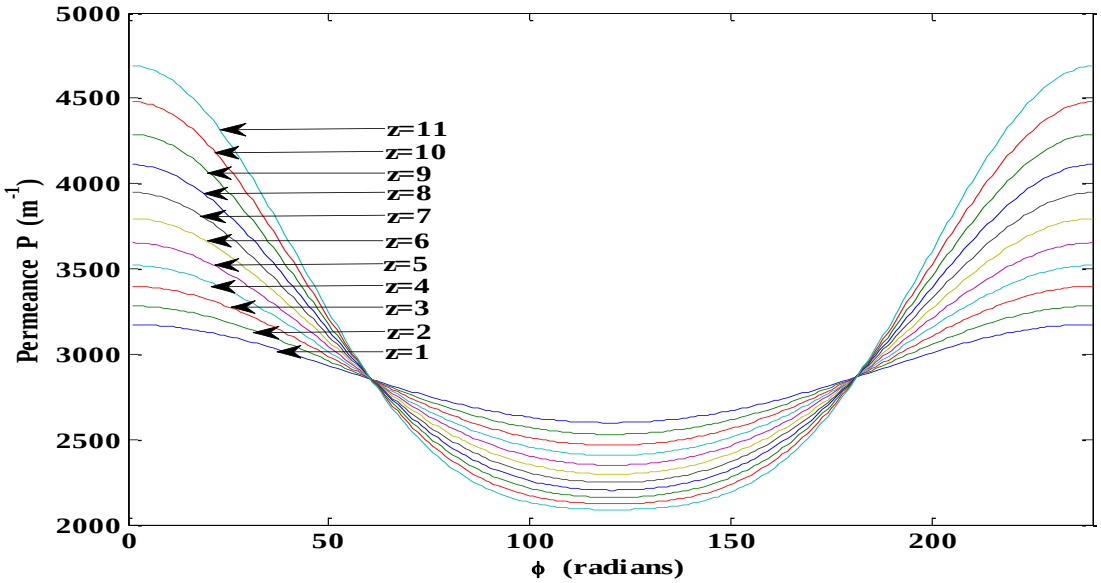

Figure 4.2 Variation of permeance for different sections along the axial length of the rotor over the rotor circumferential angle

*Refer Sections 3.1.6 and 3.1.7 for equations used to plot the curves

From Figure 4.2, following observations are made

- All the permeance curves meet at $\phi=\pi/2$ and $\phi= 2\pi-\pi/2$.
- The permeance increases with the increase in the static eccentricity level along the rotor axial length for the rotor circumferential angle $0 < \phi < \pi/2$ and $\phi > (2\pi- \pi/2)$.
- It decreases with the increase in mixed eccentricity level for the rotor circumferential angle $\pi/2 < \phi < 2\pi-\pi/2$.

The three dimensional view of the variation of permeance over the rotor circumferential angle for different sections along the axial length of the rotor of the machine having inclined eccentricity i.e. $\delta_{s0}=0$, $\delta_{s1}=0.3$, $\delta_d=0.1$ is shown in Figure 4.3.

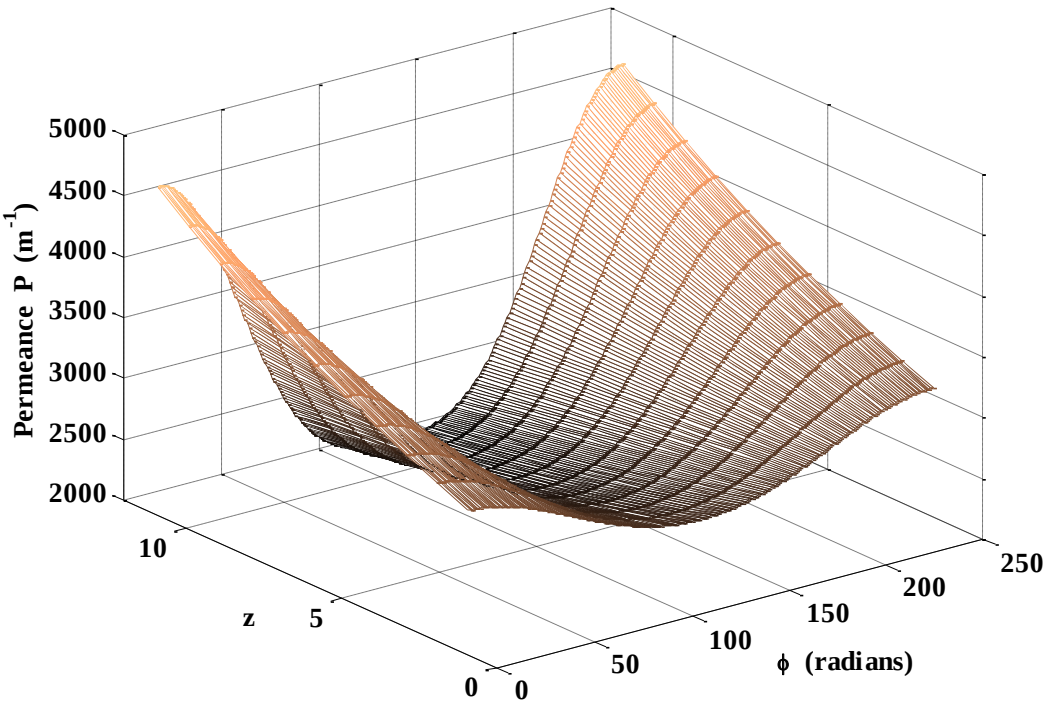

Figure 4.3 3Dimensional View of variation of permeance along the rotor length over the rotor circumferential angle

From the above figure, it can be deduced that in case of axial non uniformity conditions prevailing in the machine, the magnitude of permeance varies along the axial length of the rotor.

4.2 Inductance variation with rotor position

Most of the machines have skewed rotor slots. The rotor slots are skewed to get uniform torque, reduce the magnetic locking (also called cogging effect) between stator and rotor, and thirdly to reduce the magnetic humming noise during running condition. To study the effect of skewing of rotor slots on the mutual inductance between stator phase A and rotor loop1, the healthy machine model is simulated for the following two conditions

- Without skewing of rotor bars.
- With skewing of rotor bars

The simulation results are compared to study the effect of skewing on mutual inductance between stator phase A and rotor bar1. Variation in mutual inductance between stator phase A and rotor loop1 for different rotor position angle θ_r with and without the consideration of skewing angle is as shown in Figure 4.4

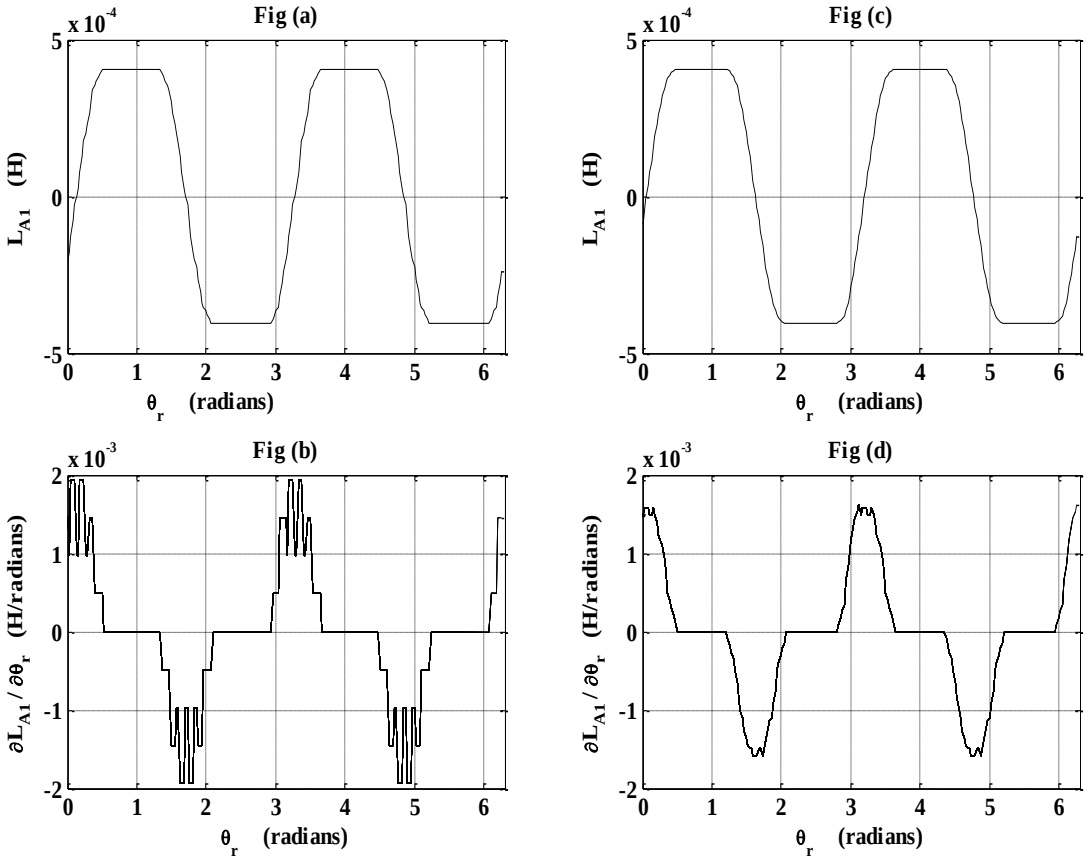

Figure 4.4 Variation of mutual inductance between stator phase A and rotor loop1 and its derivative: Fig (a) and (b) without skewing Fig (c) and (d) with skew (5°)

From Figure 4.4, the following observations are made

- There is no change in the mutual inductance magnitude and remains the same in both cases with and without skewing of rotor bars.
- The slope is smooth in the presence of the skew, mainly in the region where the inductance varies and can be seen very clearly in their derivative plots.

The model is simulated for healthy conditions of the motor for various skewing angles of the rotor bars. 3D plots of the simulated mutual inductance between the stator phase A and rotor bar 1 along the axial length of rotor for skewing angles $\gamma=0^{\circ},5^{\circ},9^{\circ}$ are shown in Figure 4.5.

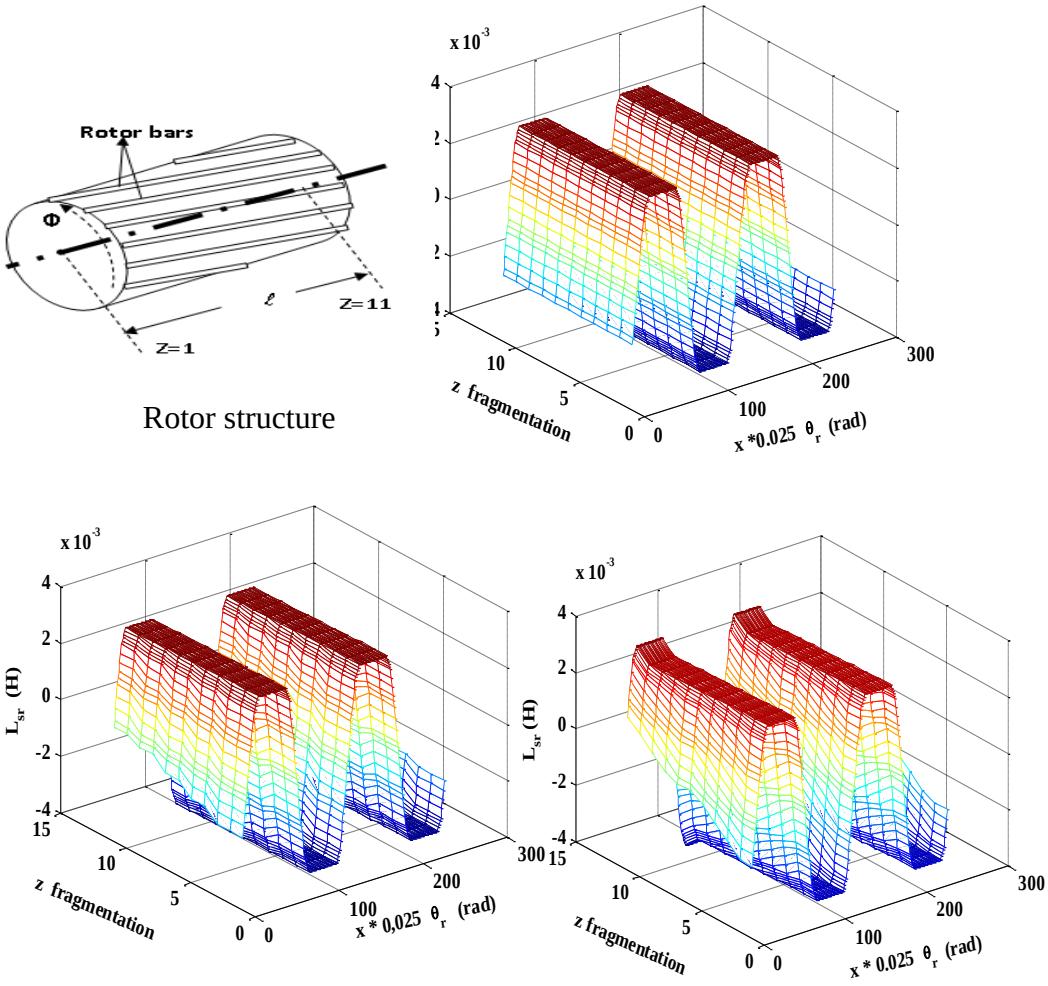

Figure 4.5 Mutual inductance between stator phase A and rotor bar 1 in the axial direction with skew=0º, 5º, 9º

From the 3D plots, it can be seen that with skewing of rotor bars, the mutual inductance between stator phase A and rotor loop1 varies along the rotor axial length in the skewing region but its peak magnitude remains unaltered.

The mutual inductance between stator phase A and rotor bar1 waveforms for both axial uniform eccentricity condition (δ_s=0.3 and δ_d=0.1) and inclined eccentricity condition (static eccentricity of (δ_{s0}=0 at one end, δ_{s1}=0.3 at the other end) and dynamic eccentricity of δ_d=0.1) are as shown in Figure 4.6.

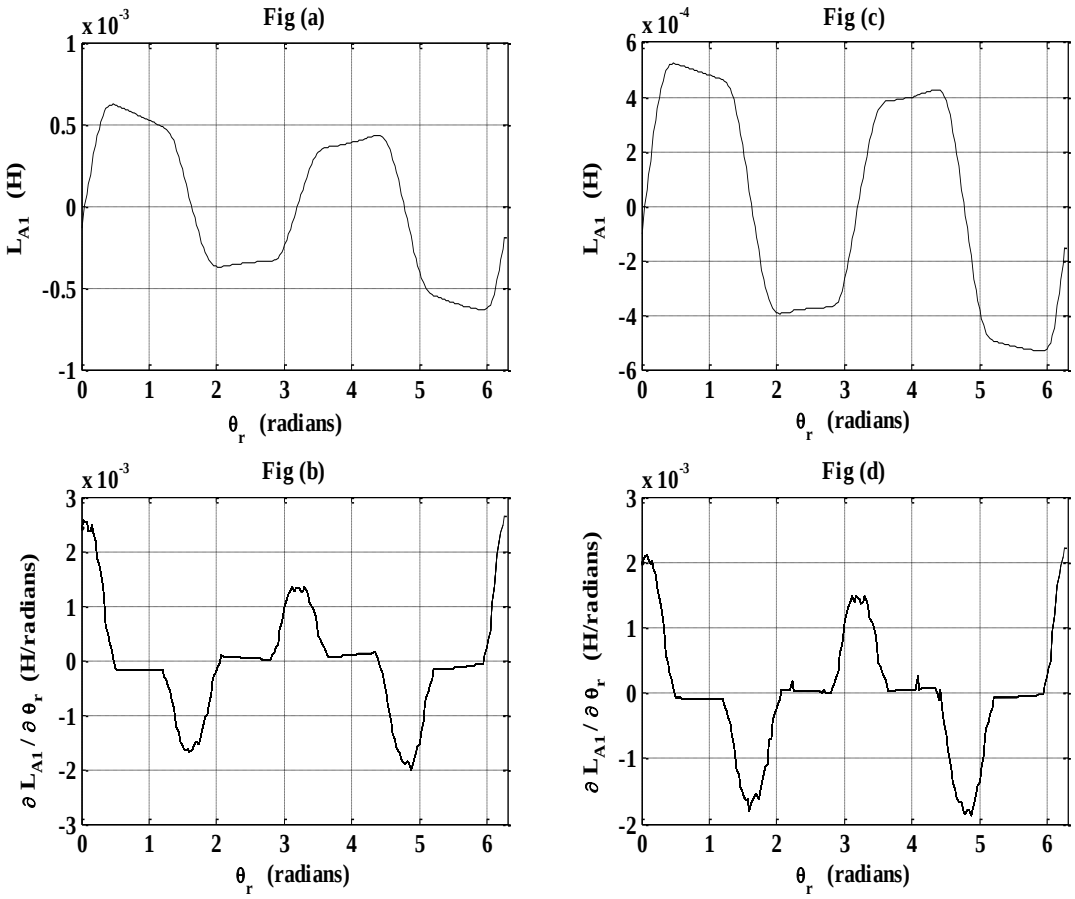

Figure 4.6 Variation of mutual inductance between stator phase A and rotor loop1 and its derivative: Fig (a) (b) uniform axial eccentricity Fig (c) (d) inclined eccentricity

From Figure 4.6, the following observations are made

- The magnitude of mutual inductance is higher in case of uniform axial eccentricity conditions.
- The derivative waveform shows more peaks in case of inclined eccentricity but its magnitude is lesser than that of uniform eccentricity condition.

The observations made are similar to those reported in the literature [Guillermo et al. (2002), Ghoggal et al. (2006)]. The mutual inductance waveforms between rotor loop1 and rotor loop2 for uniform eccentricity condition (δ_s=0.3 and δ_d=0.1) and inclined eccentricity condition (static eccentricity of (δ_{s0}=0, δ_{s1}=0.3) and dynamic eccentricity of δ_d=0.1) are as shown in Figure 4.7

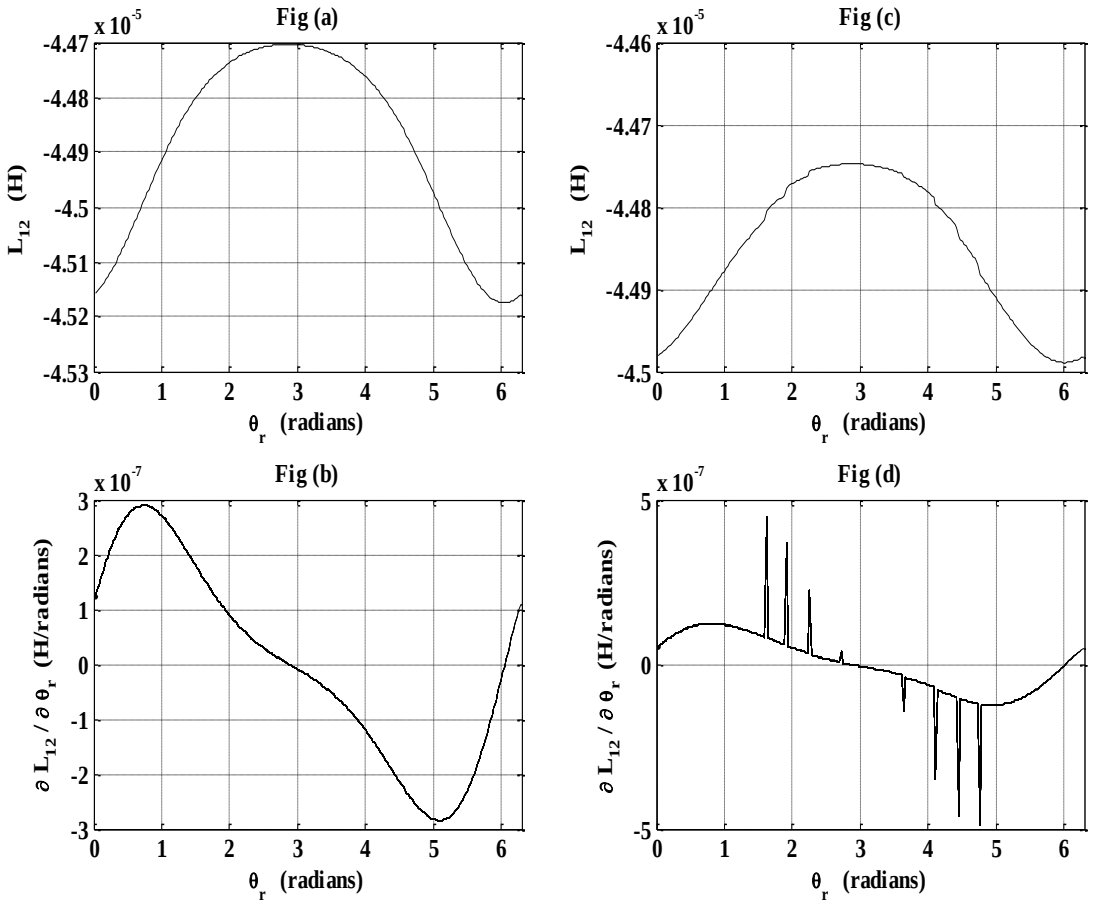

Figure 4.7 Variation of mutual inductance between rotor loop1 and rotor loop2 and its derivative: Fig (a) (b) uniform axial eccentricity Fig (c) (d) inclined eccentricity

From Figure 4.7, following observations are made

- Magnitude of mutual inductance between rotor loop1 and rotor loop2 (L_{12}) is higher in uniform eccentricity condition as compared to inclined eccentricity condition.
- The derivative waveform of L_{12} has more peaks in inclined eccentricity condition as compared to uniform eccentricity condition.

The self inductance waveforms of rotor loop1 for uniform eccentricity condition (static eccentricity of δ_s=0.3 and dynamic eccentricity of δ_d=0.1) and

inclined eccentricity condition (static eccentricity of (δ_{s0}=0, δ_{s1}=0.3) and dynamic eccentricity of δ_d=0.1) are as shown in Figure 4.8

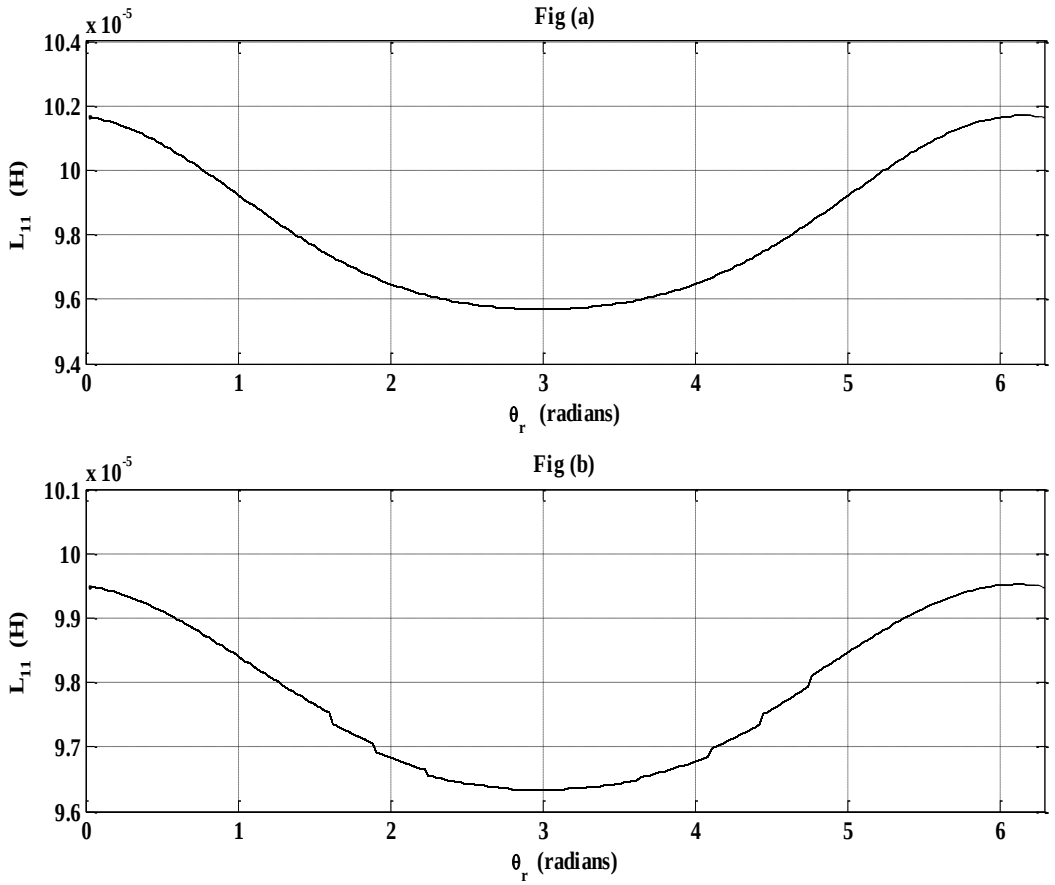

Figure 4.8 self inductance of rotor loop1 Fig (a) uniform axial eccentricity condition Fig (b) inclined eccentricity condition

From Figure 4.8, it can be seen that self-inductance of rotor loop1 has higher magnitude in the case of uniform eccentricity condition as compared to the inclined eccentricity condition.

The mutual inductance waveform between stator phase A and stator phase B for uniform eccentricity condition (static eccentricity of δ_s=0.3 and dynamic eccentricity of δ_d=0.1) and inclined eccentricity condition (static eccentricity of (δ_{s0}=0, δ_{s1}=0.3) and dynamic eccentricity of δ_d=0.1) are as shown in Figure 4.9

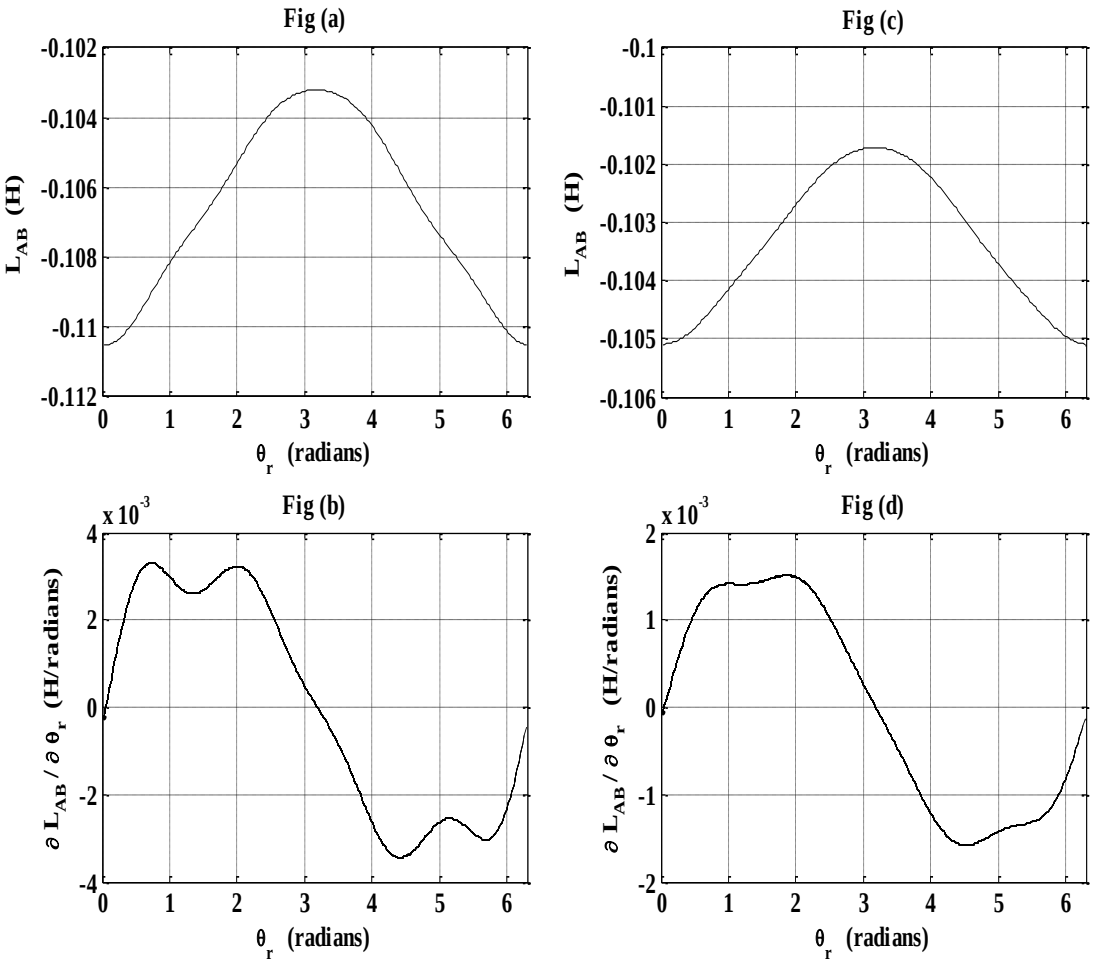

Figure 4.9 Variation of mutual inductance between stator phase A and stator phase B and its derivative: Fig (a), (b) uniform axial eccentricity Fig (c), (d) inclined eccentricity

From Figure 4.9, following observations are made

- Magnitude of mutual inductance between stator phase A and B (L_{AB}) is higher in case of uniform eccentricity as compared to inclined eccentricity condition.
- Derivative of L_{AB} also has higher magnitude in uniform eccentricity condition as compared to inclined eccentricity condition.

The self-inductance waveforms of stator phase A for uniform eccentricity condition (static eccentricity of δ_s=0.3 and dynamic eccentricity of δ_d=0.1) and inclined eccentricity condition (static eccentricity of (δ_{s0}=0, δ_{s1}=0.3) and dynamic eccentricity of δ_d=0.1) are as shown in Figure 4.10

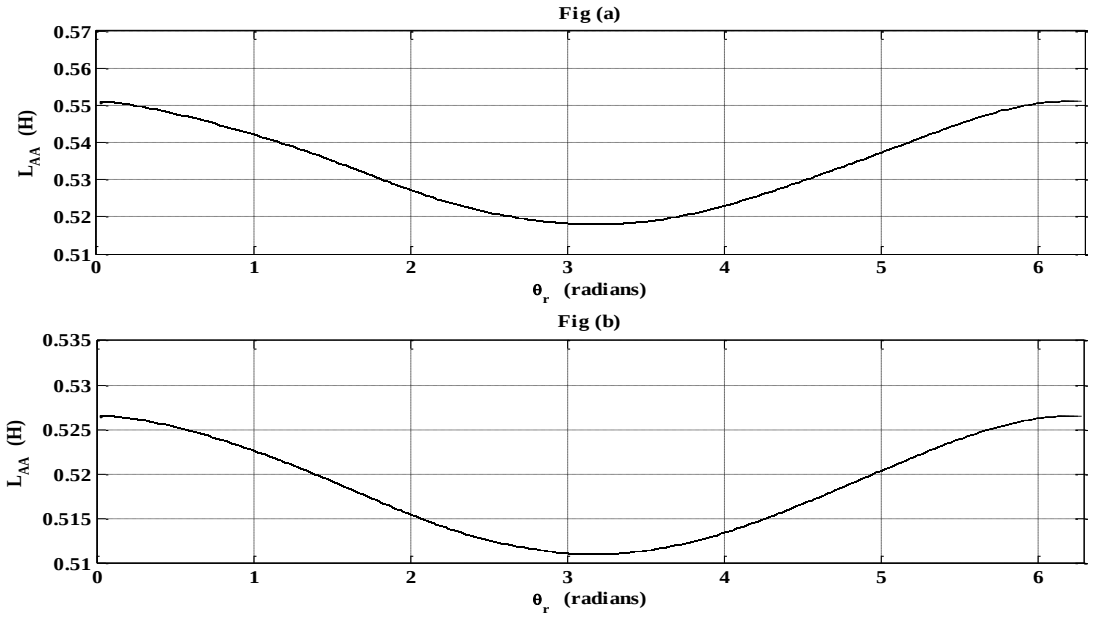

Figure 4.10 Self inductance of stator phase A Fig (a) uniform axial eccentricity condition Fig (b) inclined eccentricity condition

From Figure 4.10, it is seen that self inductance magnitude of stator phase A is slightly higher in uniform eccentricity condition of the machine as compared to that of the inclined eccentricity condition.

4.3 Simulation of dynamic behavior of machine

The dynamic model of induction motor is simulated using Runge-Kutta4 with a fixed step size of 0.00005 seconds for both healthy and eccentricity conditions. The obtained dynamic waveforms such as speed vs time, dynamic torque vs time, stator phase currents vs time and fluxes vs time, rotor loop currents vs time and fluxes vs time, d-q components of stator phase currents vs time from simulating the model are shown in this section.

4.3.1 Dynamic behaviour of healthy machine

The speed, torque, stator phase currents and flux, rotor loop currents and flux, and dq0 components of stator current waveforms are obtained from simulating the machine model under no load condition for 0-0.5 seconds, under 53.7% load from

0.5-1 second and under full load (14.89 Nm) from 1-1.5 seconds and are shown in Figures 4.11-4.14.

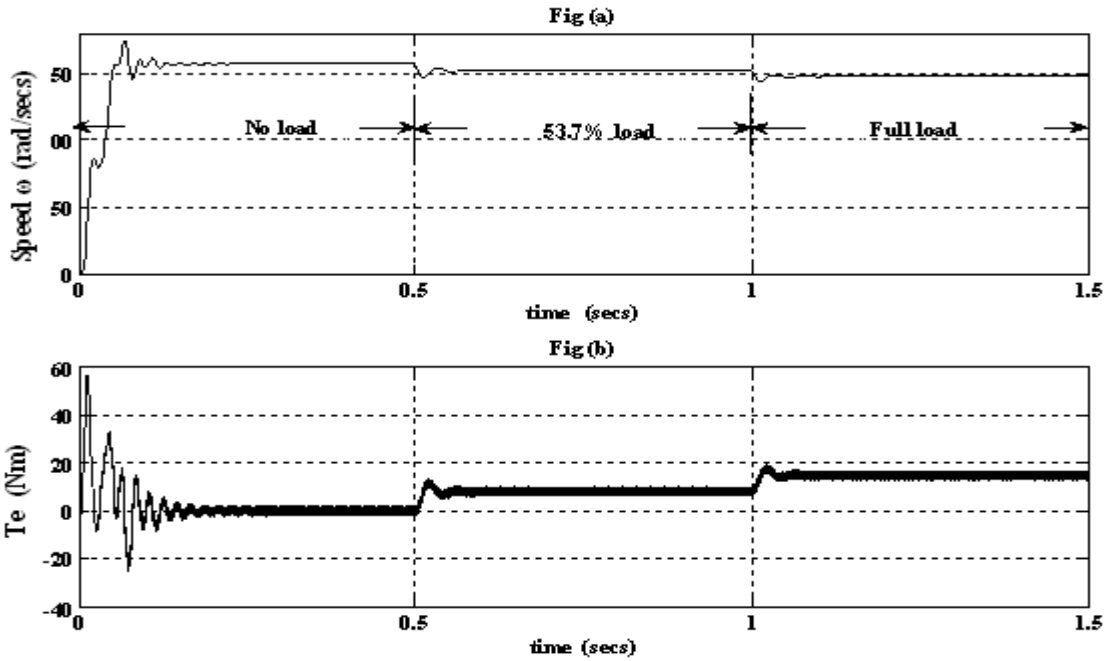

Figure 4.11 Speed and dynamic torque waveforms of the healthy machine Fig (a) speed vs time Fig (b) dynamic torque vs time

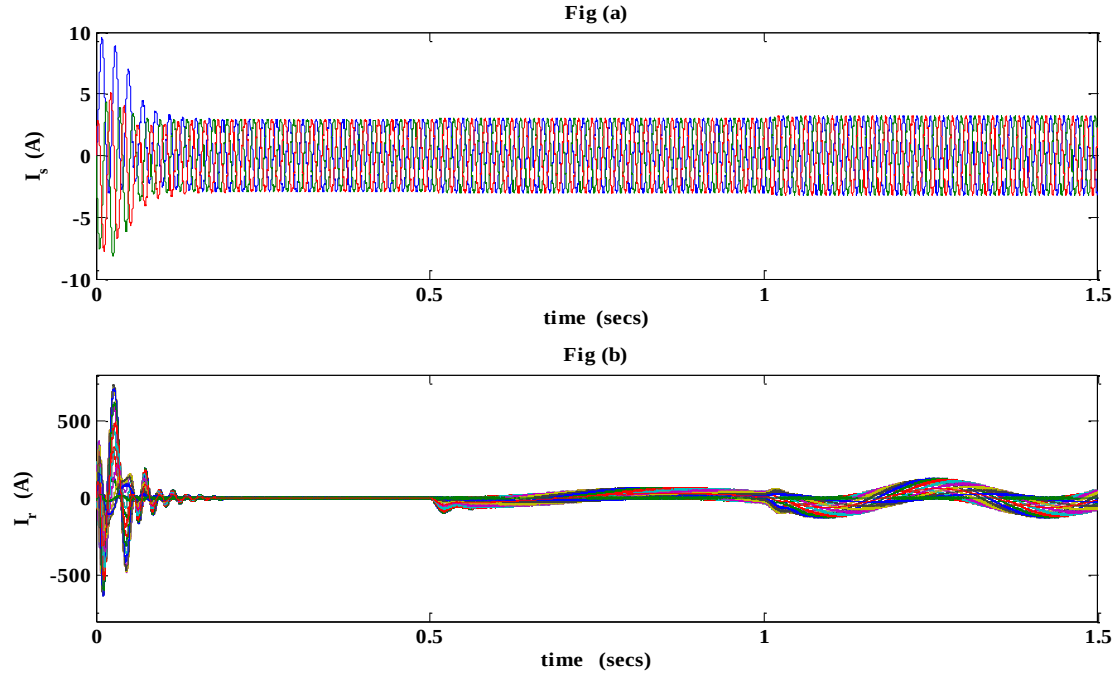

Figure 4.12 Stator phase current and rotor loop current waveforms

Fig (a) I_s vs time Fig (b) I_r vs time

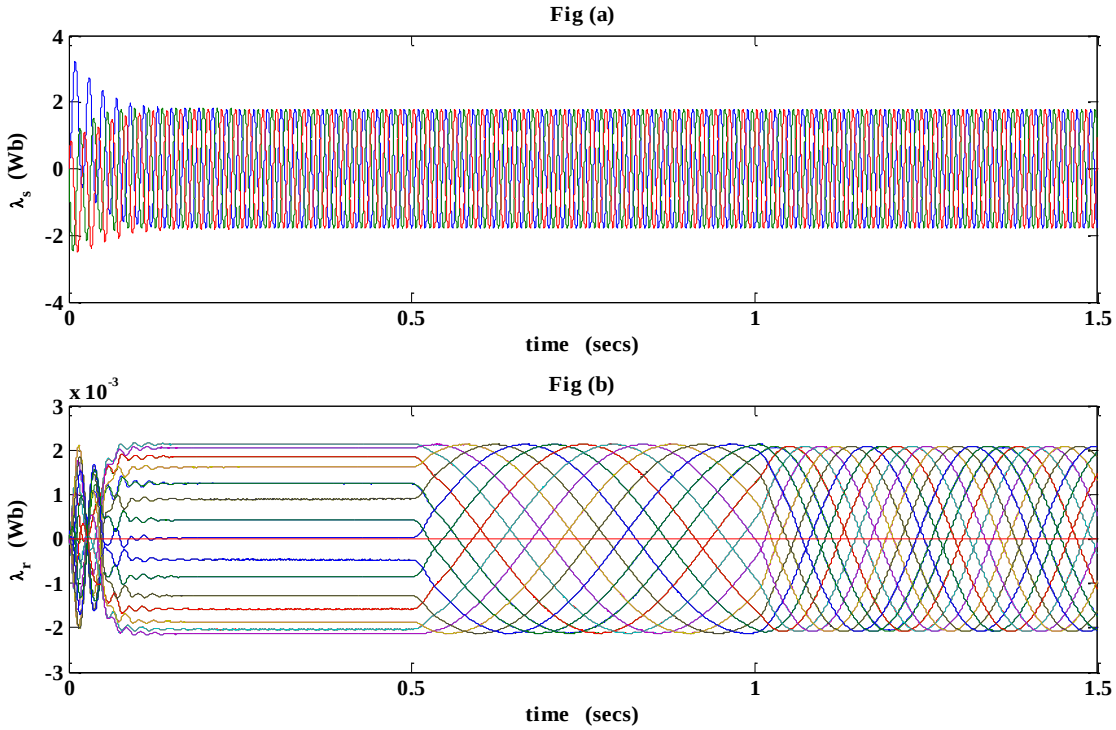

Figure 4.13 Stator phase flux linkage and rotor loop flux linkage waveforms of the healthy machine Fig (a) $\lambda_s$vs time Fig (b) λ_r vs time

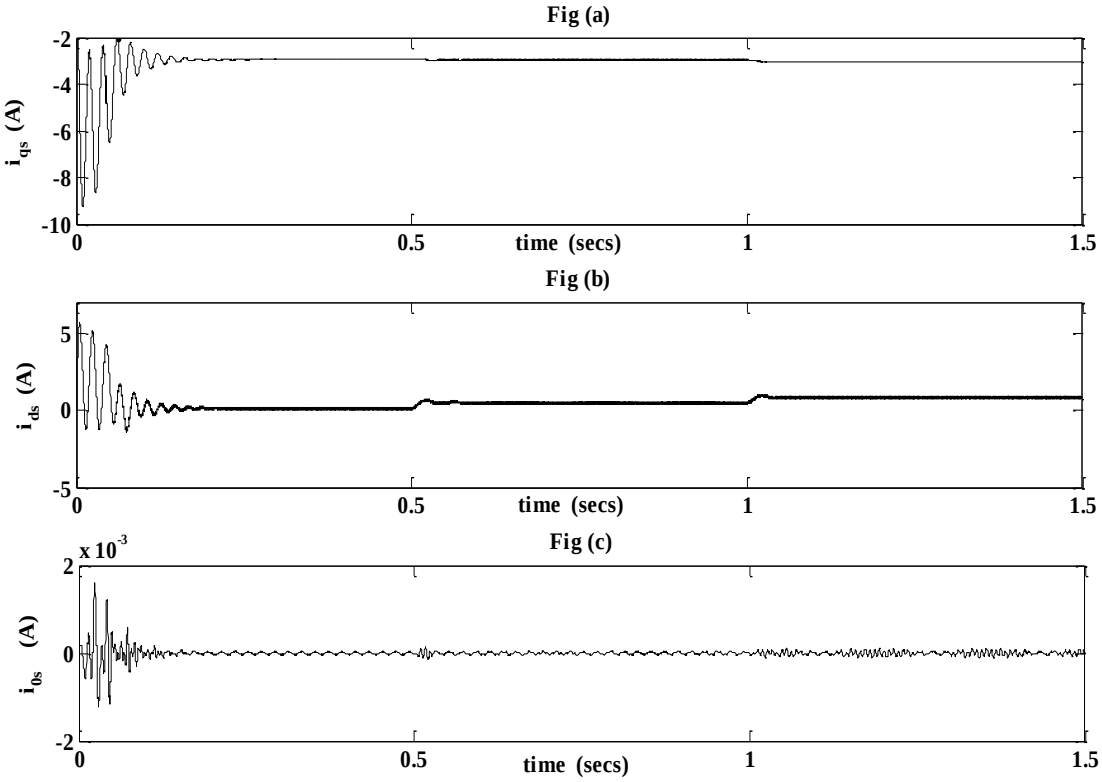

Figure 4.14 i_{qd0} components of stator phase current waveforms of the healthy machine Fig (a) i_{qs} vs time Fig (b) i_{ds} vs time Fig (c) i_{0s}vs time

From the dynamic waveforms obtained for healthy machine conditions (Figures 4.11-4.14) following observations can be made

- Dynamic machine model developed responds very well to the changes in load.
- The machine speed falls as the load increases and settles very quickly to new speed whenever there is a change in the applied load on it.
- Under no load condition, the rotor loop flux linkages are constant and under loaded conditions, they are sinusoidal having frequency (sf_1).
- Rotor end ring current and flux linkage are negligible.

From i_{qd0} waveforms following observations are made

- i_{qs} settles to a negative value in synchronous reference frame.
- i_{ds} settles positive value under loaded conditions in synchronous reference frame.
- i_{0s} remains at zero in synchronous reference value.
- Under loaded conditions both i_{qs} and i_{ds} current magnitude increase.

In the next section dynamic behaviour of the machine model for both uniform and inclined eccentricity conditions are discussed.

4.3.2 Dynamic behaviour of eccentric machine

The machine model is simulated for both uniform and inclined conditions of the machine to obtain the speed vs time, torque vs time, stator phase currents vs time, rotor loop currents vs time, stator phase flux vs time and rotor loop flux vs time. The model developed for the machine operates at full load and its dynamic behaviour is studied. The dynamic waveforms are obtained for both operating conditions:
(i) uniform axial eccentricity condition (δ_s=0.3 and δ_d=0.1) and
(ii) inclined axial eccentricity condition (static eccentricity conditions (δ_{s0}=0, δ_{s1}=0.3) and dynamic eccentricity condition, δ_d=0.1).

The waveforms are as shown in Figure 4.15. These waveforms are obtained for full load running conditions of the machine. From the plots, it can be seen that the effect of eccentricity on these parameters are more in case of uniform eccentricity as compared to inclined eccentricity.

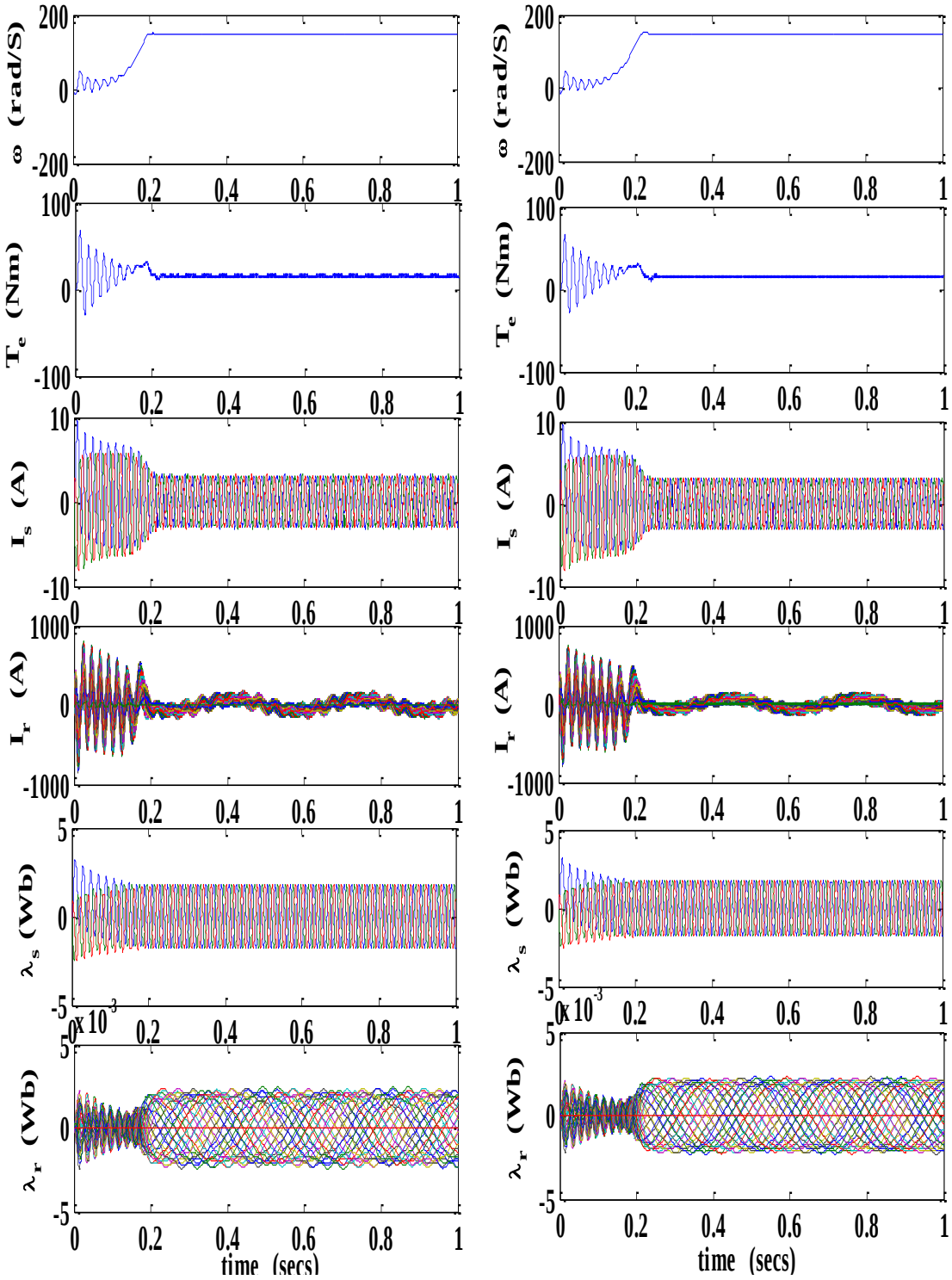

Figure 4.15 Dynamic waveforms: speed vs time, dynamic torque vs time, stator phase currents vs time, rotor loop currents vs time, stator phase flux linkages vs time, rotor loop flux linkages vs time Fig (a) uniform axial eccentricity with δ_s=0.3 and δ_d=0.1 Fig (b) inclined axial eccentricity with δ_{s1}=0 , δ_{s2}=0.3 and δ_d=0.1

The simulated i_{qd0} components of stator current for both uniform axial eccentricity condition (δ_s=0.3 and δ_d=0.1) and inclined axial eccentricity condition (δ_{s0}=0, δ_{s2}=0.3 and δ_d=0.1) are as shown in Figure 4.16.

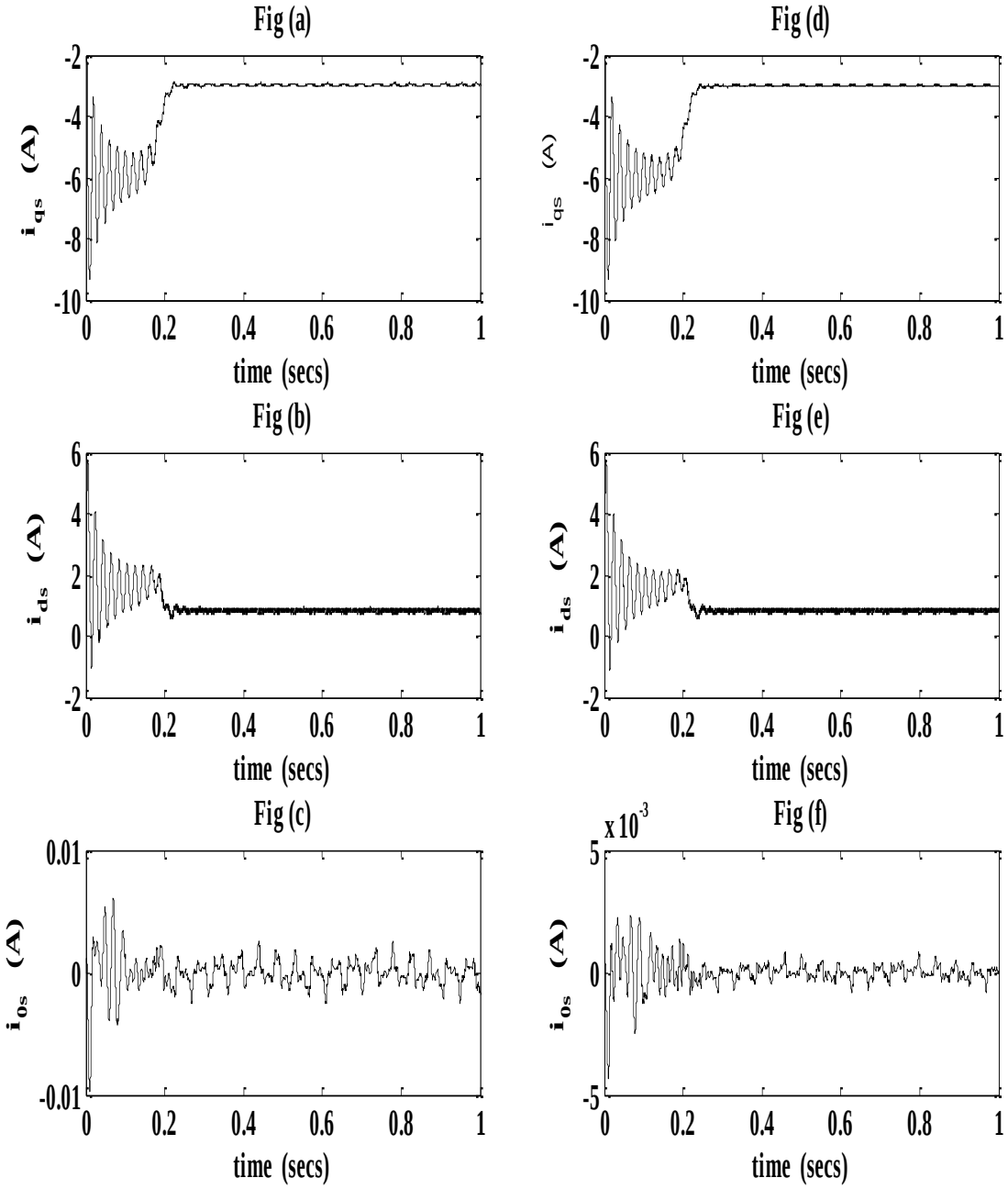

Figure 4.16 i_{qd0} components of stator phase current waveforms of the eccentric machine under full load conditions Fig (a) i_{qs} vs time Fig (b) i_{ds} vs time Fig (c) i_{0s}vs time (uniform eccentricity condition) Fig (d) i_{qs} vs time Fig (e) i_{ds} vs time Fig (f) i_{0s}vs time (inclined eccentricity condition)

From the Figure 4.16, it can be seen that both i_{qs} and i_{ds} will have a DC component superimposed with oscillations unlike healthy conditions of the machine.

4.4 Signature analysis of simulated signals

Non uniformity in the air gap results in non uniform distribution of the flux. Many quantities such as stator current (Motor current), power, power factor are affected by the air gap eccentricity. Air gap eccentricity induces eccentricity related harmonics in these quantities which can be detected by frequency analysis of these parameters.

The model is simulated for both uniform and inclined eccentricity conditions. During the analysis, the machine model is run under constant load and the model is fed with balanced sinusoidal three phase supply. Since the load is not fluctuating and the machine is not fed with inverter, the output stator current signals remain stationary. The Fourier Transform (FT) is suitable if the signal has no time varying frequency components (stationary). It can provide information only about whether certain frequency components exist or not. The information is independent of where in time each frequency component exists. By identifying the fault characteristic frequency components present in the stator current, type of fault can be detected. Usually, Fast Fourier Transform (FFT) and Power Spectral Density (PSD) analysis are performed on the stator current to detect the presence of eccentricity in the machine. Fourier Transform (FT) may not exist for a wide sense stationary random signal whereas PSD exists for all signals as average power is considered as it is the finite quantity. In this section, results and waveforms obtained by Power Spectral Density (PSD) performed on instantaneous stator currents and its d-q components, instantaneous power and power factor and obtained spectra are presented.

4.4.1 Motor Current Signature Analysis (MCSA)

All the asymmetrical faults can be detected by identifying specific frequency components characterising the faults in the motor current. It is a very popular and reliable method. They produce fault specific harmonics in the stator currents which can be calculated by the equations as listed in Table 4.1. Fast Fourier Transforms

(FFT) or Power Spectral Density (PSD) analysis is performed on the stator currents to extract these fault specific harmonics.

Table 4.1 Type of Fault and Frequency related component detection equations (Jeffrey et al. 1995)

Frequency Signature of	Equation for Identifying frequency components	Equation Number
Stator fault	$f_s = (k \pm n\frac{(1-s)}{p})f_1$ k=1,3…,n=1,2,3…..(2p-1)	(4.1)
Stator voltage asymmetry	$f_s = [v(1 \pm s) \pm 1]f_1$ for v=1,3,5,7	(4.2)
Rotor fault	$f_b = (1 \pm 2ks)f_1$ $f_b = \left[\left(\frac{k}{p}\right)(1-s) \pm s\right]f_1$ where k/p=1,3,5,……	(4.3) (4.4)
Eccentricity fault	$f_e = \left[(kR \pm n_d)\left(\frac{(1-s)}{p}\right) \pm v\right] f_1$ n_d= 0 for static eccentricity =1,2,3.. v=±1,±3… order of the stator time harmonics that are present in the power supply driving the motor $f_e = f_1 \pm kf_r = \left[1 \pm k\frac{(1-s)}{p}\right]f_1$ f_r= Nr/60 k=1,2,3…….	(4.5) (4.6)

PSD analysis is one of the powerful tool used for frequency analysis of stator current. Stator current spectra obtained from simulating the model for healthy,

uniform eccentric machine (δ_s=0.3 and δ_d=0.1) and inclined eccentric machine (δ_{s0}=0.0, δ_{s1}=0.3 and δ_d=0.1) conditions are as shown in Figure 4.17.

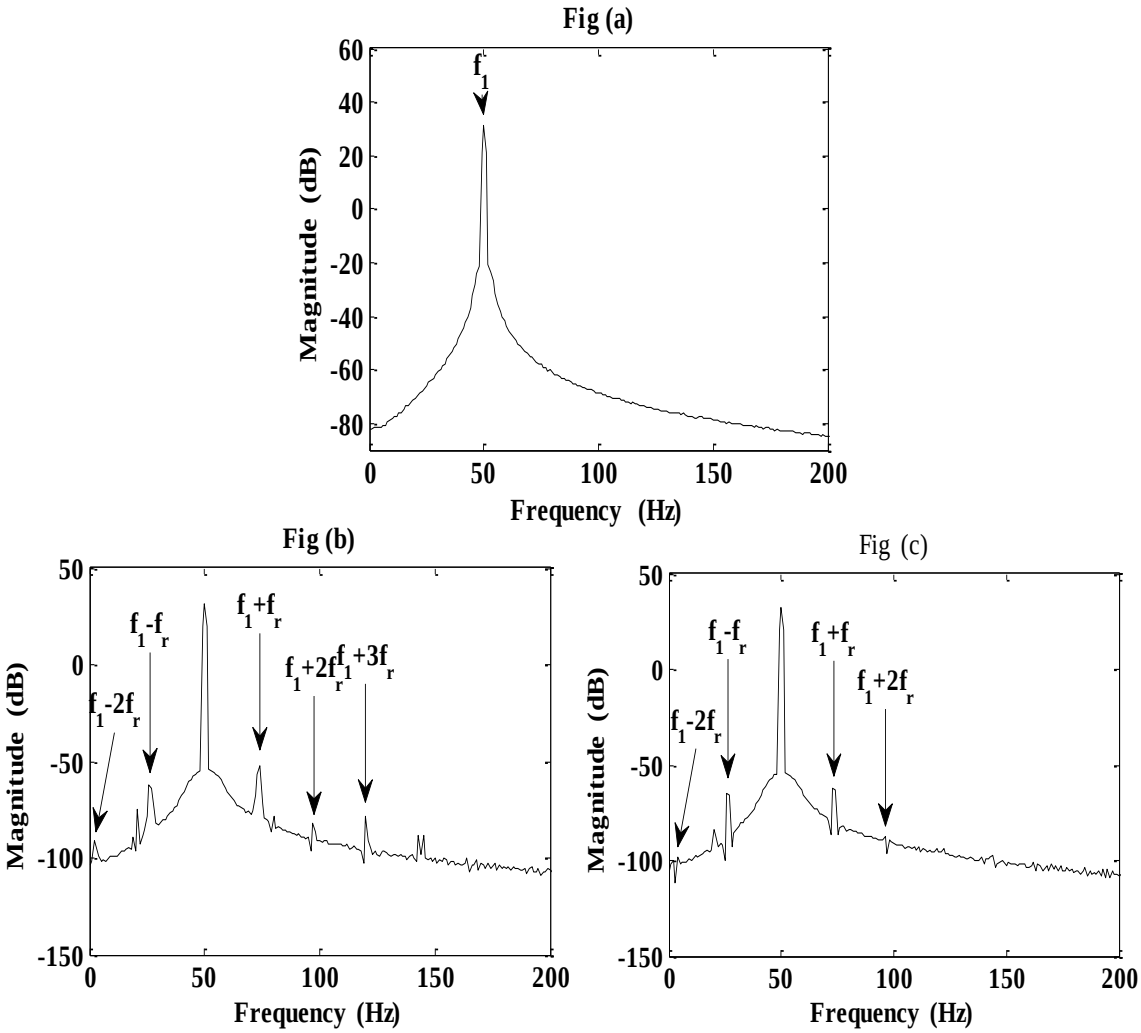

Figure 4.17 Stator phase A current spectra Fig (a) Healthy Fig (b) Uniform axial eccentricity (δ_s=0.3 and δ_d=0.1) Fig (c) Inclined axial eccentricity (δ_{s0}=0.0, δ_{s1}=0.3 and δ_d=0.1)

From Figure 4.17, it can be seen that current spectra obtained from air gap eccentric machine has side band harmonics around the fundamental. (f_1-f_r) and (f_1+f_r) are the eccentricity characteristic lower (LSB) and upper side band (USB) frequency components respectively. PSD analysis is performed on the extracted stator phase A current data samples after passing the samples through a digital filter having cut off frequency 1kHz. The designed filter is low pass Finite Impulse Response (FIR) filter

and Hanning window is used during filtering. The lower and upper side band frequency components are found from the spectra. They are obtained for both uniform eccentricity (δ_s=0.3 and δ_d=0.1) and inclined eccentricity (δ_{s0}=0.0, δ_{s1}=0.3 and δ_d=0.1) conditions of the machine. They are compared with the theoretical values computed using Equation (4.6) and are shown in Table 4.2.

Table 4.2 Lower and upper side band frequency components in the simulated PSD

Machine condition	Uniform Eccentric		Inclined Eccentric	
	PSD	Theoretical	PSD	Theoretical
Lower side band frequency (f_1-f_r)	26 Hz	26.48 Hz	26 Hz	26.48 Hz
Upper side band frequency (f_1-f_r)	74 Hz	73.52 Hz	74 Hz	73.52 Hz

The assumed frequency resolution is 1Hz for the frequency analysis. From the Table 4.2, it can be observed that LSB and USB frequency components found from the stator current spectra and from the Equation (4.6) agree with each other.

PSD analysis gives information about the existence of eccentricity, but interpreting the degree of eccentricity is very difficult as the margin of variation between these frequencies is not significant. However authors [Faiz et al. 2009] in their paper illustrate that dynamic eccentricity increases the amplitude of sideband components around Partial Slot Harmonic (PSH). This feature can be used for detection of dynamic eccentricity. Further, it is worth noting that, when the static eccentricity is increased, the amplitude of the sideband components also increases. Particularly for a fixed load, the frequencies of sideband components due to the static eccentricity fault remain constant. In the same paper, it is also reported that noise can affect this index and fault diagnosis may produce an error.

The machine model is simulated for the mixed eccentricity conditions of 20% dynamic eccentricity with static eccentricity being varied. Table 4.3-4.4, gives the details about sideband frequencies around the base frequency for the machine under full load (14.89 Nm), 53.7% load (8Nm) and no load conditions respectively. Frequency resolution considered is 1 Hz for PSD analysis.

Table 4.3 Full load with 20% dynamic eccentricity

%Static Eccentricity	$(f_1 - f_r)$ (Hz)	Magnitude (dB)	f_1 (Hz)	Magnitude (dB)	(f_1+f_r) (Hz)	Magnitude (dB)
10	26	-52.79	50	-3.9	74	-44.94
20	26	-47.8	50	-4	74	-43.81
30	26	-45.34	50	-4.07	74	-40.31
40	26	-43.07	50	-4.13	74	-38.03
50	26	-36.42	50	-4.15	74	-36.98

Table 4.4 53.7 % load with 20% dynamic eccentricity

%Static Eccentricity	$(f_1 - f_r)$ (Hz)	Magnitude (dB)	f_1 (Hz)	Magnitude (dB)	(f_1+f_r) (Hz)	Magnitude (dB)
10	26	-50.99	50	-4.35	74	-43.55
20	26	-43.78	50	-4.46	74	-42.92
30	26	-40.91	50	-4.53	74	-40.37
40	26	-38.82	50	-4.61	74	-38.09
50	26	-34.76	50	-4.65	74	-37.22

Table 4.5 No load with 20% dynamic eccentricity

%Static Eccentricity	$(f_1 - f_r)$ (Hz)	Magnitude (dB)	f_1 (Hz)	Magnitude (dB)	(f_1+f_r) (Hz)	Magnitude (dB)
10	25	-46.25	50	-4.51	74	-54.82
20	25	-39.45	50	-4.63	74	-47.89
30	25	-37.79	50	-4.71	74	-44.78
40	25	-36.36	50	-4.61	74	-40.15
50	25	-32.5	50	-4.88	74	-36.09

From Table 4.3-4.5, the following observations are made

- Amplitude of fundamental frequency in dB marginally decreases with increase in static eccentricity.
- Amplitude of side band frequencies in dB increases with increase in static eccentricity.
- The side band frequency components around fundamental remain practically the same with increase in static eccentricity.
- The above observation can be attributed to the facts that speed, and hence slip is not greatly affected with the increase in static eccentricity.

The machine model is run for the mixed eccentricity conditions of 40% static eccentricity with dynamic eccentricity being varied. Table 4.6-4.8, gives the details about the variation in the amplitude of sideband frequencies around the base frequency for the machine operating under full load (14.89 Nm), 53.7% load (8Nm) and no load conditions respectively.

Table 4.6 Full load with 40% static eccentricity

%Dynamic Eccentricity	$(f_1 - f_r)$ (Hz)	Magnitude (dB)	f_1 (Hz)	Magnitude (dB)	(f_1+f_r) (Hz)	Magnitude (dB)
3	27	-59.59	50	-4.01	73	-55.08
5	27	-55.48	50	-4.01	73	-50.52
7	27	-52.58	50	-4.02	73	-47.61
10	26	-49.48	50	-4.04	74	-44.53
20	26	-43.07	50	-4.13	74	-38.03
30	26	-38.62	50	-4.28	74	-33.94
40	26	-33.32	50	-4.46	74	-29.83

Table 4.7 53.7% load with 40% static eccentricity

%Dynamic Eccentricity	$(f_1 - f_r)$ (Hz)	Magnitude (dB)	f_1 (Hz)	Magnitude (dB)	(f_1+f_r) (Hz)	Magnitude (dB)
3	26	-55.38	50	-4.64	74	-54.82
5	26	-50.96	50	-4.47	74	-50.39
7	26	-48.09	50	-4.49	74	-47.43
10	26	-44.92	50	-4.49	74	-44.53
20	26	-38.82	50	-4.61	74	-38.03
30	26	-35.28	50	-4.79	74	-33.66
40	26	-32.38	50	-5.03	74	-29.18

Table 4.8 No load with 40% static eccentricity

%Dynamic Eccentricity	$(f_1 - f_r)$ (Hz)	Magnitude (dB)	f_1 (Hz)	Magnitude (dB)	(f_1+f_r) (Hz)	Magnitude (dB)
3	26	-52.14	50	-4.64	74	-58.81
5	26	-47.49	50	-4.47	74	-54.48
7	26	-44.56	50	-4.49	74	-51.24
10	26	-41.78	50	-4.49	74	-47.48
20	26	-36.36	50	-4.61	74	-40.15
30	26	-36.82	50	-4.79	74	-33.65
40	26	-34.44	50	-5.03	74	-31.64

From Table 4.6-4.8, the following observations are made

- Amplitude of fundamental frequency in dB decreases marginally with the increase in dynamic eccentricity.
- Amplitude of side band frequencies in dB increases with increase in static eccentricity.
- The side band frequency components around fundamental change with increase in dynamic eccentricity.(refer Table 4.6)
- Above observation can be attributed to the fact that with the increase in dynamic eccentricity, speed with which machine runs increases and slip decreases marginally

4.4.1.1 Detection of severity of air gap eccentricity fault by Eccentricity Severity Factor

Eccentricity Severity Factor (ESF) is proposed to detect the severity of mixed eccentricity level using the amplitudes of these side band frequency components and is defined as

$$ESF_1 = \frac{(\text{Amplitude of base frequency in dB} - \text{Amplitude of lower side band frequency in dB})}{\text{Amplitude of base frequency in dB}} \quad (4.7)$$

or

$$ESF_2 = \frac{(\text{Amplitude of base frequency in dB} - \text{Amplitude of upper side band frequency in dB})}{\text{Amplitude of base frequency in dB}} \quad (4.8)$$

Total Indicated Reading (TIR) of the motor provided by the manufacturer controls the dynamic eccentricity level in the machine. Even though 10% total eccentricity is permissible, the manufacturer keeps this value as low as possible [Nandi et al. 2005]. Static eccentricity exists in the machine even at the assembly stage. For a stiff rotor shaft assembly like the chosen machine for analysis, static eccentricity is unlikely to change. Hence ESF are calculated for fixed static eccentricity value, with dynamic eccentricity values being varied.

From the tables 4.3-4.8, it is observed that for a given load on the machine, the amplitude of the fundamental decreases marginally (almost remains constant) with the increase in mixed eccentricity level whereas the side band components magnitude increases significantly. Hence the magnitude of these side band frequency components are compared with those of the fundamental and Eccentricity Severity Factors (ESF) are defined to assess the degree of eccentricity in the machine. Eccentricity severity factors are calculated from the extracted stator currents obtained via simulation of the machine model for the machine running condition of 40% static eccentricity and varied dynamic eccentricities. Calculated ESF_1 and ESF_2 values for the machine under full load, 53.7% load and no load are presented in Table 4.9.

Table 4.9: ESF1 and ESF2 values vs % Dynamic Eccentricity

	Full load		53.7% load		No load	
%DE	ESF_1	ESF_2	ESF_1	ESF_2	ESF_1	ESF_2
3	-13.86	-12.74	-10.94	-10.81	-10.26	-11.70
5	-12.84	-11.60	-10.40	-10.27	-9.26	-10.77
7	-12.08	-10.84	-9.71	-9.56	-8.60	-10.04
10	-11.25	-10.02	-9.00	-8.92	-7.97	-9.19
20	-9.43	-8.21	-7.42	-7.25	-6.59	-7.38
30	-8.02	-6.93	-6.37	-6.03	-6.38	-5.74
40	-6.47	-5.69	-5.44	-4.80	-5.59	-5.05

Using Table 4.9, variation of ESF_1 and ESF_2 are plotted against % dynamic eccentricity as shown in Figures 4.18 for full load, 53.7% load and no load conditions of the machine

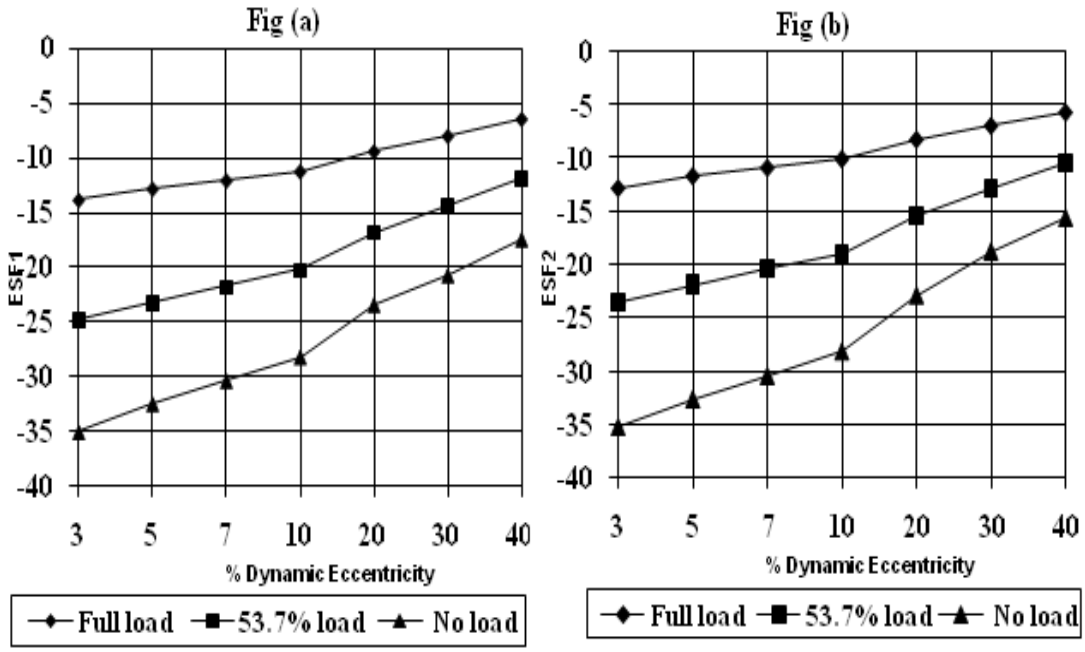

Figure 4.18 Variation of eccentricity severity factor with dynamic eccentricity
Fig (a) ESF1vs % Dynamic Eccentricity Fig (b) ESF2 vs Dynamic Eccentricity

From Figure 4.18, it is observed that eccentricity fault severity factor increases with the increase in dynamic eccentricity for an existing 40% static eccentricity in the machine. Hence ESF_1 and ESF_2 can be used as eccentricity severity detection factors.

4.4.1.2 Detection of severity of air gap eccentricity fault by Eigenvalue

The proposed Eigenvalue based fault severity detection compares the amplitude of the frequency components of stator current of an eccentric machine with those obtained under healthy condition and is a better indicator to indicate the deterioration in the health of the machine over the period. It can be used as a tool to predict the degree of air gap eccentricity fault in the machine and hence avoid the total failure of the machine.

The Eigenvalues represent the distribution of the source data's energy among each of the Eigen vectors. The cumulative energy content of Eigen vector is the sum of the energy content across all of the Eigenvalues. The amplitudes of the eccentricity characteristic harmonics (f_1-f_r), (f_1+f_r) and (f_1+2f_r) components are obtained for different mixed uniform eccentricity conditions and are compared to those obtained under healthy condition. Co-variance matrix is formed from which Eigenvalues are evaluated. The lowest Eigenvalues obtained for different eccentricity conditions are plotted as shown in Figure 4.19.

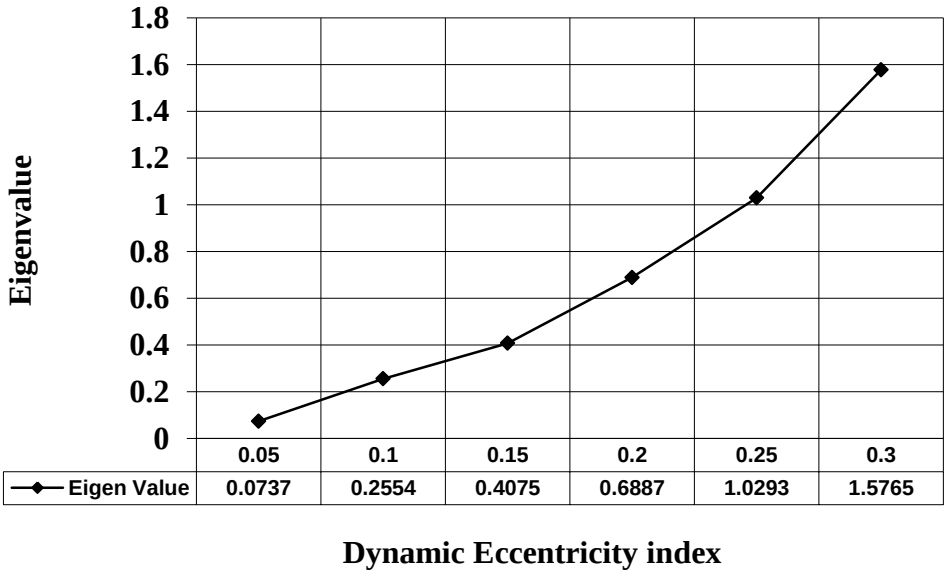

Figure 4.19 Variation of Eigenvalue with dynamic eccentricity index

From Figure 4.19, it is observed that Eigenvalues increase with the increase in dynamic eccentricity level in the machine. Hence, it can be used as a fault severity predictor to assess the degree of mixed eccentricity fault in the machine. This method has an added advantage that severity index is defined by evaluating the amplitudes of

many eccentricity related harmonics and these values being compared to those of a healthy machine (or the installation condition of the machine). This index, along with 'Total Indicated Reading (TIR)' or 'total run out' provided by the manufacturer can be used to take a decision whether to send the machine to manufacturer's workshop or not.

4.4.1.3 Motor current signature analysis for inclined eccentric machine

Power Spectral Density (PSD) analysis is conducted on the stator phase A current samples obtained by simulating the model for the mixed eccentricity condition of 5% dynamic eccentricity and inclined static eccentricity of 20% at one end and 35% on the other end and the resulting current spectra is shown in Figure 4.20.

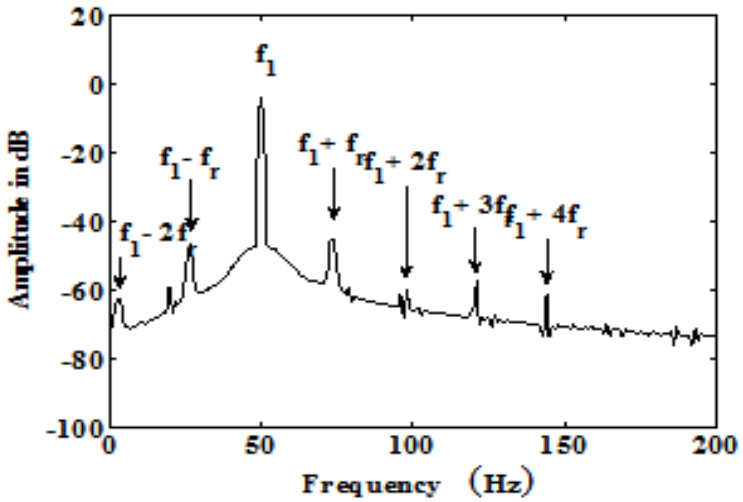

Figure 4.20 Stator current spectra for eccentric condition (δ_d=0.05 and inclined static eccentricity with δ_{s1}=0.2 and δ_{s2}=0.35)

The chosen frequency resolution to obtain the current spectra is 1Hz. Side band eccentricity characteristic frequency components around the fundamental (f_1-f_r) (LSB) and (f_1+f_r) (USB) values are detected in the stator phase current spectra by Power Spectral Density analysis. The LSB and USB frequency components are found to be at 26 Hz and 74 Hz respectively in the stator phase A current spectra. The steady state speed of the machine is found to be 148 rad/sec (s=0.0584). Theoretical values of (f_1-f_r) and (f_1+f_r) calculated by using Equation (4.6), are found to be 26.46 Hz and 73.54 Hz. respectively.

The variation in the degree of mixed eccentricity can be achieved in three ways

- by keeping the static eccentricity constant and varying the dynamic eccentricity.
- by keeping the dynamic eccentricity constant and varying the static eccentricity.
- by varying both the static eccentricity and the dynamic eccentricity.

If the rotor- shaft assembly is sufficiently stiff, the level of static eccentricity does not change [Nandi et al. 2005]. In this study, data of a 3 hp machine having rigid rotor-shaft assembly is considered for modeling. Hence simulations are carried out keeping the static eccentricity index constant while the dynamic eccentricity index is being varied.

The machine model is simulated for the condition of inclined static eccentricity of 20% at one end and 35% on the other end with dynamic eccentricity values being varied. Table 4.10 shows the eccentricity related frequency components and its amplitude obtained by PSD analysis. The assumed frequency resolution is 1 Hz.

Table 4.10 Eccentricity related frequency components (f_1-f_r) and (f_1+f_r) and its amplitudes

%Dynamic Eccentricity index	(f_1-f_r), amplitude in dB		(f_1+f_r), amplitude in dB	
5	26	-56.80	74	-54.32
10	26	-50.85	74	-48.24
15	26	-47.06	74	-44.59
20	26	-44.37	74	-41.82
25	26	-42.52	74	-39.41
30	26	-41.98	74	-37.09

From Table 4.10, it is observed that with the increase in dynamic eccentricity (mixed eccentricity), amplitudes of mixed eccentricity related frequency components also increase. The frequency at which these components exist remains the same as the change in slip is very small at different eccentric conditions and hence not noticeable.

4.4.2 Instantaneous Power Signature Analysis

Instantaneous power signature analysis is used to extract the air gap related harmonic component from the power fed to the machine. The main advantage is that it contains air gap eccentric component f_r which is independent of synchronous speed and it contains information about the voltage asymmetry. The instantaneous power is calculated by using the Equation (4.9) [Hsu.John 1998].

$$p_{phasor} = (v_a - v_0)(i_a - i_0) + (v_b - v_0)(i_b - i_0) + (v_c - v_0)(i_c - i_0) \quad (4.9)$$

where $v_0 = (v_a + v_b + v_c)/3$

$i_0 = (i_a + i_b + i_c)/3$ and v_a ,v_b and v_c are the instantaneous phase voltages, i_a, i_b and i_c are the instantaneous phase currents.

Equation (4.9) is selected as compared to the classic instantaneous power measurement equation, because it is in a more generalised form and is valid for both balanced and unbalanced supply voltage conditions. The instantaneous power spectrum obtained from simulating the machine model for the eccentricity condition of 5% dynamic eccentricity and inclined static eccentricity of 20% at one end and 35% at the other end is as shown in Figure 4.21.

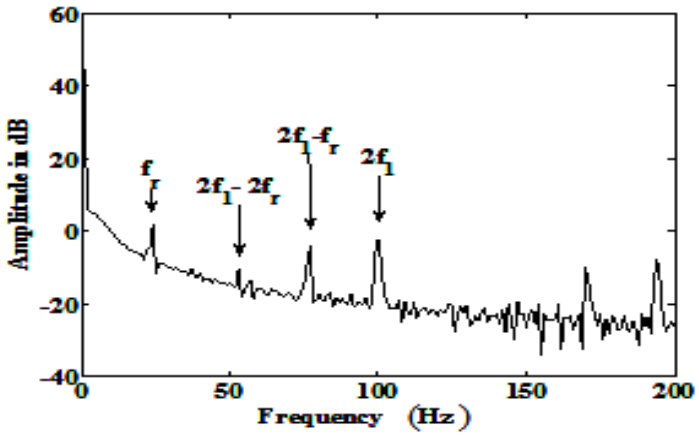

Figure 4.21 Instantaneous Power spectra for eccentric condition (δ_d=0.05 and inclined static eccentricity with δ_{s1}=0.2 and δ_{s2}=0.35)

In the instantaneous power signature spectrum, besides the fundamental and the two sideband components at ($2f_1$-f_r) and ($2f_1$+f_r), it contains an additional component at the modulation frequency f_r [Drif et al. 2006]. It also has an added advantage that it can be used to identify the voltage asymmetry in the supply. But the

main disadvantage is that it requires additional voltage transducers besides the current transducers.

From the power spectrum, eccentricity characteristic harmonics, f_r, $(2f_1-f_r)$ and $(2f_1-2f_r)$ are obtained at 24 Hz, 76 Hz and 53 Hz respectively and corresponding theoretical values are found to be at 23.54 Hz, 76.46 Hz and 52.92 Hz respectively.

The model is simulated for various inclined eccentricity conditions of inclined static eccentricity of 20% at one end and 35% at the other end and dynamic eccentricity being varied. The amplitudes of eccentricity characteristic frequency components are computed. The variation in the amplitudes of f_r, $(2f_1-f_r)$ and $(2f_1-2f_r)$ frequency components in the power spectra with the variation in dynamic eccentricity is shown in Table 4.11.

Table 4.11 Eccentricity related frequency components, f_r, $(2f_1-f_r)$ and $(2f_1-2f_r)$ and its amplitudes

%Dynamic Eccentricity index	f_r, amplitude in dB		$(2f_1-f_r)$, amplitude in dB		$(2f_1-2f_r)$, amplitude in dB	
5	24	-0.84	76	-6.17	53	-16.40
10	24	5.54	76	-0.13	53	-8.89
15	24	9.02	76	4.03	53	-1.79
20	24	11.88	76	6.94	53	3.56
25	24	14.43	76	9.72	53	8.01
30	24	17.25	76	12.15	53	11.59

From Table 4.11, it is seen that with the increase in the eccentricity level in the machine, amplitudes of eccentricity related harmonic components also increase.

4.4.3 Instantaneous Power Factor Signature Analysis

Flux distribution in the air gap of induction motor gets affected with the non uniformity in the air gap. Power factor is the primary factor to get affected by the unequal distribution of flux in the air gap. The instantaneous power factor, $\cos(\Phi)$ is

defined by the ratio of the active and the apparent instantaneous powers [Hsu.John 1998].

$$\cos(\varphi) = p_{phasor} / s_{phasor} \tag{4.10}$$

where s_{phasor} is the three-phase instantaneous apparent power and the product of 3 times the rms voltage and current and is defined as

$$s_{phasor} = 3VI/2$$

$$\text{where } V = \sqrt{2}\sqrt{[(v_a - v_0)^2 + (v_b - v_0)^2 + (v_c - v_0)^2]/3}$$

$$I = \sqrt{2}\sqrt{[(i_a - i_0)^2 + (i_b - i_0)^2 + (i_c - i_0)^2]/3}$$

Since instantaneous power factor depends on the instantaneous power, the eccentricity related characteristic frequency component f_r which appears in the power spectrum is also present in the power factor spectrum. PSD analysis is performed on the filtered instantaneous power factor data samples obtained by simulating the machine model with 20% static eccentricity at one end and 35% at the other end and 5% dynamic eccentricity conditions. The power factor spectrum obtained is as shown in Figure 4.22.

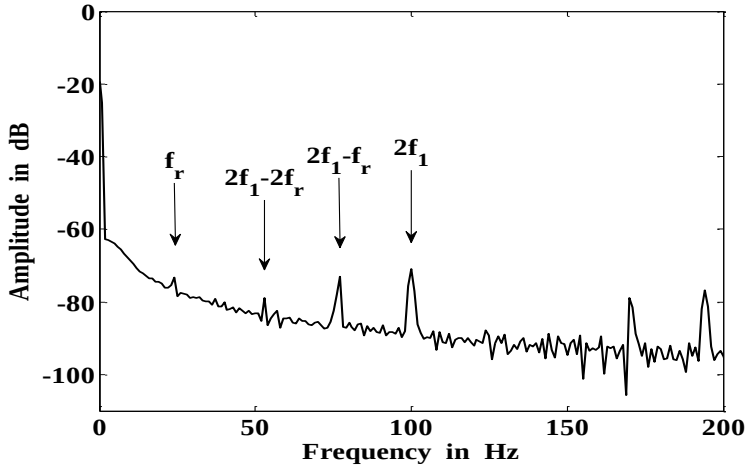

Figure 4.22 Instantaneous Power factor spectra for δ_d=0.05 and inclined static eccentricity with δ_{s1}=0.2 and δ_{s2}=0.35

Amplitudes of eccentricity related harmonic components f_r (24Hz), ($2f_1$-f_r) (76Hz) and ($2f_{1.}$-$2f_r$) (53Hz) varies with the variation in dynamic eccentricity in the machine and is shown in Table 4.12.

Table 4.12 f_r, $(2f_1-f_r)$ and $(2f_1-2f_r)$ frequency components and their amplitude in power factor spectra.

%Dynamic Eccentricity index	f_r, amplitude in dB		$(2f_1-f_r)$, amplitude in dB		$(2f_1-2f_r)$, amplitude in dB	
5	24	-80.13	76	-74.91	53	-85.51
10	24	-73.63	76	-68.91	53	-77.58
15	24	-70.78	76	-64.63	53	-70.39
20	24	-67.88	76	-61.62	53	-64.99
25	24	-63.91	76	-58.71	53	-60.37
30	24	-57.92	76	-56.23	53	-56.65

From Table 4.12, it is seen that with the increase in the eccentricity level in the machine, amplitudes of eccentric related characteristic harmonic components also increases.

The authors in paper [Drif et al. 2008], have defined a power factor fault severity factor as the ratio of the amplitude of the f_r component of the instantaneous power factor of the motor and the corresponding dc value to predict the severity of the fault. The observation made by them is that fault severity factor (ratio) increases with the increase in the air gap eccentricity. The dynamic model of the machine is simulated for various dynamic eccentricity conditions (mixed eccentricity) and power factor fault severity factors are obtained. The power factor fault severity factor variation with the dynamic eccentricity indices is as shown in Figure 4.23.

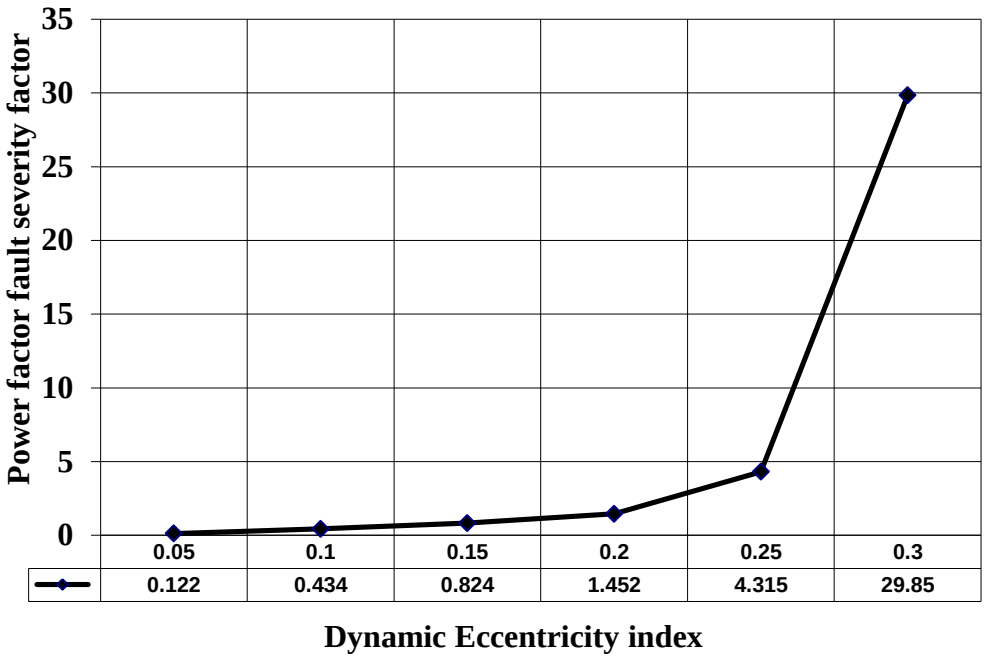

Figure 4.23 Power factor severity factor vs dynamic eccentricity index

From the Figure 4.23, it can be observed that as the dynamic eccentricity increases in the machine, power factor fault severity factor also increases. Hence, the slope of the power factor severity factor curve is a better fault severity indicator in field applications (please refer Figure 4.24).

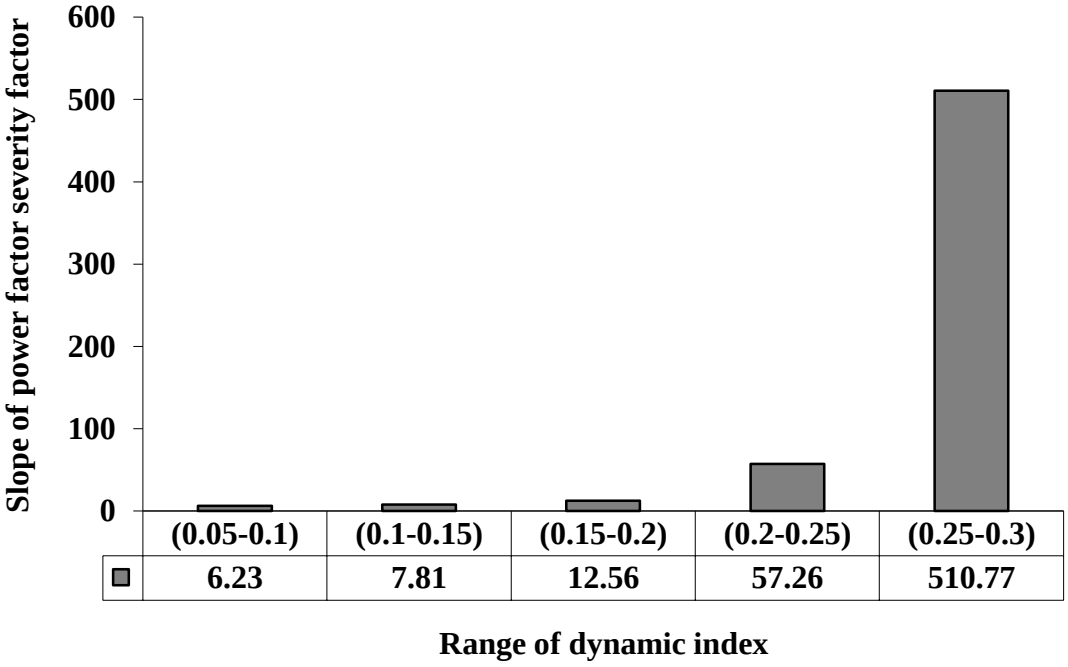

Figure 4.24 Slope of power factor severity factor curve

From Figure 4.24, it is inferred that the slope of the power factor severity curve contains more information about the severity of eccentricity fault in the machine and can be used for fault detection.

4.4.4 Instantaneous d-q current Signature Analysis

d-q components of stator currents are obtained by transforming stator currents in 3 phase form to 2 phase form using the Equations (3.16) and (3.17). The machine model is simulated for the uniform mixed eccentricity conditions (δ_s=0.3, δ_d=0.1). The stator current samples along with its d-q components are obtained and stored. PSD analysis is performed on the extracted data samples of d-q components of stator currents. The i_q and i_d current spectra obtained under this condition is compared with those of healthy condition in Figure 4.25.

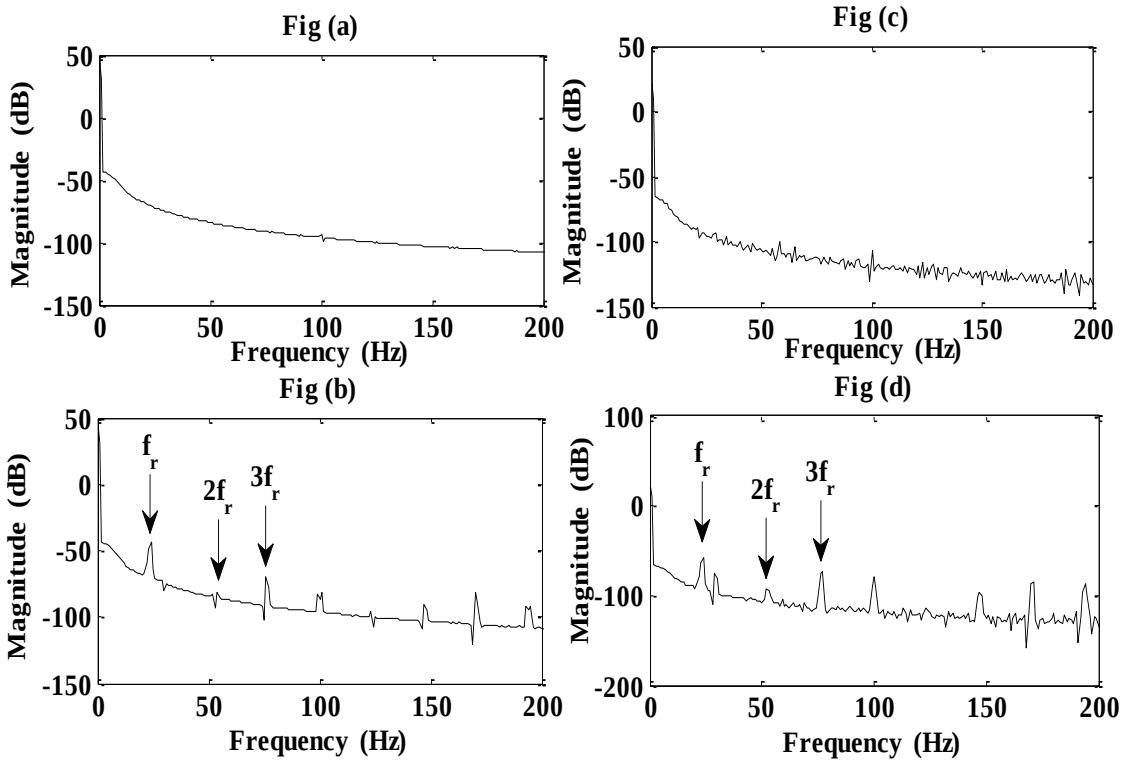

Figure 4.25 Current spectra under healthy and uniform eccentricity conditions (δ_s=0.3,δ_d=0.1)

Fig (a) i_{qs} current spectra –Healthy condition

Fig (b) i_{qs} current spectra – Eccentric condition

Fig (c) i_{ds} current spectra –Healthy condition

Fig (d) i_{ds} current spectra – Eccentricity condition

It can be seen from Figure 4.25 that both i_{qs} and i_{ds} current spectra contain f_r, $2f_r$, $3f_r$ ….components in them. Similarly current spectra are obtained for inclined eccentricity condition (δ_{s0}=0, δ_{s1}=0.3, δ_d=0.1) and are compared with those obtained under healthy conditions in Figure 4.26.

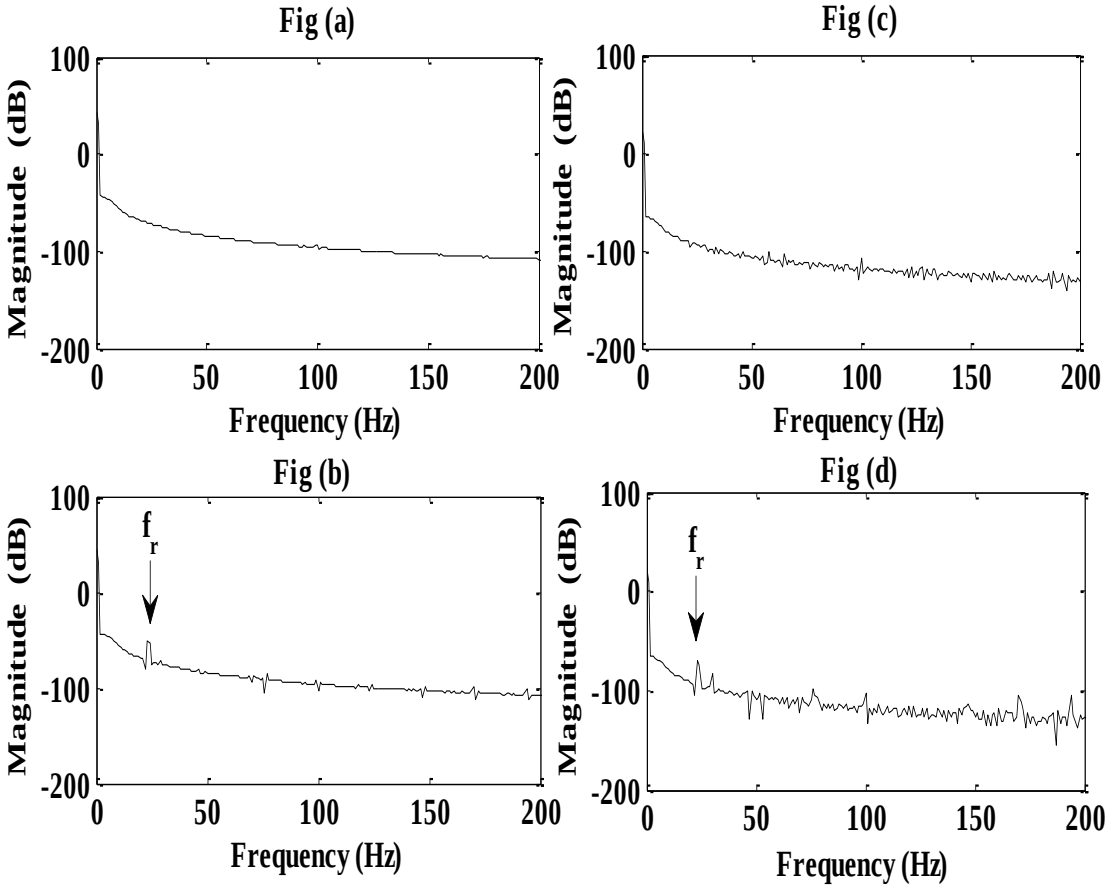

Figure 4.26 Current spectra under healthy and inclined eccentricity conditions (δ_{s0}=0, δ_{s1}=0.3, δ_d=0.1)

Fig (a) i_{qs} current spectra –Healthy

Fig (b) i_{qs} current spectra – Eccentricity

Fig (c) i_{ds} current spectra –Healthy

Fig (d) i_{ds} current spectra – Eccentricity

On comparing Figure 4.26 with that of Figure 4.25, it can be inferred that the magnitudes of eccentricity characteristic harmonics are less (severity of the fault is less) when the air gap eccentricity is non uniform throughout the length of the rotor.

Figure 4.27, shows the current spectra of i_{as}, i_{qs} and i_{ds} obtained by PSD analysis performed on the filtered (1kHz) machine data samples obtained by simulation of the machine model in which static eccentricities on two ends of the rotor are maintained at δ_{s0}=0 and δ_{s1}=0.2857. The machine suffers from dynamic eccentricity of 0.1.

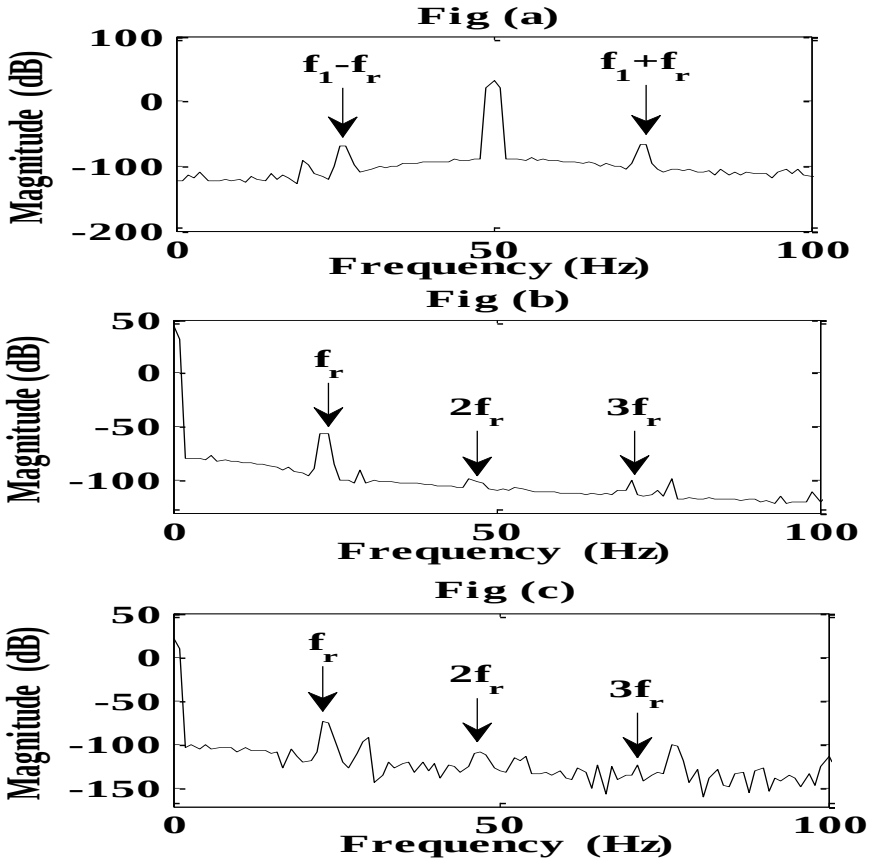

Figure 4.27 Current spectra Fig (a) i_{as} current spectra Fig (b) i_{qs} current spectra Fig (c) i_{ds} current spectra

It is seen from the stator phase A current spectra that it contains air gap non uniformity characteristic frequency components (f_1-f_r) (26 Hz) and (f_1+f_r) (74 Hz) and f_r (24Hz), 2f_r (47 Hz), 3f_r (71 Hz) components are present in d-q axis components of stator current extracted in synchronous reference frame.

The simulation of the model for different inclined static eccentricity conditions for a constant 10% dynamic eccentricity condition is carried out and data samples of stator phase A current, d-q components of stator currents are stored. The PSD analysis are performed on the stored data samples of i_{as}, i_{qs}, i_{ds} obtained from simulating the

machine model for four different conditions of inclined eccentricity. The frequency resolution is 1 Hz. The variation in amplitudes of (f_1-f_r) (26 Hz) and (f_1+f_r) (71 Hz) eccentricity related harmonic components in i_{as} current spectrum, amplitudes of f_r (24 Hz) component in i_{qs} and i_{ds} are plotted in Figure 4.28.

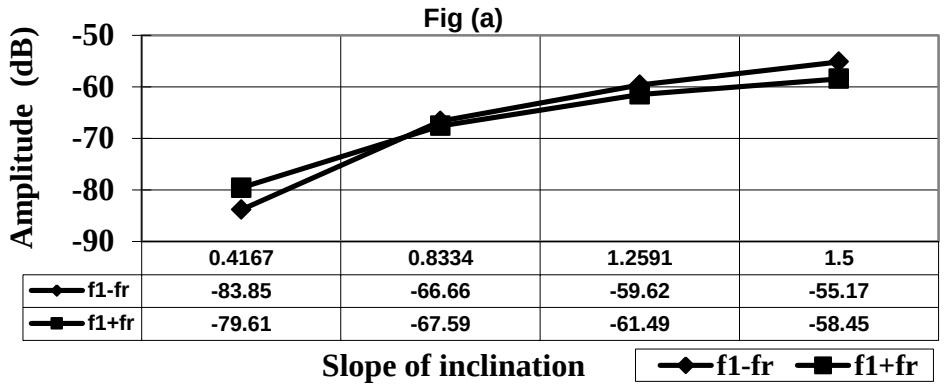

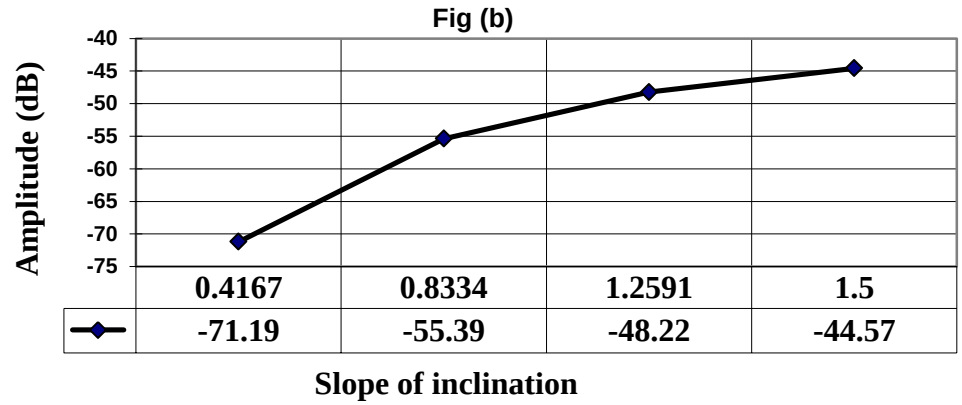

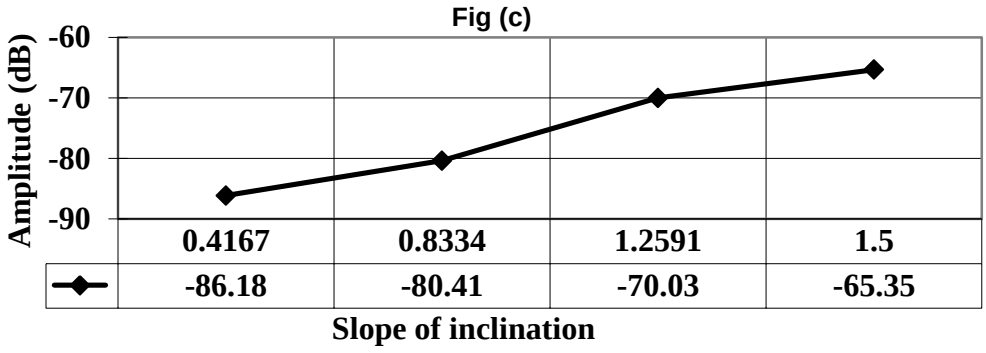

Figure 4.28 Variation of amplitudes of eccentricity characteristic harmonics

Fig (a) (f_1-f_r), (f_1+f_r) in i_{as} current spectrum with variation in slope of inclination

Fig (b) f_r in i_{qs} current spectrum with variation in slope of inclination of rotor

Fig (c) f_r in i_{qs} current spectrum with variation in slope of inclination of rotor

From the waveforms shown in Figure 4.28, it is observed that eccentricity characteristic frequency components amplitude increases with the increase in the inclined eccentricity level. Hence eccentricity characteristic frequency component f_r found in i_{ds}, i_{qs} components of stator currents can be used to predict the fault severity in the machine. It is also observed that amplitude of fundamental frequency component in i_{as} spectrum marginally decreases with the increase in inclined eccentricity level.

In the following Chapter, details of experimental set up developed in the laboratory as well as experimental results obtained to validate the modeling and simulation results are presented.

CHAPTER 5

5.0 DEVELOPMENT OF MOTOR ECCENTRICITY DETECTION SCHEME

From the mathematical equations derived and from simulating the machine model for different air gap eccentricity conditions, it is seen that d-q components extracted from the stator phase currents of an eccentric induction motor contains the eccentricity characteristic harmonics mf_r in it. Also it is shown in Chapter 4 that Eigen Values obtained from comparision of the frequency spectral components of stator current of the eccentric condition of the machine with those of healthy machine condition can be used to predict the fault severity in the machine. To validate the claims made in earlier chapters, experiments are conducted on an air gap eccentric machine in the laboratory. For this purpose, a custom made machine in which mixed air gap eccentricity can be created artificially is used in the laboratory. Frequency analysis is performed on the instantaneous power, stator current and its d-q components, for different conditions of eccentricity under various loading conditions of the machine. The experimental part has two parts: data acquisition of the stator currents for offline studies and data analysis of the acquired stator currents. The description of experimental set up along with the creation of eccentricity in the machine is given below.

5.1 Creation of artificial eccentricity in the machine

3 hp induction motor whose machine parameters are used for modeling is sent to workshop to fabricate the rotor mounting mechanism so that air gap eccentricity can be created artificially in the machine. The machine is a 4 pole, 50 Hz, 2.2 kW squirrel cage induction motor whose performance figures are given below:

Frame-100L, Efficiency-81%, cos ϕ-0.8, Rated speed-1410, Inertia-0.024 kgm^2

The chosen induction motor is a foot mounted type whose sectional view showing the front end bearing cap and rear end bearing cap is shown in Appendix IV-I. The changes made in the rotor mounting mechanism of the machine to create air gap eccentricity artificially in the machine are explained in the following sections.

5.1.1 Creation of static eccentricity

The machine is modified as shown in Figure 5.1.

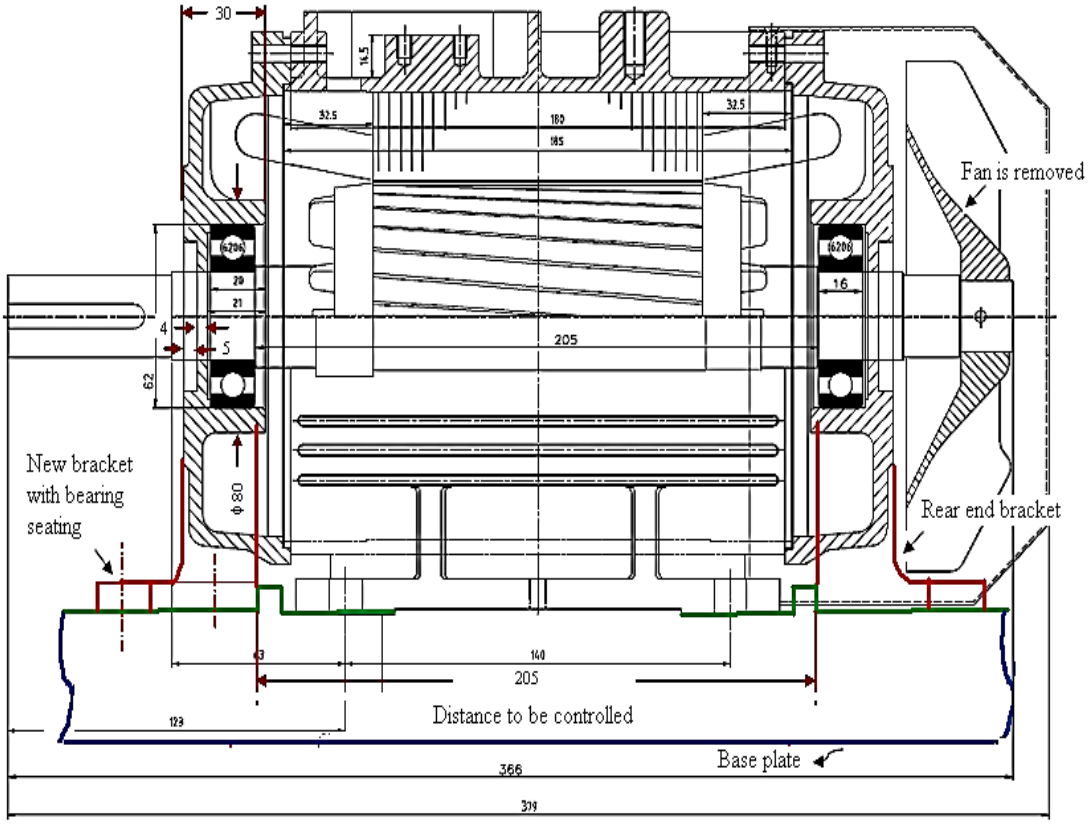

Figure 5.1 Sectional view of the machine with modifications.

The fan is removed and the machine is mounted on a base plate. Two L shaped brackets with shaft seating are placed on either side of the machine. The bracket design is as shown in Figure 5.2.

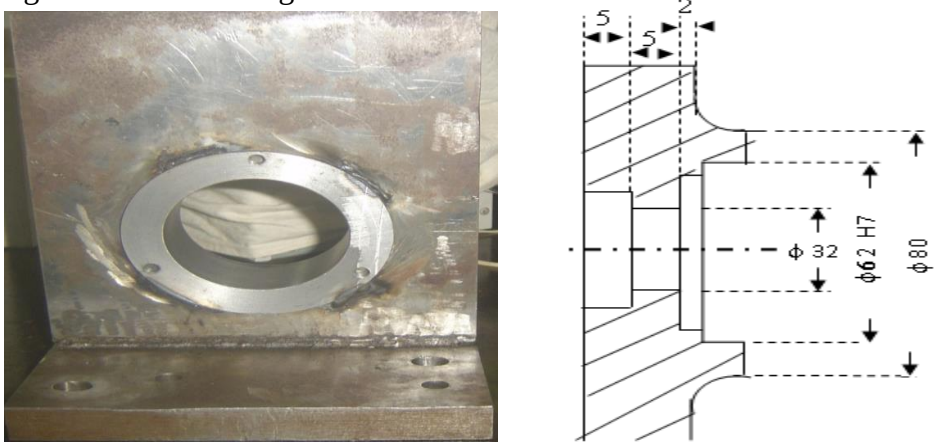

Figure 5.2 Bracket with shaft seating arrangement and its dimensions

These brackets are placed on the base plate. These brackets can be moved horizontally to create static eccentricity in the machine. Both the brackets can be moved simultaneously to create uniform static air gap eccentricity in the machine. By moving only one bracket horizontally, inclined static eccentricity is created in the machine. Circle gauge indicators and digital Vernier calipers are used to measure the bracket movement in the horizontal direction. The least count of both circle gauge indicator and Vernier caliper is 10μ.

5.1.2 Creation of dynamic eccentricity

Dynamic eccentricity is introduced by using bushings placed in these brackets. The bushing is as shown in Figure 5.3.

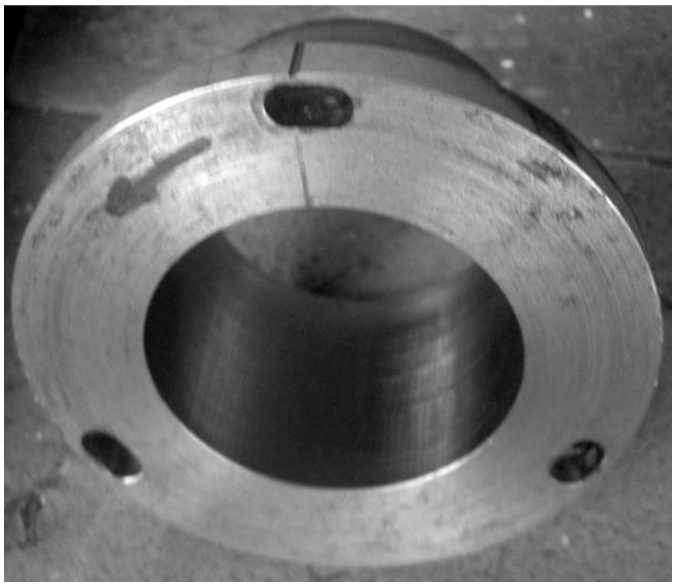

Figure 5.3 Bushing to be placed inside the shaft seating arrangement

Two bushings are placed in the brackets placed on either side of the rotor shaft of the motor. The arrow mark on the bushing indicates the direction in which it must be moved to create dynamic eccentricity in the machine. Both the bushings are rotated in opposite direction to create an air gap dynamic eccentricity in the machine. These bushings can be moved from true value position in the direction marked on it to vary dynamic air gap eccentricity in the machine. Figure 5.4 shows the front and back view of the bracket along with the bushing.

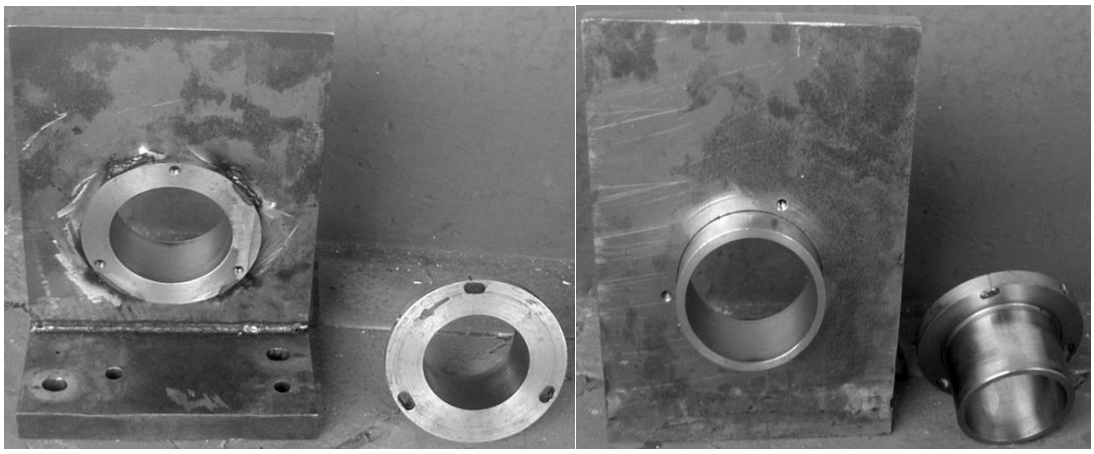

Figure 5.4 Front and back view of the bracket

The fabricated machine side view and top view are shown in Figure 5.5

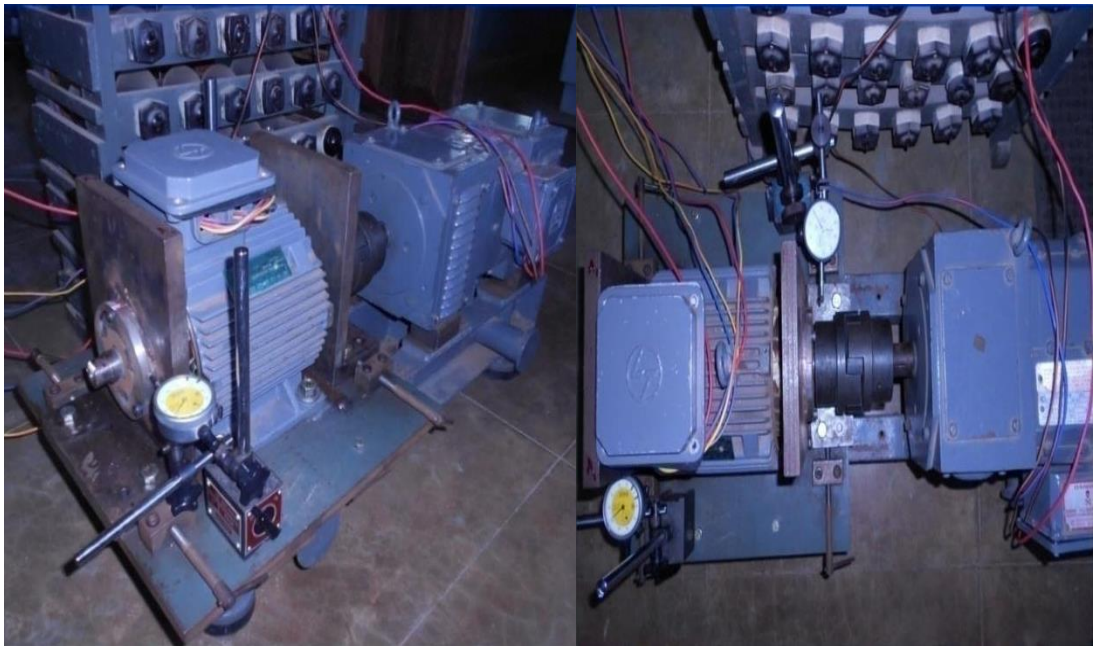

Figure 5.5 Modified machine (a) side view (b) top view

The experimental induction motor needs to be coupled to a load so that experiments are conducted on the machine for various loading conditions. Out of the two options: mechanical loading and electrical loading, electrical loading is chosen. A DC generator is procured which can be coupled to the motor under test. The rating of the DC machine is 11A, 220V, 2 KW, 1500rpm. Lamp loads are used for electrical loading. The experiments are conducted on the machine and stator currents data

samples are extracted using the Data Acquisition Hardware configured in the laboratory whose details are given in the next section.

5.2 Data Acquisition Hardware

The developed Data Acquisition System (DAS) should be capable of acquiring both stator phase currents and stator voltages and analyzing these data. Basically it should contain the following blocks:

- Sensors to sense both stator currents and stator voltages
- An analog interface between the sensors and data acquisition card
- A personal computer acting as a host

and is as shown in Figure 5.6.

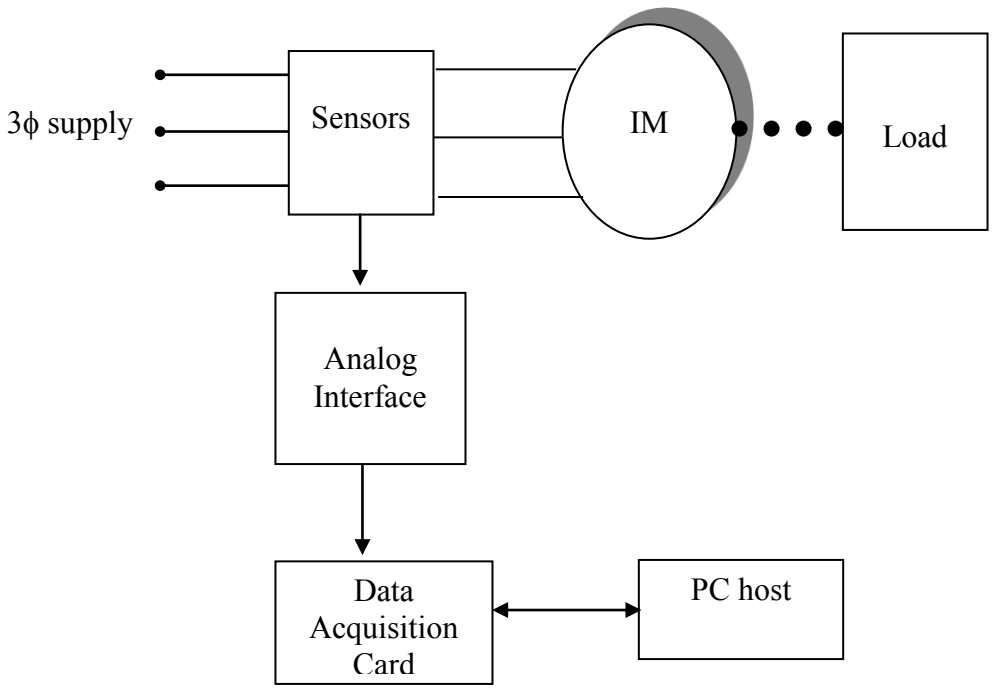

Fig 5.6 Data Acquisition block diagram

The experimental machine is a 2.2kW, 3 hp, 400/415V, 50Hz, 3ϕAC, 1500rpm, 4 pole squirrel cage induction motor which is coupled to a DC generator. Lamp loads are connected across the generator to load the motor-generator set.

To extract the air gap eccentric characteristic harmonics from the instantaneous stator currents and its d-q components, there is a need to acquire the

stator phase currents. Each stator phase winding is designed to carry full load current 2.77 A rms. During starting of the machine, primary winding of the transducer has to carry approximately 7-8 times the full load current (approximately 22.16 A rms). Hence current transducers should have a primary winding whose measuring peak current rating should be more than 32 A (max peak current). Conversion ratio of the current transducer should be such that core will not saturate due to very high current during starting of the machine. The eccentricity characteristic harmonics in the stator currents can be computed using the Equation $\left| f_1 \pm m f_r \right|$. The fundamental frequency f_1 is 50Hz. The expected rotor speed frequency f_r under full load condition is around 23.5 Hz. As the requirement is to compute only side band low frequency components around the fundamental, it is required for the current samples to carry frequency components up to 1kHz. Based on the requirement, the following decisions are taken

- Signal acquisition must be done at a sampling frequency of 20 kHz.
- Signal conditioning must be done by passing through an antialiasing analog filter having cut off frequency 10kHz.
- Further signal conditioning is to be done by passing through a digital filter having cut off frequency of 1kHz.

Hence three LA 55-P Hall Effect Current Transducers are used to extract three phase stator currents as they have conversion ratio as high as 1:1000 and frequency resolution of 200 kHz. Primary winding peak current rating of the transducer is 50A. Three sets of LA 55-P Hall Effect Current transducers placed in each of the stator phases are used to extract three stator phase currents in the laboratory. For more details about the LEM current transducer LA 55-P, please refer Appendix V.

The analog interface block should contain the following units

(i) Stator currents into equivalent voltages conversion block.

(ii) Signal conditioning block for both stator currents and voltages.

Under full load running conditions of the machine, secondary winding of current transducer will be carrying 2.77 mA rms. The stator phase currents in mA flowing in the secondary of current transducers need to be converted into equivalent voltages so that it can be acquired by the data acquisition card. To achieve current to voltage conversion, extracted stator phase currents have to be passed through three

sets of standard resistors and the precision of conversion should be very high. The voltage measured range for 0-2.77 mA should be within 0-5V DC.

NI based Current Input, High-Voltage Terminal Block SCXI-1338, has the capability to measure from both current and voltage sources. It contains a precision 249 Ω, 0.1%, 10ppm, ¼ W resistors, hence can be used for current to voltage conversion. It also has the ability to measure current from 0-20 mA and 4-20 mA sources.

To convert the voltage read by the SCXI module to the actual current being measured, the following formula can be used:

current = measured voltage / 249

The voltage measured for a 4-20 mA current source is in the range of 0.996-4.98 V DC. As the maximum current carried by the secondary winding of the transducer is 2.77 mA, SCXI-1338 can be used for current to voltage conversion. For more details about SCXI-1338, please refer Appendix V.

At the same time, three phase stator voltages (line voltages) supplied to the machine also needs to be acquired. These are extracted to detect the harmonics due to asymmetry in the supply voltages. The chosen machine for experiment has rated voltage 400/415 V. Three stator phase voltages have to be sensed by using voltage sensors. The voltage sensors should be capable of measuring voltage up to 587 V DC ($\sqrt{2}$ x 415 V).

For this purpose, TBX 1316, High-Voltage Attenuator Terminal Block is used to sense three stator phase voltages as it can be used to measure high-voltage signals of up to 600V. It has 8 different input channels and has a fixed attenuation ratio of 200:1. The TBX-1316 is a lockable shielded metal enclosure with a built-in high-voltage attenuator. Please refer Appendix V for more details.

Three stator phase currents (converted into equivalent voltages in SCXI-1338) and three stator phase voltages (sensed by TBX-1316) needs to be passed through an analog anti aliasing filter so that they are free from noises. Hence signal conditioner unit SCXI-1125 is procured as it has the following features

- It is a jumper less eight-channel isolated analog input conditioning module with programmable gain and filter settings on each channel (as 6 signals (three current and three voltage signals)) have to be signal conditioned.

- Each channel has 12 programmable gain settings from 1 to 2000 and two programmable filter settings of either 4 Hz or 10 kHz (As the sampling frequency chosen is 20 kHz and cut off frequency of the filter can be chosen as 10 kHz to meet the Nyquist criteria). SCXI-1125 block diagram is as shown in Figure 5.7

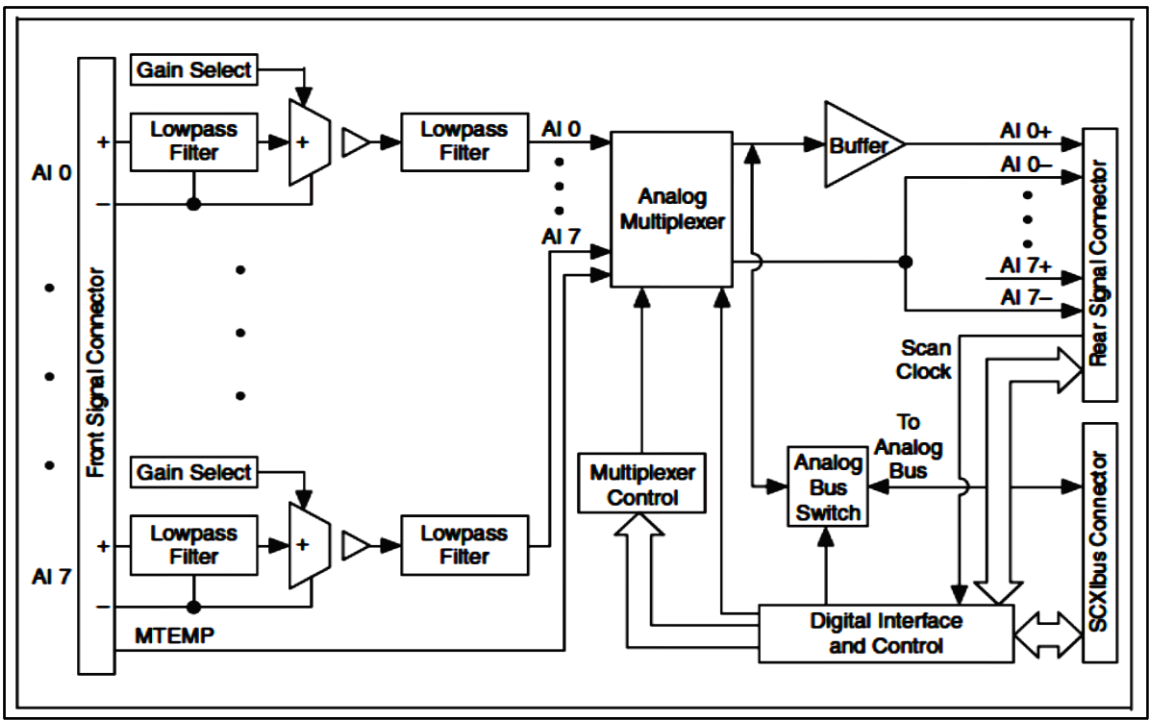

Figure 5.7 SCXI-1125 block diagram (courtesy: www.NI.com)

The SCXI-1125 provides two filtering stages with an overall response of a four-pole Butterworth filter. Also it has an added advantage is that the cutoff frequency of the filter can be controlled through software.

- The SCXI-1125 supports both multiplexed and parallel output modes of operations. Please refer Appendix V for more information.

To mount both the SCXI-1125 and SCXI-1338, a housing unit is required. SCXI-1000 is chosen as interfacing unit between signal conditioning unit and data acquisition card. Both SCXI-1125 are housed in SCXI-1000 Chassis as it provides low-noise signal conditioning environment. The SCXI-1000 chassis is a rugged, compact 4-slot AC-powered chassis to house SCXI modules. For more information, please refer Appendix V.

Both the voltage and current signals have to be converted into digital signals using A/D converter. DAQ card 6024-E is procured as it has the following features

●It makes use of 12 bit A/D converter with programmable gain settings of 0.5, 1.0,10 or 100 and can provide high precision. Precision is defined as the value of 1 LSB of the 12-bit ADC; that is, the voltage increment corresponding to a change of one count in the ADC 12-bit count. Precision with which data conversion takes place for different gain setting are given below

Gain	Input Range	Precision
0.5	–10 to +10 V	4.88 mV
1.0	–5 to +5 V	2.44 mV
10.0	–500 to +500 mV	244.14 µV
100.0	–50 to +50 mV	24.41 µV

●Sampling rate 200 kS/s is guaranteed (as the requirement is 20 kS/s in the work).

●The 6024E features 16 channels of analog input, two channels of analog output, a 68-pin connector and eight lines of digital I/O.

Figure 5.8 shows the internal block diagram of DAQ 6024-E.

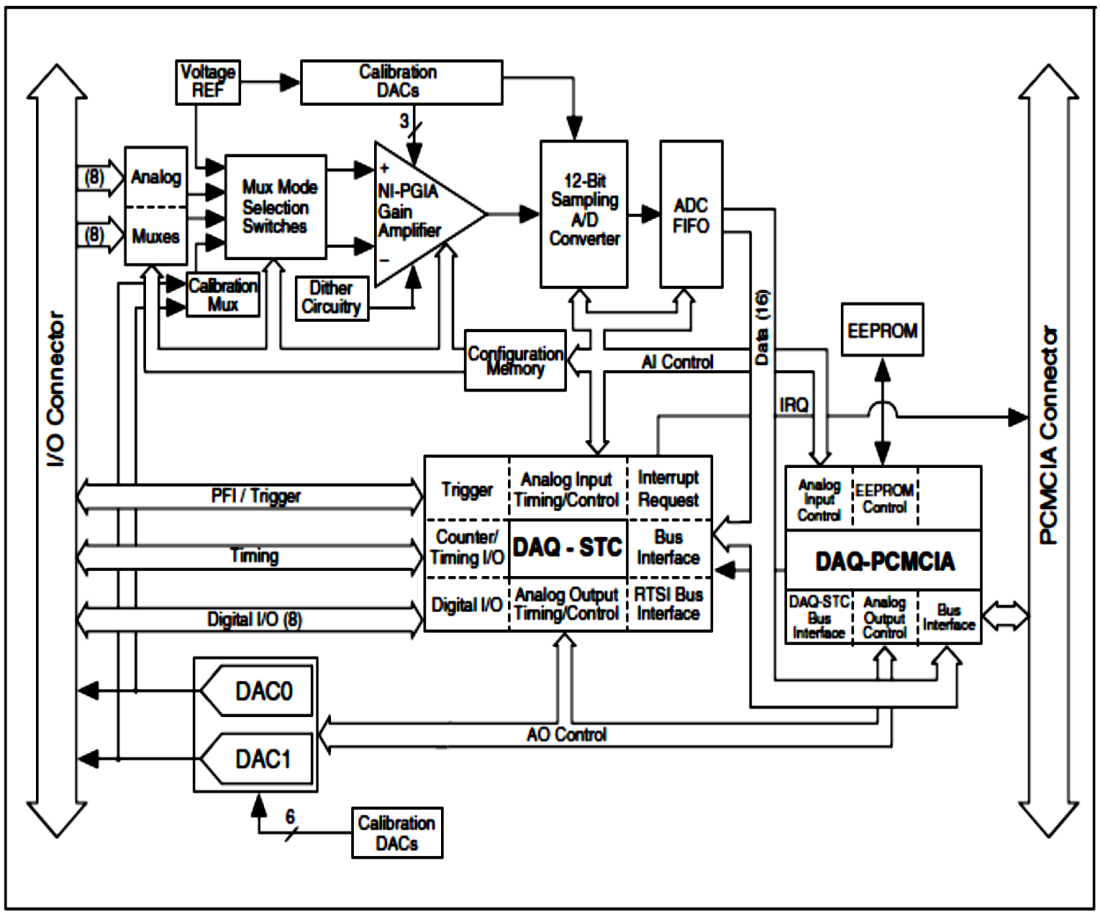

Figure 5.8 Block diagram of DAQ 6024E (courtesy: www.ni.com)

This device has two channels of analog output voltage at the I/O connector. The bipolar range is fixed at ±10 V. The devices contain eight lines of digital I/O for general-purpose use and each line for either input or output is software configurable.

The signal conditioned current and voltage signals are acquired using a Data Acquisition (DAQ) card 6024-E embedded in CPU. For more detailed information about transfer characteristics and amplifier characteristics of DAQ card, please refer Appendix V.

Using all the units described above in the section, Data Acquisition System (DAS) is configured and developed DAS in the laboratory to acquire stator currents and the applied voltages of the three phase squirrel induction machine is shown in Figure 5.9.

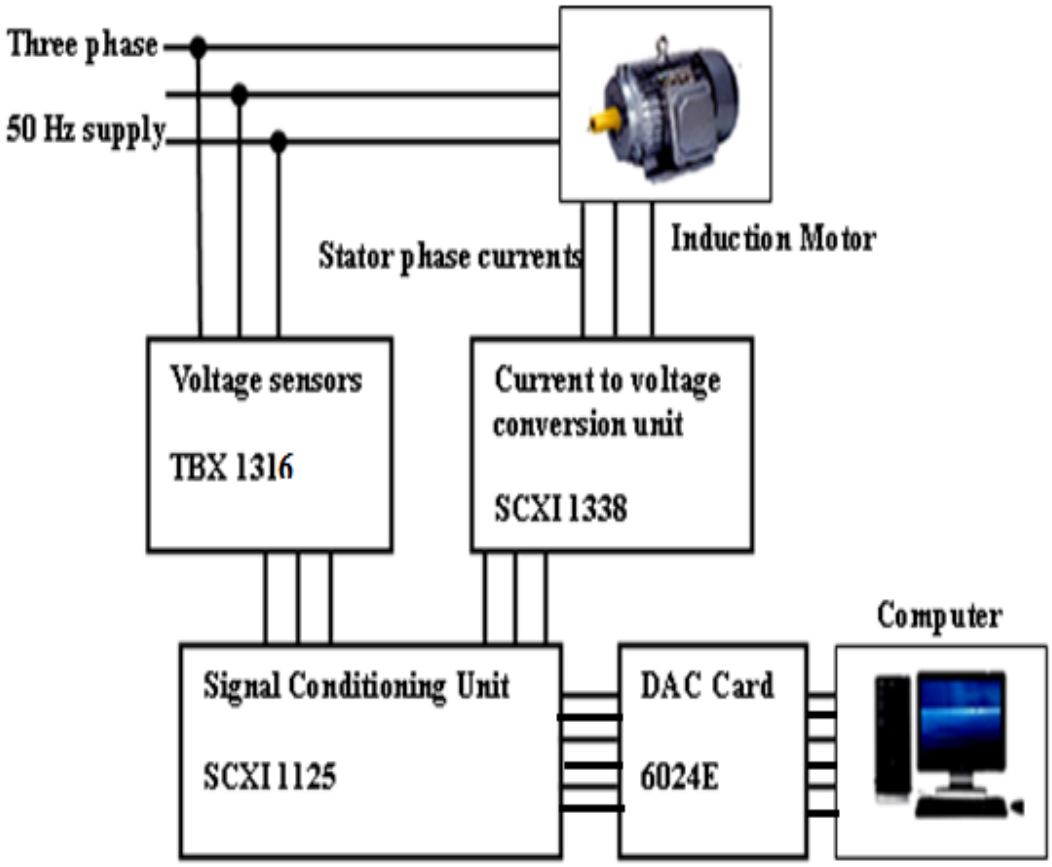

Figure 5.9 Data Acquisition System- block diagram

The experimental hardware set up built in the laboratory to acquire 3 stator phase currents and 3 stator phase voltages (line voltages because machine is connected in delta) are as shown in Figure 5.10.

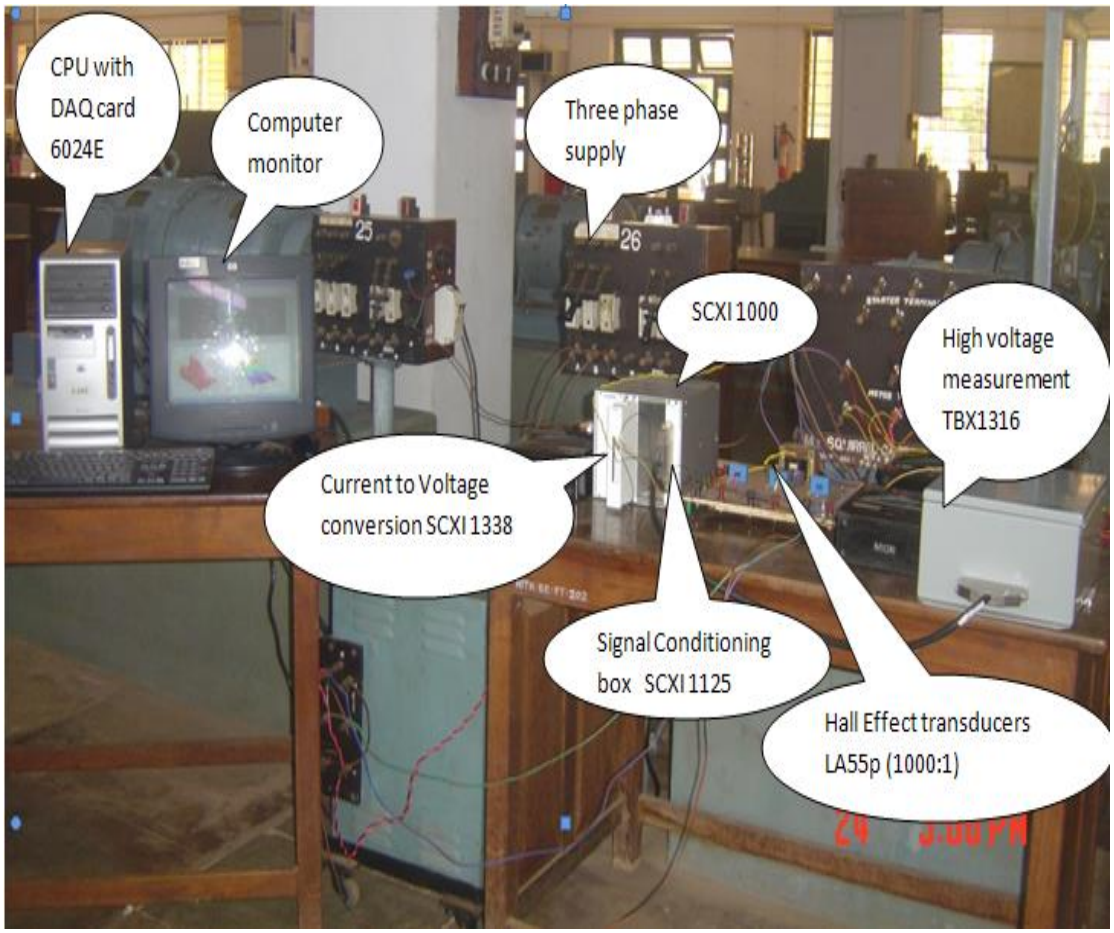

Figure 5.10 Data acquisition experimental set up

The data acquisition is done using configured using NI Hardware set up and processing of data is done using LabView software whose details are given in the next section.

5.3 Data acquisition software

The current and voltage data samples should be acquired and stored for offline studies and can be used for further analysis. The software must be capable of both acquiring and analysing the data. Using LabVIEW software, these data samples are acquired and analysed in the Personal Computer (PC). It features interactive graphics, a state-of-the-art user interface, and a powerful graphical programming language.

Data acquisition program is used to perform real time current and voltage monitoring, detection and data recording whereas data analysis program is for post acquisition data analysis. The NI-DAQ driver software DAQmx-8.9 is used which is compatible with the DAQ device for data acquisition. It has an extensive library of functions that can be called from the user application programming environment. The LabVIEW Data Acquisition VI Library, a series of virtual instruments for using LabVIEW with National Instruments DAQ hardware, is included with LabVIEW. The LabVIEW Data Acquisition VI Library is functionally equivalent to NI-DAQ software.

5.4 Development and performance evaluation of eccentricity detection schemes

The experiments are conducted on the machine under balanced supply voltage conditions. The stator phase current and voltage data samples are extracted at sampling frequency of 20 kHz. They are stored in excel sheet as .lvm files for off line studies using LabVIEW software VI as shown in Appendix VI-1. Stator currents are used to generate its d-q components in synchronous reference frame using the developed VI as shown in Appendix VI-2.

The machine is run under full loading condition. The instantaneous i_q and i_d current waveforms obtained from stator currents of the machine having

- Inclined static eccentricity of 0% eccentricity at one end (coupling end) and 28.57% eccentricity at the other end of the rotor and inherent dynamic eccentricity.
- Inclined static eccentricity of 0% eccentricity at one end (coupling end) and 51.43% eccentricity at the other end of the rotor and inherent dynamic eccentricity.

The obtained aveforms are as shown in Fig 5.11. The d-q components of the stator currents of a healthy machine fed from a balanced 3 phase sinusoidal three phase supply will be pure DC if they are extracted in synchronous reference frame. It is shown in earlier Chapters by both modeling-simulation and mathematical expressions that they contain harmonics if they are extracted from the eccentric machine. From the obtained waveforms it is seen that i_d and i_q will contain a DC component but it is superimposed with oscillations produced by the presence of eccentricity characteristic harmonics in them.

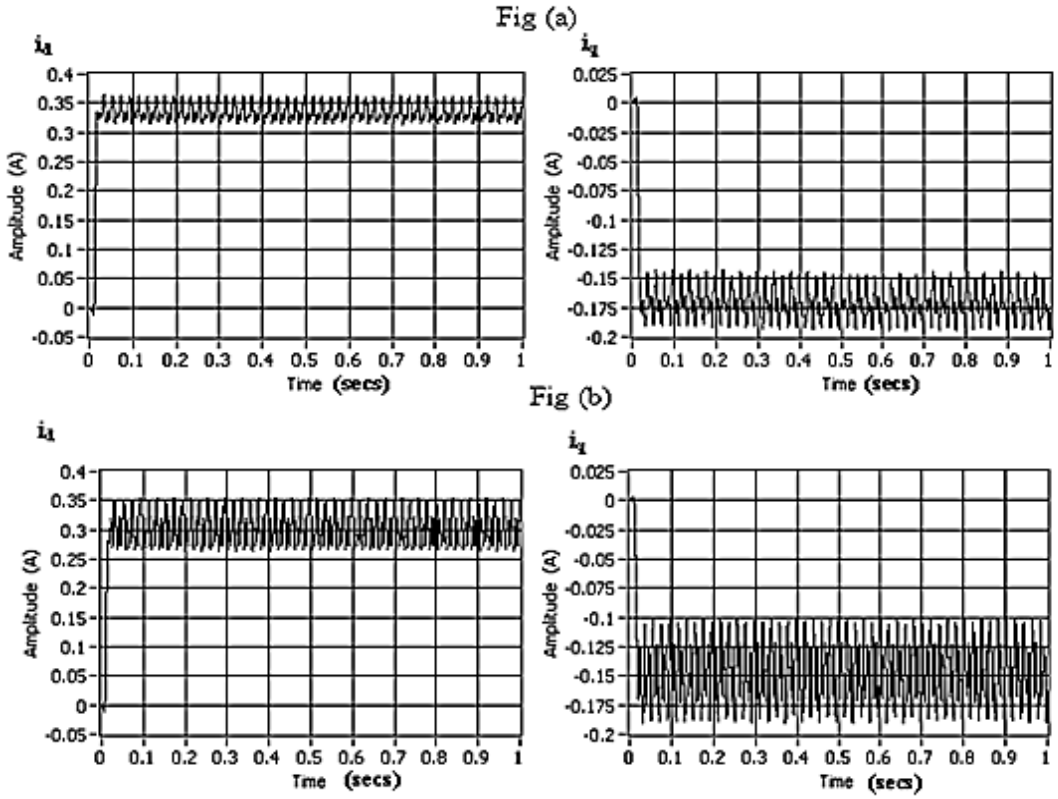

Figure 5.11 i_d and i_q components of stator currents Fig (a) inclined static eccentricity of slope 0.8333 (k=2.3809*) Fig (b) inclined static eccentricity of slope of 1.5 (k=4.2857*)

(*k value in $\delta_s(z)=\delta_{s0}+kz$)

On comparing Fig (b) with Fig (a), it can be noticed that the oscillations in the waveforms have increased with the increase in eccentricity level. Also it is observed that the amplitude of oscillation increases with the increase in inclined eccentricity.

5.4.1 Eccentricity fault detection by eccentricity characteristic harmonics in stator current and its d-q components

Stator phase A current spectrum, d-q components of stator current spectrum obtained from conducting experiments on the machine suffering from inclined static eccentricity of slope 2.3809 (inclined static eccentricity of 0% eccentricity at one end and 28.57% eccentricity at the other end of the rotor) are as shown in Figure 5.12.

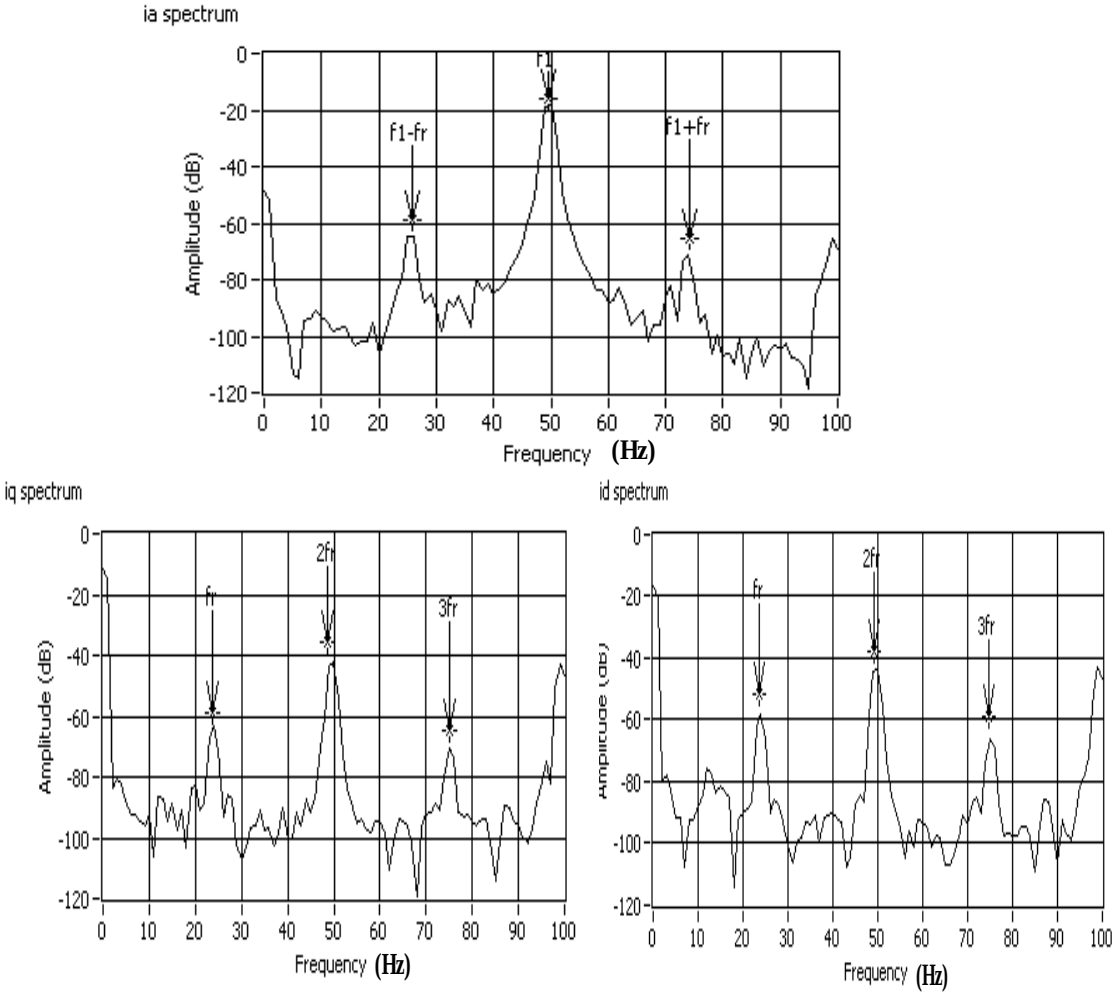

Figure 5.12 i_a, i_q and i_d current spectra

From Figure 5.12, it can be seen that mixed eccentricity related harmonics (f_1-f_r), (f_1+f_r) (lower and upper side band frequencies respectively) in i_a spectra, f_r, $2f_r$, $3f_r$ components in i_q and i_d spectra are present.

For different loading conditions, experiments are conducted on the eccentric machine (with mixed eccentric condition of inclined static eccentricity of 0% eccentricity at one end and 28.57% eccentricity on the other end of the rotor and inherent dynamic eccentricity). Table 5.1-5.3 gives the comparison between theoretical and experimental values of eccentricity related harmonic components found in the stator phase A current for different loading conditions on the motor.

Table 5.1 Eccentricity related characteristic components in current spectra for the eccentric machine under no load condition

Characteristic frequency components	No load	
	Equation (2.16)	Experimental (PSD)
f_1-2f_r (Hz)	0.21	0.35
f_1-f_r (Hz)	**25.07**	**24.98**
f_1+f_r (Hz)	**74.79**	**74.95**
f_1+2f_r (Hz)	99.65	99.58

Table 5.2 Eccentricity related characteristic components in current spectra for the eccentric machine under 85% load condition

Characteristic frequency components	85% load	
	Equation (2.16)	Experimental (PSD)
f_1-2f_r (Hz)	1.57	0.7
f_1-f_r (Hz)	**25.68**	**25.69**
f_1+f_r (Hz)	**73.9**	**73.90**
f_1+2f_r (Hz)	98.01	99.23

Table 5.3 Eccentricity related characteristic components in current spectra for the eccentric machine under full load condition

Characteristic frequency components	Full load	
	Equation (2.16)	Experimental (PSD)
f_1-2f_r (Hz)	2.05	0.7
f_1-f_r (Hz)	**26.02**	**26.04**
f_1+f_r (Hz)	**73.96**	**73.9**
f_1+2f_r (Hz)	97.93	99.23

From the Tables 5.1-5.3, it is inferred that theoretically obtained air gap eccentric related side band frequency components at (f_1-f_r) and (f_1+f_r) in stator phase A current of the motor match with those of experimental values.

Tables 5.4-5.6 lists eccentricity related frequency components f_r, $2f_r$, $3f_r$ in the d-q components of stator currents and gives the comparison between the theoretically calculated values with those of experimental for the machine under no load, 85% load and full load conditions respectively.

Table 5.4 Eccentricity related characteristic components in i_q and i_d current spectra for no load condition.

Characteristic frequency components	No load		
	Equation (mf_r=mNr/60)	Experimental (PSD)	
		i_q	i_d
f_r (Hz)	**24.86**	**25**	**25**
$2f_r$ (Hz)	49.72	50	50
$3f_r$ (Hz)	74.58	75	75

Table 5.5 Eccentricity related characteristic components in i_q and i_d current spectra for 85% load condition

Characteristic frequency components	85% load		
	Equation (mf_r=mNr/60)	Experimental (PSD)	
		i_q	i_d
f_r (Hz)	**24.11**	**24.21**	**24.21**
$2f_r$ (Hz)	48.22	50	50
$3f_r$ (Hz)	72.33	72.52	72.52

Table 5.6 Eccentricity related characteristic components in i_q and i_d current spectra for Full load condition

Characteristic frequency components	Full load		
	Equation ($mf_r=mNr/60$)	Experimental (PSD)	
		i_q	i_d
f_r (Hz)	**23.97**	**23.95**	**23.95**
$2f_r$ (Hz)	47.94	50	50
$3f_r$ (Hz)	71.91	76.05	76.05

From the Tables 5.3-5.6, it can be observed that eccentricity characteristic components extracted from PSD analysis match very well with those computed theoretically only in case of no load running conditions of the machine. It is also seen that the rotor frequency components f_r found in the i_q and i_d current spectrum in all three cases agree with those computed using the equation. Hence it can be used to predict the presence of air gap eccentricity in the machine. Hence it can be used as an index to detect mixed air gap eccentricity in the machine.

The variation of amplitude of (f_1-f_r), (f_1+f_r), f_1 in stator phase current i_a spectra, f_r in i_q and i_d spectra with the variation of mixed eccentricity level is shown in Figure 5.13. It is also observed that the magnitude of the fundamental frequency component in the current spectra will vary marginally with increase in mixed eccentricity level in the machine.

The results obtained by experimentation validate the fact that amplitude of (f_1-f_r), (f_1+f_r) components of stator currents increases with the increase in the level of inclined eccentricity. From experimental results, it is also observed that the amplitude of f_r component in i_q and i_d increases with increase in the eccentricity level. Hence it can be used to characterise the eccentricity fault in the machine.

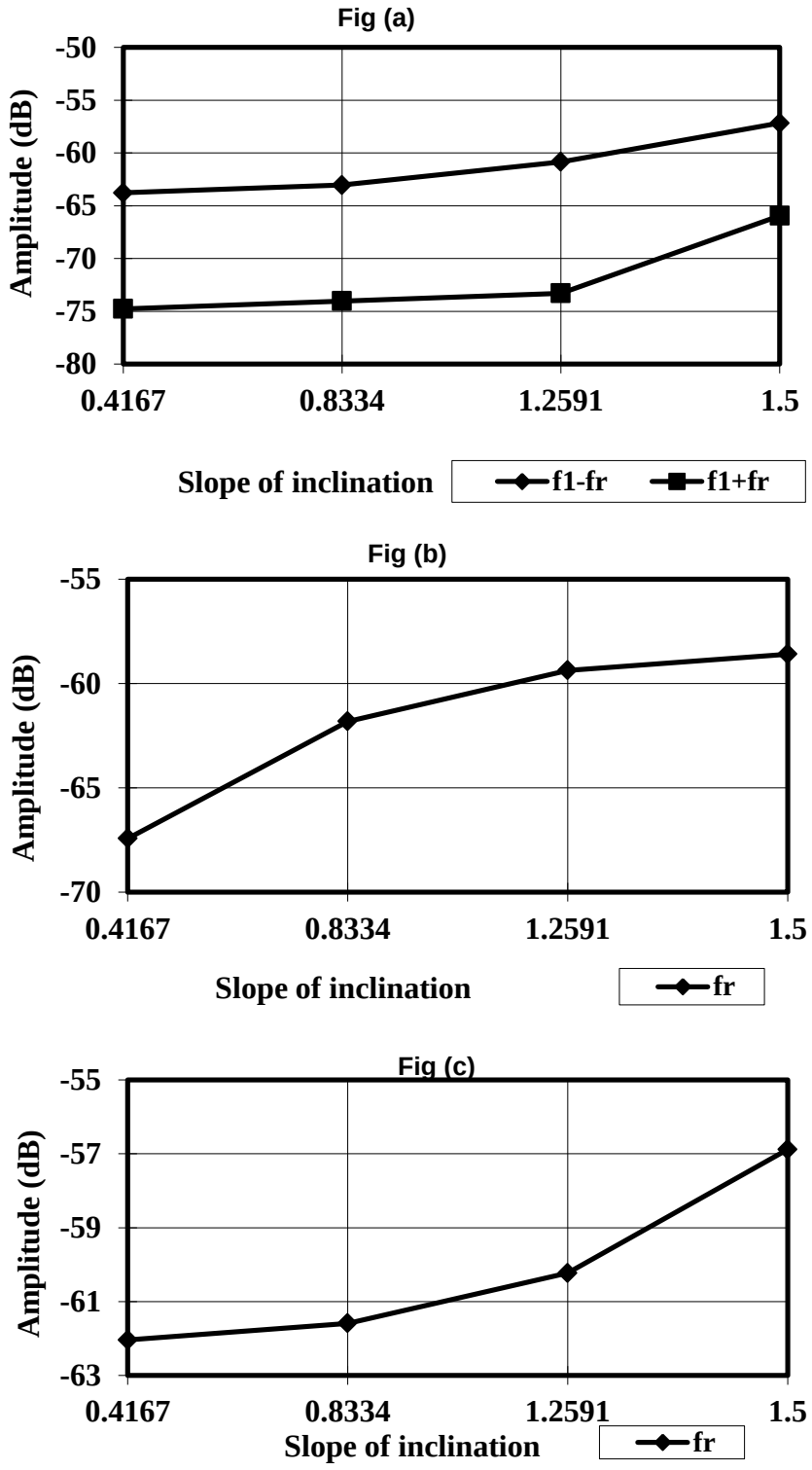

Figure 5.13 Variation of amplitudes of eccentric characteristic harmonics

Fig (a) (f_1-f_r), (f_1+f_r) in i_{as} current spectrum with variation in slope of inclination

Fig (b) f_r in i_{qs} current spectrum with variation in slope of inclination of rotor

Fig (c) f_r in i_{qs} current spectrum with variation in slope of inclination of rotor

5.4.2 Eigenvalue based fault severity detection

In Chapter 4, it is shown that the Eigenvalues computed from comparision of eccentricity characteristic harmonics magnitude with those of healthy condition (or installation condition) can be used as an indicator to assess the air gap non uniformity fault in the machine. To validate this claim made in Chapter 4, experiments are carried out in the laboratory on the air gap eccentric machine in the laboratory.

The fabricated machine suffers from inclined static eccentricity of 0% at one end and 14.28% (slope of inclination- 0.4167) on the other end and has inherent dynamic eccentricity. This machine is run under full load condition for balanced supply voltages of 400V. The stator current samples are extracted under this condition and Power Spectral Density analysis is performed on these samples to obtain the magnitude of air gap eccentricity harmonics (f_1-f_r), (f_1+f_r) and (f_1+2f_r).

Similarly experiments are conducted on the machine under following eccentricity conditions of the machine.

(i) static inclined eccentricity of 0% at one end and 28.57% on the other end (slope of inclination- 0.8334) and inherent dynamic eccentricity.

(ii) static inclined eccentricity of 0% at one end and 42.86% on the other end (slope of inclination- 1.2591) and inherent dynamic eccentricity.

(iii) static inclined eccentricity of 0% at one end and 51.43% on the other end (slope of inclination- 1.5) and inherent dynamic eccentricity.

(f_1-f_r), (f_1+f_r) and (f_1+2f_r) eccentric characteristic harmonics magnitudes are found from the stator phase A current spectra for various inclined static eccentric conditions of the machine.

(f_1-f_r), (f_1+f_r) and (f_1+2f_r) eccentric characteristic harmonics magnitudes obtained for each of the above said eccentric conditions of the machine are compared with those obtained for the initial condition of the machine. Covariance matrix is formed for each case and Eigenvalues are found

The obtained Eigenvalue for various inclined static eccentric conditions represented by the slope of inclination is as shown in the Figure 5.14.

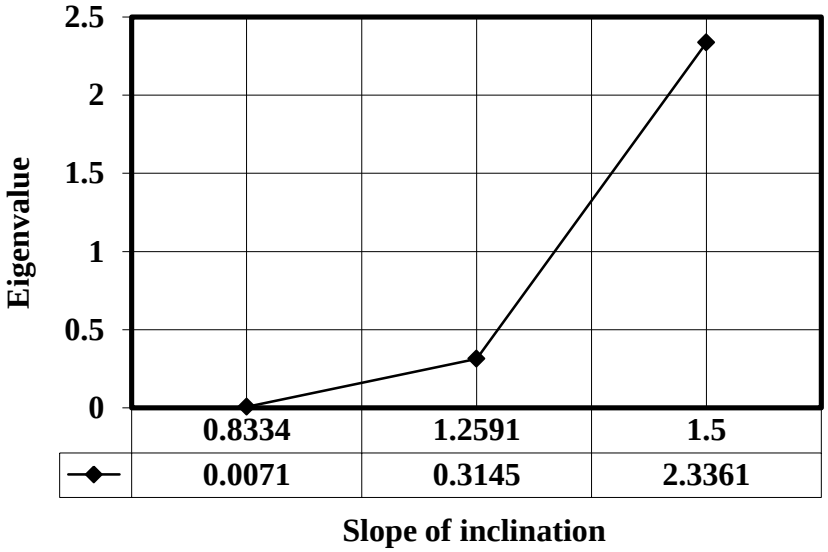

Figure 5.14 Variation of Eigenvalue with static eccentricity (experiment)

From Figure 5.14, it can be seen that the Eigenvalue increases with the increase in the mixed eccentricity level in the machine. In Chapter 4, the response of the model (whose machine parameters are same as those of the experimental machine) for various mixed uniform eccentricity conditions are studied. The Eigenvalues obtained by simulation (please refer Figure 4.19) shows similar behaviour as those obtained by experimentation.

To validate the experimental results, dynamic machine model is simulated for the same experimental inclined static eccentricity conditions keeping the dynamic eccentricity at 10%. The Eigenvalues are computed and its variation with static eccentricity is shown in Figure 5.15.

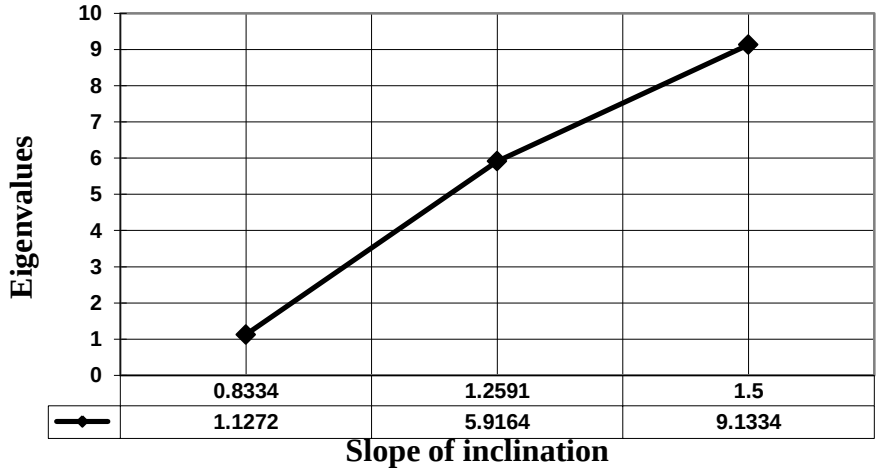

Figure 5.15 Variation of Eigenvalue with static eccentricity (simulation)

By comparing Figures 5.15 and 5.16, it is seen that experimental and simulation results show similar trend that Eigenvalues increase with increase in mixed eccentricity level in the machine. Hence this can be used as an indicator to predict the eccentricity fault severity in the machine. It is a better indicator compared to other severity fault indicators as it is obtained by comparing several eccentricity characteristic harmonics magnitudes with those of installation

5.4.3 Laboratory experiments to evaluate eccentricity detection techniques

Dynamic eccentricity is created by moving the bush by 0.5mm marked on the bush and inclined static eccentricity is created by moving the plate by 0.1mm (28.57%) on the free end of the rotor. PSD analysis is performed on the stator phase A current i_a and the spectrum are obtained for no load, 72.7% loaded, full load conditions and are shown in Figure 5.16.

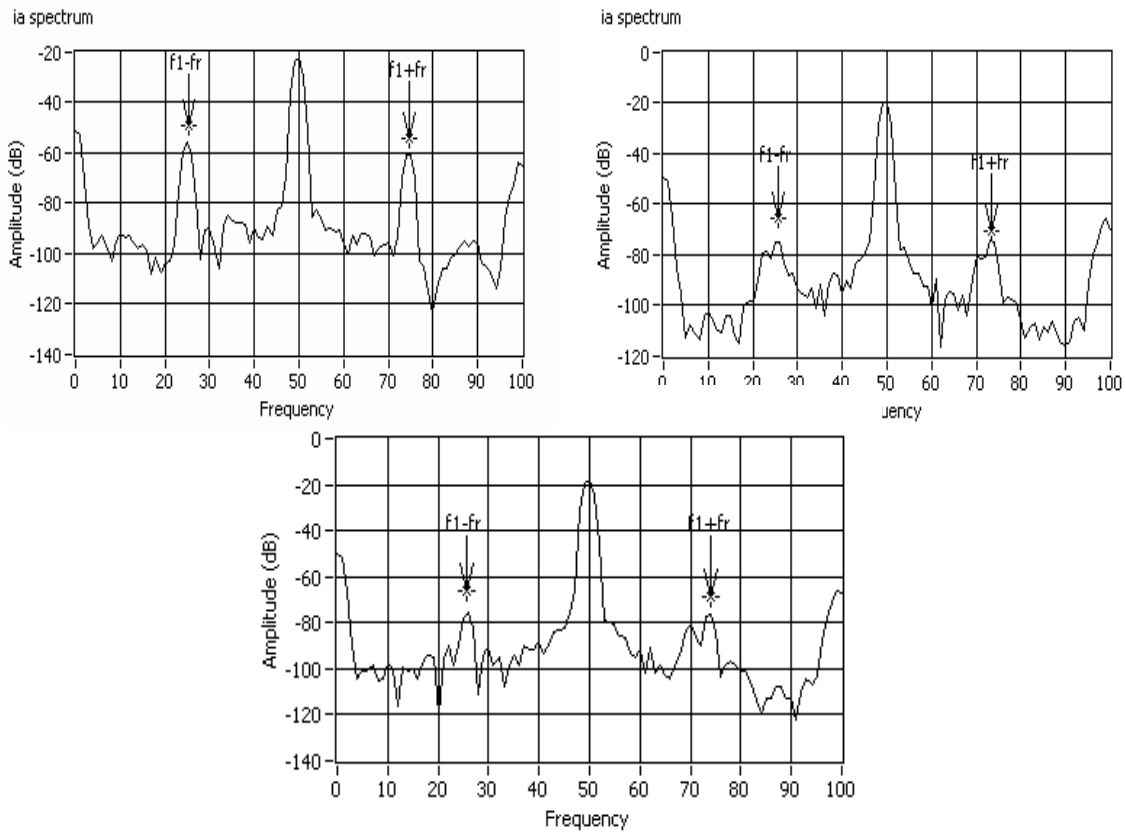

Figure 5.16 Stator phase A current spectra under no load, 72.7% and full load conditions

Theoretical and experimental eccentricity characteristic frequency components are compared in the Tables 5.7. Theoretically, frequency of rotor speed f_r is calculated by the expression $N_r/60$ where N_r is the rotor speed.

Table 5.7 Eccentricity characteristic frequency components in stator phase current i_a

Eccentricity characteristic frequency	No load		72.7% load		Full load	
	Equation	PSD	Equation	PSD	Equation	PSD
f_1-f_r (Hz)	24.92	25	25.47	25.32	25.84	25.6
f_1+f_r (Hz)	74.48	74.35	73.47	73.38	73.6	73.7
f_1+2f_r (Hz)	99.28	99.35	97.47	98.7	97.48	99.0

Similarly PSD analysis is performed on the extracted d-axis component of stator currents and spectra obtained are shown in Figure 5.17.

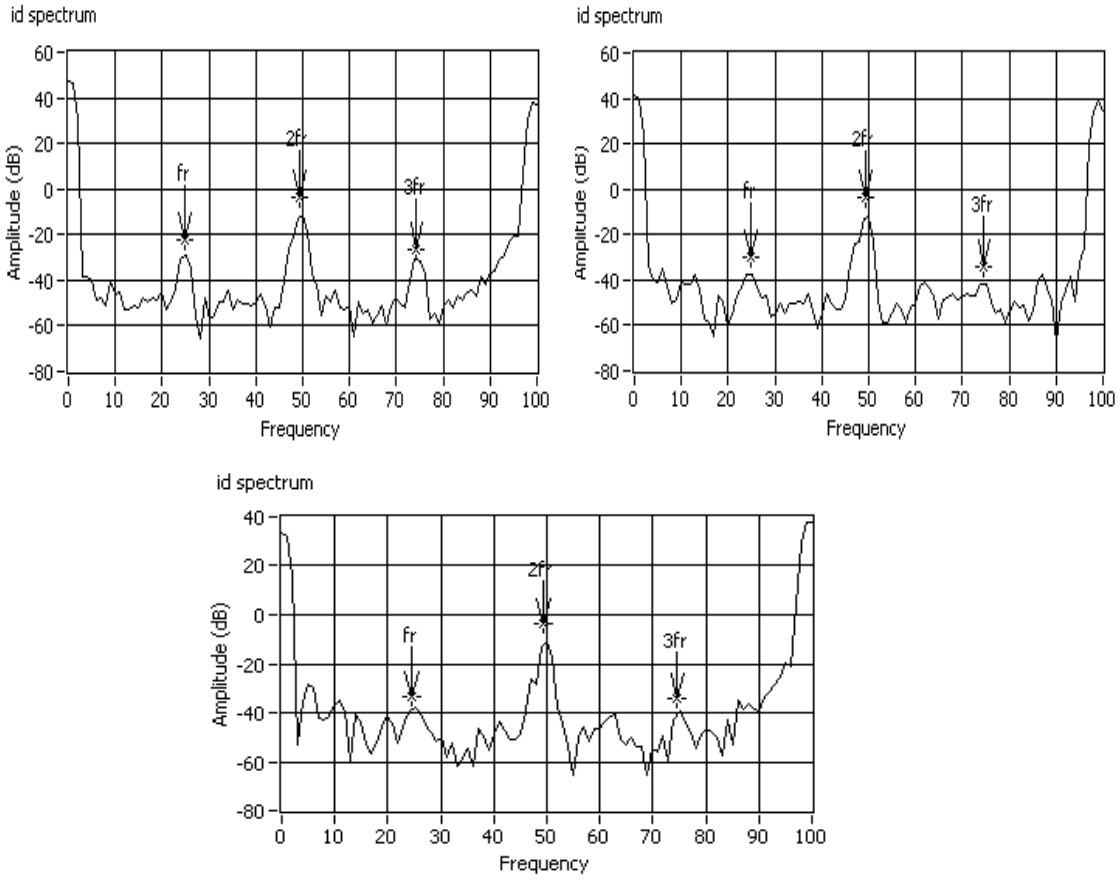

Figure 5.17 d-axis component of stator phase currents spectra under no load condition, 72.7% load condition and full load condition

Table 5.8 compares the frequency components obtained by PSD analysis with those of theoretically calculated frequency components.

Table 5.8 Eccentricity characteristic frequency components in i_d spectra

Eccentricity characteristic frequency components	No load		72.7% load		Full load	
	Equation	PSD	Equation	PSD	Equation	PSD
f_r (Hz)	24.78	24.8	24	24.5	23.88	24.5
$2f_r$ (Hz)	49.56	49.6	48	49.3	47.76	49.6
$3f_r$ (Hz)	74.34	74.1	72	74.1	71.64	74.8

Figure 5.18 shows the spectra obtained by performing PSD analysis on the q-axis component of stator currents for no load, 72.7% load and full load condition.

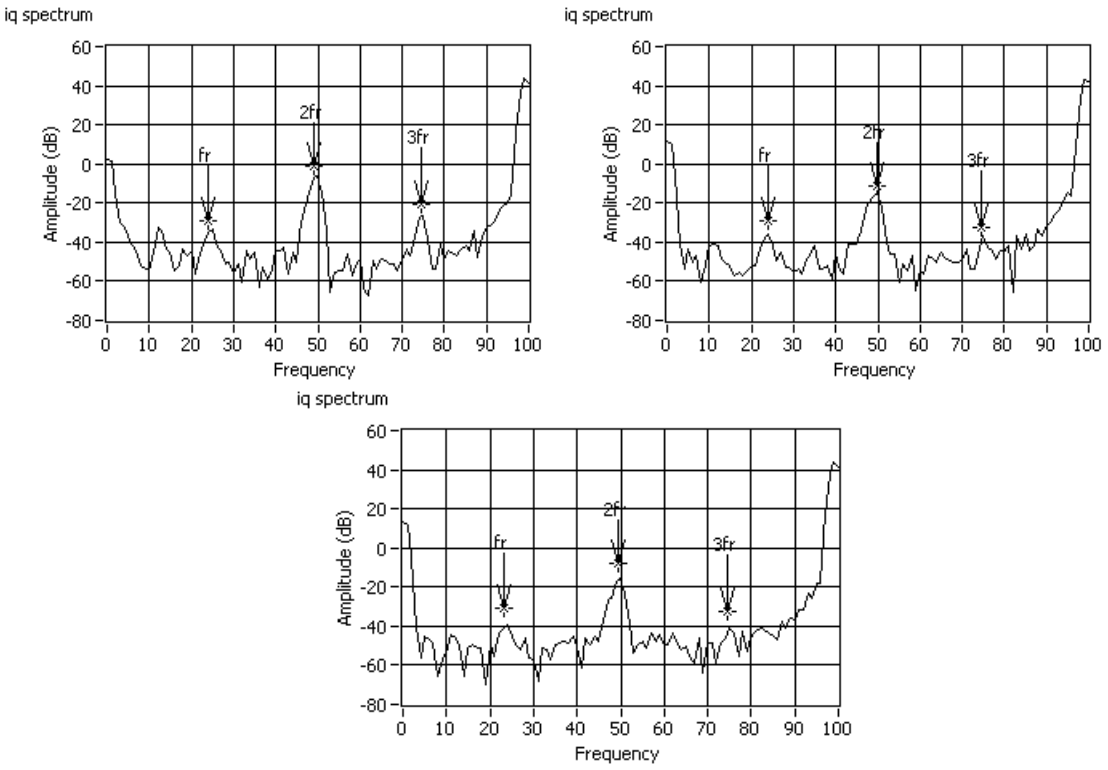

Figure 5.18 q-axis components of stator phase currents spectra under no load condition, 72.7% load condition and full load condition.

The eccentricity characteristic frequency components obtained by PSD analysis on q-axis component of stator currents are listed in Table 5.9 and are compared with those obtained theoretically.

Table 5.9 Eccentricity characteristic frequency components in i_q spectra

Eccentricity characteristic	No load		72.7% load		Full load	
	Equation	PSD	Equation	PSD	Equation	PSD
f_r (Hz)	24.78	24.71	24	23.57	23.88	23.57
$2f_r$ (Hz)	49.56	49.43	48	49.43	47.76	49.43
$3f_r$ (Hz)	74.34	74.52	72	74.52	71.64	74.9

Power spectral density analysis performed on the instantaneous power under no load, 72.27% load and full load gave the spectra as shown in Figure 5.19.

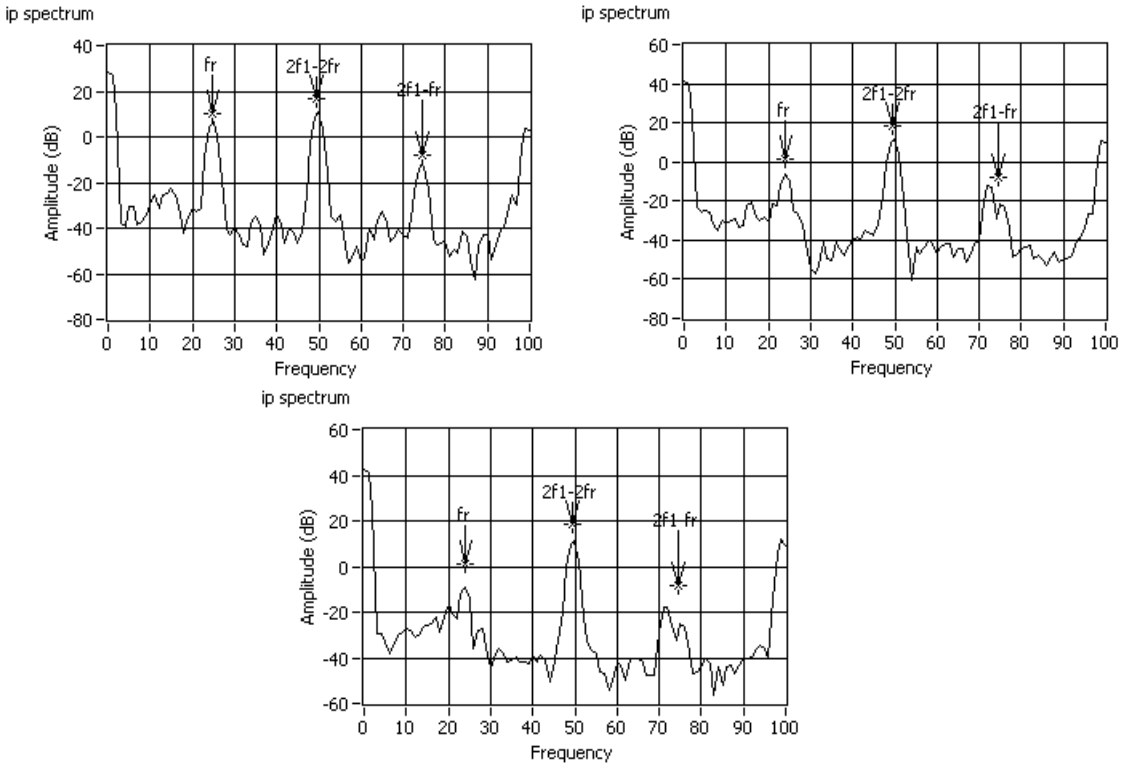

Figure 5.19 Instantaneous power spectra under no load condition, 72.7% loaded condition and full load condition.

Table 5.10 compares the eccentricity related frequency components obtained by PSD analysis with those values obtained theoretically

Table 5.10 Eccentricity characteristic frequency components in power spectra

Eccentricity Characteristic frequency components	No load		72.7% load		Full load	
	Equation	PSD	Equation	PSD	Equation	PSD
f_r (Hz)	24.78	24.71	24	24.3	23.88	23.9
$2f_1$-$2f_r$ (Hz)	49.56	49.43	50.94	49.4	51.68	49.8
$2f_1$-f_r (Hz)	74.34	74.52	74.94	75.2	75.56	71.4

From the Tables 5.7-5.10 following observations are made

(i) Eccentricity related harmonic frequencies obtained by PSD analysis on the parameters under no load conditions matched very well with those obtained theoretically.

(ii) As the machine is loaded, the error between the eccentricity characteristic frequency components computed by PSD analysis and of calculated theoretically has increased.

(iii) As the machine is loaded, the frequencies at which eccentricity characteristic frequency components are found, decreases. This can be attributed to the fall in speed as the machine is loaded.

(iv) The frequency component f_r found in both i_d and i_q spectra can be used for mixed eccentricity detection as its values are very close to those obtained theoretically and also it is independent of fundamental frequency.

Thus by both modeling-simulation results and experimental results, it is shown that f_r component which is independent of synchronous speed can be extracted from the current samples itself by taking d-q transformation on them. The extraction of d-q components are usually done in the controller circuit of the induction motor. Hence the same can be used for eccentricity fault detection and is cost effective.

Unbalance in supply voltages can cause unbalance in currents also. Hence in the next chapter, a study conducted on the eccentric motor to observe the impact of supply voltage unbalances on the eccentricity characteristic harmonics found in the stator currents are presented.

CHAPTER 6

6.0 INFLUENCE OF UNBALANCE IN SUPPLY ON DETECTION OF MIXED AIR GAP ECCENTRICITY

Motor Current Signature Analysis (MCSA) is one of the fault detection methods employed for eccentricity fault detection. Many research papers have been published on eccentricity fault detection by MCSA under balanced voltage supply condition [Nandi et al. 2005, Thomson 2009, Faiz et al. 2009]. The mixed eccentricity fault in an induction motor is detected by identifying the eccentricity characteristic side band frequency components around the fundamental [Nandi et al. 2005]. The amplitude of these frequency components is used as an indicator to assess the degree of air gap non uniformity in the machine. In this chapter, investigations conducted on an induction motor to study the effect of unbalance in supply voltage on the amplitude of these frequency components and hence on the mixed eccentricity detection by MCSA method are presented.

6.1 Introduction

Unbalance in voltage supply fed to the induction motor can result in the performance degradation of the motor and also shortens its life. Small percentage of voltage unbalance may result in large current unbalance in the motor currents resulting in temperature rise and hence insulation failure in the motor. National Electrical Manufacturers Association (NEMA) and International Electro technical Commission (IEC) standards introduce independent definition for voltage unbalance and one of these is normally used for analysis of electrical machine [Pillay et al. 2001, Faiz et al. 2005, Jong-Gyeum et al.2005].

(i) NEMA Definition

The voltage unbalance percentage (VUP) at the terminal of a machine, based on the NEMA definition can be expressed as

$$VUP = \frac{\text{maximum deviation from average voltage}}{\text{average voltage}} \times 100\% \quad (6.1)$$

where only the value of the line voltages have been considered.

(ii)IEEE Definition

The IEEE definition of voltage unbalance, also known as the Phase Voltage Unbalance rate (PVUR), is given by

$$PVUR = \frac{\text{maximum deviation from average phase voltage}}{\text{average phase voltage}} \times 100\% \quad (6.2)$$

The IEEE uses the same definition of voltage unbalance as NEMA, the only difference being that the IEEE uses phase voltages rather than line-to-line voltages. Here again, phase angle information is lost since only magnitudes are considered.

(iii) IEC or Symmetrical Components Definition or True definition

The voltage unbalance factor at the terminal of a machine based on the IEC definition, is as follows

$$VUF = \frac{V_2}{V_1} \times 100\% \quad (6.3)$$

where V_1 and V_2 are the magnitude of positive and negative sequence components of unbalanced voltages, respectively.

Investigations to study the effect of unbalance supply voltage on the amplitude of mixed eccentricity related frequency components by MCSA are carried out by making use of NEMA definition. For example, if the three unbalanced line-line voltages are:

$V_{ab} = 400\ V \quad V_{bc} = 417\ V \quad V_{ca} = 420\ V$

The average voltage is 412.33 V and the maximum voltage deviation from the average voltage i.e. maximum of {(412.33-400=12.33), (417-412.33=4.67),(420-412.33=7.67)} is 12.33 V.

Then % of unbalance is

$$VUP = \frac{12.33}{412.33} \times 100\% = 2.99\% \approx 3\ \% \quad (6.4)$$

3% unbalance can be obtained for three different possible combinations of line voltages as given in Table 6.1

Table 6.1 Line voltage magnitude corresponding to 3% unbalance

Set	V_{ab}	V_{bc}	V_{ca}	V_{avg}	Nature
1	400	417	420	412.33	Vavg>Vrated
2	400	385	380	388.33	Vavg<Vrated
3	400	388	412	400	Vavg = Vrated

The need for clarity arises due to the fact that by application of different voltages across a three phase machine, the operating behavior of the machine also changes. Most of the time, it has been seen that only VUP has been mentioned, which leads to insufficiency of information. Hence investigations are carried out under three sub headings as given below

(i)Over Voltage unbalance Condition: In this case, line voltage V_{ab} is set at 400V and other two line voltages V_{bc} and V_{ca} are kept more than 400V- Set 1 in Table 6.1.

(ii)Under Voltage unbalance Condition: Both the line voltages V_{bc} and V_{ca} are maintained less than 400V while V_{ab} is kept constant at 400 V-Set 2 in Table 6.1.

(iii)Mixed Voltage unbalance Conditions: In this case, study is conducted by keeping V_{ab} constant at 400V while one of V_{bc} or V_{ca} is maintained above 400V and the other below 400V-Set3 in Table 6.1.

In summary, whatever may be the magnitude of line voltage, it can be clearly identified and defined the extent of voltage unbalance; the subsequent result analysis will be more logical and correct in nature.

This investigation is carried out in two phases.

In phase 1, a dynamic behavioural model of an induction motor is developed which can take unbalance supply as input and simulations are carried out and its results are analysed.

In phase 2, experiments are conducted on an eccentric induction motor operating under various unbalance supply voltage conditions. The experimental results are compared with those of modeling and simulation results.

6.2 Modeling of induction motor for unbalance supply input

The induction motor model developed in [Toliyat et al. 1995] takes stator phase voltages as input. Hence the model is suitable to study the operation of motor

under balanced conditions only. To take into account of the unbalance in supply voltages, it is necessary to modify the model which can take line voltages as input. For machines having delta connected stator windings, modifications in the model is not necessary as the line voltages will be the same as phase voltages.

But for a star connected machine modifications are necessary in the stator system equations as described below. The voltages equations for the stator loops in vector matrix can be written as given in (6.5) [Toliyat et al. 1995, Xiaogang et al. 1995].

$$V_s = \begin{bmatrix} R_a & 0 & 0 \\ 0 & R_b & 0 \\ 0 & 0 & R_c \end{bmatrix} I_s + \begin{bmatrix} \frac{d\lambda_a}{dt} \\ \frac{d\lambda_b}{dt} \\ \frac{d\lambda_c}{dt} \end{bmatrix} \tag{6.5}$$

where $V_s = [v_a\ v_b\ v_c]^t$, v_a, v_b and v_c are the stator voltages of phase A, B and C respectively , R_a, R_b and R_c are the stator resistances of phase A, B and C respectively, λ_a, λ_b and λ_c are the stator flux linkages of phase A, B and C respectively and the stator flux is given by

$$\lambda_s = \begin{bmatrix} L_{aa} & L_{ab} & L_{ac} \\ L_{ba} & L_{bb} & L_{bc} \\ L_{ca} & L_{cb} & L_{cc} \end{bmatrix} I_s + \begin{bmatrix} L_{ar} \\ L_{br} \\ L_{cr} \end{bmatrix} I_r \tag{6.6}$$

where L_{aa}, L_{bb}, L_{cc} are the self inductances of three phases A,B,C respectively and L_{ab}, L_{ac}, L_{ba}, L_{bc}, L_{ca} , L_{cb} are the mutual inductances between two stator phases, I_s, is a phase current vector $=[i_a\ i_b\ i_c]^t$,I_r is a vector of rotor loop currents and defined as $I_r = [i_1\ i_2 \ldots\ldots i_n i_e]$ and L_{ar} , L_{br} and L_{cr} are the mutual inductances between stator phases and rotor loops and are '*1x (n+1)*' row vectors.

By manipulating Equations (6.5) and (6.6), $V_{sl\text{-}l}$ and $\lambda_{sl\text{-}l}$ are obtained and are given by the Equations (6.7) and (6.8) respectively.

$$V_{sl-l} = \begin{bmatrix} v_a - v_b \\ v_b - v_c \\ v_c - v_a \end{bmatrix} = \begin{bmatrix} R_a & -R_b & 0 \\ 0 & R_b & -R_c \\ -R_a & 0 & R_c \end{bmatrix} I_s + \begin{bmatrix} \frac{d\lambda_{sl-l}}{dt} \end{bmatrix} \tag{6.7}$$

$$\lambda_{sl-l} = \begin{bmatrix} \lambda a - \lambda_b \\ \lambda_b - \lambda_c \\ \lambda c - \lambda_a \end{bmatrix} = \begin{bmatrix} L_{aa} - L_{ba} & L_{ab} - L_{bb} & L_{ac} - L_{bc} \\ L_{ba} - L_{ca} & L_{bb} - L_{cb} & L_{bc} - L_{cc} \\ L_{ca} - L_{aa} & L_{cb} - L_{ab} & L_{cc} - L_{ac} \end{bmatrix} I_s + \begin{bmatrix} L_{ar} - L_{br} \\ L_{br} - L_{cr} \\ L_{cr} - L_{ar} \end{bmatrix} I_r \qquad (6.8)$$

It does not matter, whether the phases are balanced, symmetrical and identical or not, if the stator is star connected then it can be written as

$$i_a + i_b + i_c + \frac{d(i_a + i_b + i_c)}{dt} = 0 \qquad (6.9)$$

where i_a, i_b, i_c are line currents.

Replacing the third row in Equation (6.7) by Equation (6.9), Equation (6.7) can be rewritten as

$$V_{sl-l} = \begin{bmatrix} V_a - V_b \\ V_b - V_c \\ 0 \end{bmatrix} = \begin{bmatrix} R_a & -R_b & 0 \\ 0 & R_b & -R_c \\ 1 & 1 & 1 \end{bmatrix} I_s + \begin{bmatrix} \frac{d\lambda'_{sl-l}}{dt} \end{bmatrix} \qquad (6.10)$$

where λ'_{sl-l} is given by

$$\lambda'_{sl-l} = \begin{bmatrix} \lambda a - \lambda_b \\ \lambda_b - \lambda_c \\ 0 \end{bmatrix} = \begin{bmatrix} L_{aa} - L_{ba} & L_{ab} - L_{bb} & L_{ac} - L_{bc} \\ L_{ba} - L_{ca} & L_{bb} - L_{cb} & L_{bc} - L_{cc} \\ 1 & 1 & 1 \end{bmatrix} I_s + \begin{bmatrix} L_{ar} - L_{br} \\ L_{br} - L_{cr} \\ 0 \end{bmatrix} I_r \qquad (6.11)$$

Although three stator phases have been considered here explicitly, it can be extended for an arbitrary number of stator circuits. Since the rotor winding are short circuited, there is no need for modification of equations on the rotor side. The rotor equations and mechanical equation remain the same.

Under unsymmetrical unbalanced conditions, the magnitude and phase angles of the line voltages will not remain the same. In order to obtain the phase angle of line voltages, the triangle theorem and properties of line voltages are used and are calculated as follows

With V_{ab} as reference, three line voltages are defined as

$$\begin{aligned} v_{ab} &= V_{ab} \angle 0 \\ v_{bc} &= V_{bc} \angle 180 - \beta \\ v_{ca} &= V_{ca} \angle -180 + \alpha \end{aligned} \qquad (6.12)$$

where α and β are defined as (refer Figure 6.1)

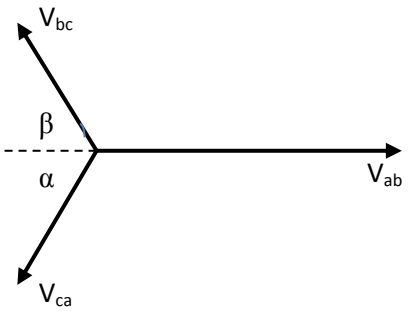

$$\alpha = \frac{V_{ab}^2 + V_{bc}^2 + V_{ca}^2}{2V_{ab}V_{ca}}$$

$$\beta = \frac{V_{ab}^2 + V_{bc}^2 + V_{ca}^2}{2V_{ab}V_{bc}}$$

Figure 6.1 Line voltage triangle

where V_{ab}, V_{bc} and V_{ca} are the magnitude of line voltages.

For different unbalance supply voltage conditions, phase angles are computed as given in Figure 6.1 and line voltage magnitudes along with their phase angles are fed to the machine model. The dynamic behavioural machine model is developed for the mixed eccentricity conditions which is uniform throughout the axial length of the rotor. The developed mathematical model of the machine behavior is studied for various unbalanced supply voltage conditions and the results obtained are discussed in the next Sections.

6.3 *Validation of proposed model through experimental verification*

The machine is simulated considering stator phase A turn function and rotor loop1 turn function as shown Figure 6.2

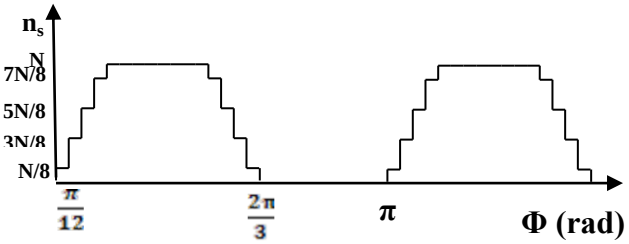

Fig 6.2 (a)

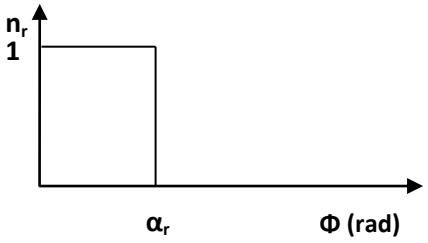

Fig 6.2 (b)

Figure 6.2 (a) stator phase A turn function (b) rotor loop1 turn function

Skewing angle of the rotor bar is neglected. The model is simulated using RungeKutta 4 method using a step size of 0.00005 seconds for mixed eccentricity conditions for both conditions of balanced and unbalanced supply voltages. 20000 stator data samples of stator phase currents are extracted from simulating the machine

model with full load. They are filtered using a low pass digital FIR filter having cut off frequency of 10 kHz. The chosen window is Hanning.

Frequency analysis is performed on the stator current data samples to study the effect of supply unbalance on the eccentricity characteristic harmonic frequency components in the current spectra. The spectra obtained by Power Spectral Density (PSD) analysis being performed on the data samples of stator phase A current of the machine having 30% static eccentricity and 20% dynamic eccentricity under both balance and unbalance conditions are shown in Figure 6.3. The frequency resolution is 1 Hz.

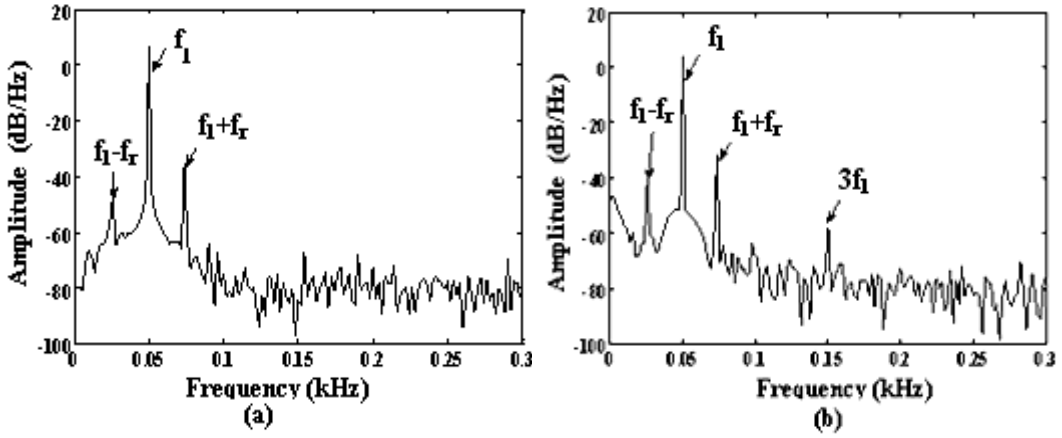

Figure 6.3 Stator phase A Current Spectra (a) Balanced condition (b) Unbalanced condition (2.03%).

From Figure 6.3, it is observed that mixed eccentricity characteristic harmonics (f_s-f_r) and (f_s+f_r) are present in both the current spectra. But under unbalance conditions, third order harmonics are also present in the current spectra. The eccentricity related side band frequency components around the fundamental are computed using Equation (2.16) and are compared with those obtained by PSD analysis performed on the stator phase A current under unbalance voltage supply condition of 2.03% in Table 6.2.

Table 6.2 Comparison of eccentricity related harmonics in stator phase A current

Frequency Components	f_1-f_r (Hz)	f_1+f_r (Hz)
PSD Analysis	26	74
Theoretical from Equation (2.16)	26.16	73.84

where $f_r=N_r/60$ where N_r is the rotor speed. From the table, it can be inferred that eccentricity characteristic frequency components obtained from PSD analysis of stator phase current A is very close to those values calculated using rotor speed. The model is simulated for the air gap eccentricity conditions of 20% static eccentricity and 20% dynamic eccentricity for the three conditions of unbalance voltage i.e Over voltage unbalance condition, Under voltage unbalance condition, Mixed voltage unbalance condition. The amplitudes of the eccentricity related frequency components found from the stator phase A current spectra for three different unbalance voltage conditions are compared in Table 6.3-6.5.

Table 6.3 Variation in magnitude of air gap eccentricity related harmonics under Over voltage unbalance

Type of unbalance	% Voltage Unbalance	f_1-f_r (26Hz) Magnitude	f_1+f_r (74Hz) Magnitude
Over Voltage Unbalance	1% (400,404,408)	-45.11	-35.53
	2% (400,410,415)	-44.43	-35.13
	3% (400,417,420)	-42.9	-35.01

Table 6.4 Variation in magnitude of air gap eccentricity related harmonics under Under voltage unbalance

Type of unbalance	% Voltage Unbalance	f_1-f_r(26Hz) Magnitude	f_1+f_r(74Hz) Magnitude
Under Voltage Unbalance	1% (400,396,392)	-46.79	-36.38
	2% (400,392,384)	-47.41	-36.95
	3% (400,385,380)	-48.97	-37.31

Table 6.5 Variation in magnitude of air gap eccentricity related harmonics under Mixed voltage unbalance

Type of unbalance	Percentage Voltage Unbalance	f_1-f_r (26Hz) Magnitude	f_1+f_r(74Hz) Magnitude
Mixed Voltage Unbalance	1% (400,396,404)	-45.83	-35.94
	2% (400,392,408)	-45.93	-35.91
	3% (400,388,412)	-45.96	-35.98

From Table 6.3-6.5, following observations are made

(i)With Over voltage unbalance, the magnitude of air-gap related harmonic component increases with increase in percentage unbalance.

(ii)With Under voltage unbalance, the magnitude of air-gap related harmonic component decreases with increase in percentage unbalance

(iii)With Mixed voltage unbalance, the magnitude of air-gap related harmonic component remain nearly constant with increase in percentage unbalance

The dynamic behaviour of the air gap eccentric machine model for various unbalance supply conditions are simulated using newly developed model up to now. The simulation results show that, the magnitude of side band harmonics signifying eccentricity characteristic get affected by the unbalance in supply voltage conditions. To validate these observations experiments are conducted on an eccentric machine for different unbalance supply voltage conditions. The experimental details and results are presented in the section that follows.

6.4 Experimental results and analysis

3 hp squirrel cage induction motor is modified to create inclined eccentricity in it.The motor is coupled to a DC generator which is supplying the lamp loads through which the machine is loaded. Inclined static eccentricity of 0.1452 is created

at one end while the other end (coupling end) is healthy. Machine suffers from inherit dynamic eccentricity.

Stator phase A current spectra obtained by PSD analysis performed on the stator phase A current data samples obtained from the machine operating 2.02% (400V, 392V,396V) under unbalance condition at full load is shown in Figure 6.4.

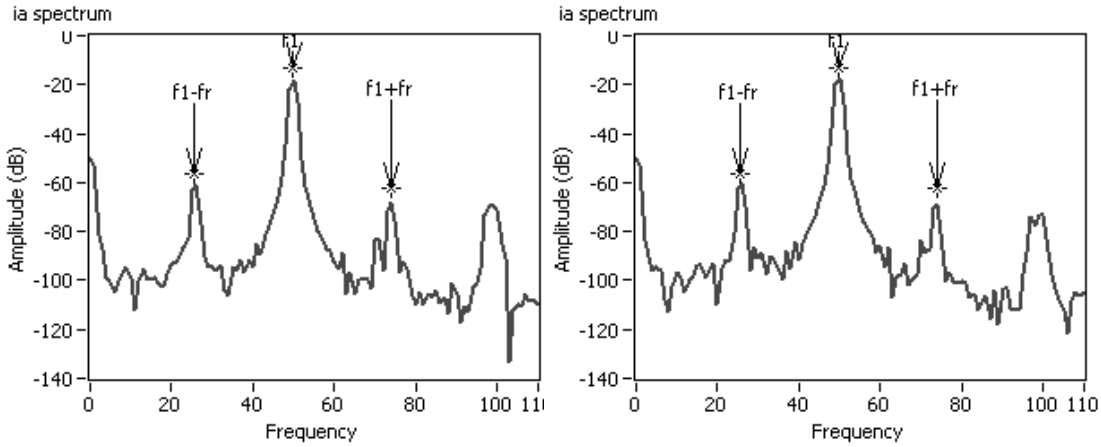

Figure 6.4 Stator phase A Current Spectra (a) Balanced condition (b) Unbalanced condition (2.02%)

The eccentricity related side band frequency components around the fundamental are computed using Equation (2.16) and are compared with those obtained by PSD analysis performed on the stator phase A current under unbalance voltage supply condition of 2.02% in Table 6.6.

Table 6.6 Comparison of eccentricity related harmonics in stator phase A current

Frequency Components	f_1-f_r (Hz)	f_1+f_r (Hz)
PSD Analysis	25.96	73.92
Theoretical from Equation (2.16)	25.39	73.95

From the table, it can be observed that eccentricity related harmonics obtained from PSD analysis of stator phase A current and theoretically calculated values are very close. The variation of amplitude of eccentricity characteristic frequency components under over, under and mixed voltage unbalance conditions are given in Table 6.7

Table 6.7 Variation of magnitude of air gap eccentricity related harmonics under Over, Under, Mixed voltage unbalance

Type of unbalance	Percentage Voltage Unbalance	f_s-f_r Magnitude in dB	f_s+f_r Magnitude in dB
Over Voltage Unbalance	1.97% (400,408,408)	-62.3	-70.36
	4.86% (400,414,420)	-60.84	-69.63
Under Voltage Unbalance	2.02% (400,392,396)	-59.37	-68.17
	3.04% (400,396,388)	-60.14	-71.09
Mixed Voltage Unbalance	2.99% (400,408,396)	-60.84	-69.63
	4.46% (400,396,414)	-61.57	-73.01
0% Unbalance	(400,400,400)	-62.23	-68.9

From the Table 6.7, following observations are made

With the increase in the percentage unbalance

(i)The magnitude of air-gap related harmonic component increases under Over voltage condition.

(ii) The magnitude of air-gap related harmonic component decreases under Under voltage condition.

(iii)The magnitude of air-gap related harmonic component decreases under, Mixed voltage condition.

From both modeling and simulation and experimental results, it can be observed that unbalance in supply voltage and type of unbalance will affect the amplitude of eccentricity characteristic harmonics marginally.

CHAPTER 7

7.0 CONCLUSION

Condition monitoring unit of induction motors has become an integral part of the drives in industries. It ensures the smooth functioning of these industries. It continuously monitors the health of the machine and detects the fault at the earliest possible. Air gap eccentricity fault results from the wear and tear of the bearings or due to the shaft misalignment or defect of rotor and stator structure. Of late more emphasis is laid on the early detection of air gap eccentricity fault.

Literature survey showed that Motor Current Signature Analysis (MCSA) and Vibration monitoring are the two popular fault diagnostic methods to detect air gap eccentricity fault. From the survey, it is also observed that MCSA could detect these faults while vibration monitoring failed to do so. In reality, both static and dynamic eccentricities tend to co-exist in the machine. An inherent level of static eccentricity exists even in newly manufactured machines due to manufacturing and assembly method. This may give rise to unbalance magnetic pull on the rotor resulting in dynamic eccentricity. Any non uniformity in the air gap alters the flux distribution in the air gap. Stator current is the primary parameter to get affected by this non uniform distribution of flux in the air gap. Hence they contain eccentricity characteristic harmonics in them. MCSA is used to identify the characteristic current signature pattern which is indicative of abnormal levels of air gap eccentricity.

The mixed air gap eccentricity fault in the machine, give rise to low frequency side band frequency components around the fundamental in the current spectrum. These frequency components are very often used to detect fault severity in the machine. The actual location of these components is a function of the number of pole pairs and slip. Instantaneous power signature analysis, instantaneous power factor signature analysis and instantaneous torque signature analysis are also used for fault detection. They produce eccentricity characteristic harmonics which are independent of fundamental frequency.

In this study, all the air gap eccentricity detection methods such as instantaneous current signature analysis, instantaneous power signature analysis, and

instantaneous power factor signature analysis are reviewed. A 3 hp squirrel cage induction motor is considered for investigation.

A dynamic model of an induction motor using the physical parameters of the machine is developed using multiple coupled circuit approach and inductances are calculated using 2D-Modified Winding Function Theory. The model is developed using numerical integration technique and has the following features:

- It responds very well to the sudden increase or decrease in the load.
- It has the capability to start with load on it.
- Skewing of rotor bar is included while defining the turn function of the rotor loop.
- Both uniform eccentricity and inclined eccentricity can be incorporated in the model.

The response of the model for both uniform eccentricity and inclined eccentricity conditions are studied. It is inferred that degree of fault is more if the degree of eccentricity is uniform throughout the axial length of the rotor in the machine.

Frequency analysis is performed on the stator currents to extract the eccentricity characteristic harmonics from them. Power Spectral Density (PSD) is performed on the instantaneous stator current obtained from simulation of the model for different eccentricity conditions. The stator phase current spectra showed the presence of lower and upper side band frequency components around the fundamental. Using the amplitude of these side band frequency components, Eccentricity Severity Factors are defined as follows

$$ESF_1 = \frac{(\text{Amplitude of base frequency in dB} - \text{Amplitude of lower side band frequency in dB})}{\text{Amplitude of base frequency in dB}}$$

and

$$ESF_2 = \frac{(\text{Amplitude of base frequency in dB} - \text{Amplitude of upper side band frequency in dB})}{\text{Amplitude of base frequency in dB}}$$

Also it is shown that this factor increases with the increase in the degree of dynamic eccentricity (mixed eccentricity). Hence these factors are proposed to assess the severity of non uniformity in the air gap of a machine.

The Eccentricity Severity Factors makes use of only side band eccentricity characteristic frequency components. It needs to be calculated and compared with the previous value to assess the way in which fault is progressing. In this research work, a new method based on Eigen Value is proposed. It is a known fact that all machines suffer from some degree of eccentricity at the manufacturing stage itself due to mechanical reasons. Eigen Value based detection method compares many side band eccentricity characteristic harmonics present in the current spectrum with those obtained during installation stage. Co-variance matrix is formed and Eigen Values are found. It is shown that this value increases with the increase of air gap eccentricity level in the machine and hence can be used to assess the severity of the fault in the machine. This method has two advantages over the other methods as

(i) It makes use of many eccentricity harmonics present in the current spectra for prediction of severity of fault.

(ii) Severity of the fault is predicted by comparing the eccentricity characteristic frequency components in the current spectra with those of installation stage.

Instantaneous Power and Power factor signature analysis are performed on the acquired signals by simulation for different eccentricity conditions. It is inferred that they contain eccentricity specific harmonics mf_r in them. This method of air gap eccentricity detection does not require the knowledge of fundamental frequency.

The power factor fault severity factors are calculated for various eccentricity conditions. It is defined as the ratio of the amplitude of the f_r component of the instantaneous power factor of the motor and the corresponding DC value. It is shown that the fault severity factor (ratio) increases with the increase in the air gap dynamic (mixed) eccentricity in the machine. It is inferred that the increase in the slope of the curve with the increase in air gap eccentricity can be used to predict the severity of air gap eccentricity fault in the machine.

Mathematical expressions are derived to show the effect of presence of mixed air gap eccentricity in the machine on the d-q components of stator currents. From the expressions derived, it is shown that

(i) The d-q components of stator currents in synchronous reference frame will not remain as pure DC.

(ii) They contain a DC component superimposed with oscillations because of the harmonics of the order mf_r present in them.

The instantaneous d-q components of stator currents in synchronous reference frame are obtained by simulation of the model for both healthy and eccentricity conditions. Frequency analysis performed on them showed the following results

(i) They contain only a dc component when the machine is healthy.

(ii) They contain eccentric specific harmonics mf_r in them.

Thus validating the claims made by the mathematical expressions. It is also shown that the amplitude of f_r harmonic present in these components increase with increase in the degree of eccentricity in the machine and hence can be used for detection of severity of mixed eccentricity in the machine.

All the observations made by simulation are validated by conducting experiments on an air gap eccentric machine in the laboratory. For this purpose, a special rotor mounting mechanism for the motor is fabricated through which both static eccentricity and dynamic eccentricity can be varied. The Data Acquisition System is developed to

(i) acquire both voltage and current signals from machine.

(ii) analyse these acquired signals.

The experimental machine is run for different load and inclined eccentricity conditions and the signals are acquired for off line studies. The frequency analysis performed on the various signals showed the following results.

(i) the current spectrum contains eccentricity characteristic harmonics $|f_1 \pm mf_r|$ in them.

(ii) the magnitude of these frequency components increase with the increase in the level of eccentricity.

(iii) Eigen Values computed for various inclined eccentricity conditions increases with the eccentricity level.

(iv) the instantaneous power signature analysis showed that they contain eccentricity specific harmonics mf_r in them.

(v) the instantaneous d-q components of stator currents obtained in synchronous reference frame for eccentric machine showed the presence of oscillations in them.

(vi) their signature analysis showed the presence of eccentricity characteristic frequency components mf_r in them.

(vii) the magnitude of eccentricity characteristic harmonic f_r increases with the increase in eccentricity level and hence can be used as a fault severity indicator.

Hence all the claims made by simulation results are validated experimentally.

The effect of supply voltage unbalance on the mixed eccentricity detection method by MCSA is also investigated for three different unbalance conditions. Modeling and simulation results and experimental results have shown that

With the increase in the percentage unbalance

(i)The magnitude of air-gap related harmonic component increases under Over voltage condition.

(ii) The magnitude of air-gap related harmonic component decreases under Under voltage condition.

(iii)The magnitude of air-gap related harmonic component marginally decreases under Mixed voltage condition.

Thus it is shown that unbalance in supply voltage conditions affect the fault detection by MCSA method marginally.

The major contributions of this research work are the following:

This study is special, in that the parameters chosen for modeling and simulation are the same as the parameters of the experimental machine.

Contributions by the current work are the following:

- A method based on numerical integration is proposed to develop the dynamic model of the induction motor. The model is developed using multiple coupled circuit approach and 2D-MWFT is used to calculate the mutual inductances. This model is capable of taking into account of skewing of rotor bars and inclined eccentricity.

- Eccentricity Severity Factors are the new indices proposed for air gap eccentricity detection in this work. They aid to assess the severity of the fault in the machine by comparing the air gap eccentricity related lower and upper side band frequency components in the stator current spectra with the fundamental.
- Eigen Value based eccentricity detection method is proposed in this work. The main advantage is that it would predict the degree of the fault by comparing the eccentricity related frequency components in stator currents with those values obtained during the installation stage.
- During the investigation, it is found that the slope of the power factor severity curve is very useful to predict the severity of the eccentricity fault in the machine.
- The study shows that d-q components of stator currents is a better parameter to characterise the eccentricity fault as compared to power, power factor and torque. The spectral analysis of instantaneous d-q components of stator currents showed that the eccentricity specific harmonics mf_r are present in them where m=1,2,3….. and f_r is the speed frequency.
- Earlier studies used to detect the air gap eccentricity by extracting the f_r component from instantaneous torque, power and power factor signature analysis. However, the current study, highlights that the air gap eccentricity characteristic f_r component can be easily extracted by the spectral analysis of d-q components of stator currents. This method is very cost effective.
- By mathematical expressions, modeling - simulation results and experimentation, it is shown in this study that d-q components of stator currents in synchronous reference frame of an eccentric squirrel cage induction motor will not remain DC. Instead they will have oscillations superimposed on the DC due to the harmonics produced by the air gap eccentricity.
- This research work proposes an integrated condition monitoring unit (eccentricity fault detection unit) and the controller unit for an induction motor in industrial drive systems.
- By both modeling-simulation and experimental results, it is shown that the unbalance in supply voltage would affect marginally, the air gap eccentricity fault detection method by Motor Current Signature Analysis (MCSA).

Many researchers have made use of instantaneous torque spectra to characterise the asymmetrical fault in the machine. Instead of computing torque (making use of expensive transducers), extraction and frequency analysis of the i_q component of stator current can be used as a fault predictor. Most of the induction motor drives are VSI fed drives. The d-q components are extracted from the stator currents in the controller unit. Most of the time, these components will not remain pure DC due to the presence of inverter or load fluctuations. Hence, to remove these harmonics, they are passed through the filter. A mixed eccentricity fault detection unit placed just before this filter in the controller unit can be used to predict the fault in the machine.

Limitation of this work:

● The developed model in this work does not account the partial slot harmonics in the machine.

●The specially designed rotor mounting mechanism is used to create dynamic eccentricity whose degree could not be measured accurately.

●The experiments are conducted on the machine only for machine inclined eccentricity conditions.

●This work deals with only one type of asymmetrical fault i.e eccentricity fault.

●In this study, load variations on the machine are ignored for fault analysis.

●This investigation is limited to only balanced and unbalanced sinusoidal supply voltage conditions.

Feature Scope of this work:

●A more robust dynamic model of the machine including rotor slot effects can be developed.

●This investigation can be extended to study the effect of variation of load on eccentricity fault detection method.

●Wavelet transforms can be used to predict the fault instead of FFT analysis which can give the information about time and line of faults.

●This study can be extended to inverter fed induction motor.

●This research work can be extended for other types of asymmetrical faults.

●Artificial intelligence methods such as neural networks and fuzzy logics, genetic algorithms can be used to predict the type and severity of the fault.

APPENDIX

Appendix I

Machine details

2.2 kW, 3 hp, 400/415V, 50Hz, 3ϕAC, 1500rpm, 4 pole squirrel cage induction motor, Single layer, integral slot winding machine.

Number of stator slots =24

Number of rotor bars =30

Length of stacks =120mm

Effective air gap =0.35mm

Mean radius of air gap=89.65mm

Number of turns/phase =400

Stator resistance =7.6Ω

Stator leakage inductance =38.43mH

Rotor bar resistance=0.00376Ω

Rotor bar leakage inductance =44.52μH

Rotor end ring segment resistance =0.0012 mΩ

Rotor end ring segment inductance =1.24μH

Rotor inertia in GD^2=0.024 kg-m^2

Appendix II

II-1: Derivation of expression for permeance for the machine having only static eccentricity [Cameron et al.1986]

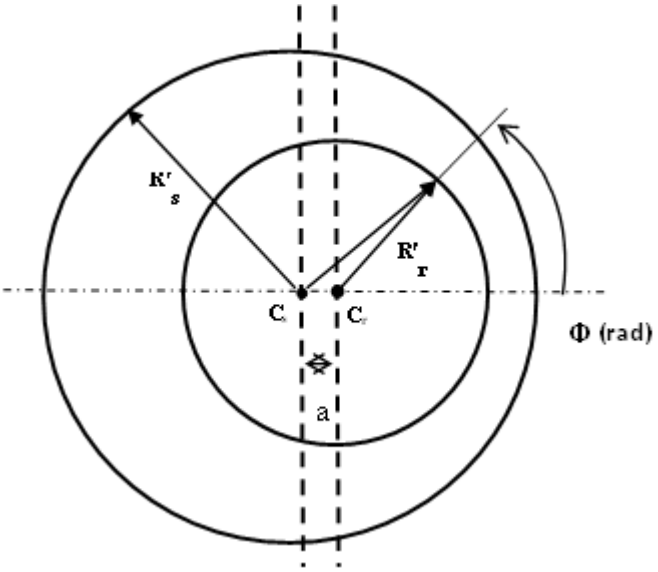

Figure II-1.1 Schematic representation of the static air gap eccentricity

In the case of static eccentricity, the position of minimum air gap length is fixed in space. If the rotor shaft assembly is sufficiently rigid, then the level of static eccentricity stays constant. If a coordinate system is placed into Figure II-1.1, with the origin on the center of the stator bore, the equation of the inner surface of the stator bore, in polar coordinates, is

$$r_1 = R'_s \qquad \text{(II-1.1)}$$

and the equation for the rotor surface, in Cartesian coordinates, is

$$(x-a)^2 + y^2 = \left(R'_r\right)^2 \qquad \text{(II-1.2)}$$

Converting this equation into polar coordinates and rearranging it in quadratic form yields the following equation

$$r_2 = a\cos(\phi) + \sqrt{\left(R'_r\right)^2 - (a\sin(\phi))^2} \qquad \text{(II-1.3)}$$

The length of the air gap is the difference between r_1 and r_2

$$g(\phi) = R_s' - a\cos(\phi) - \sqrt{\left(R_r'\right)^2 - (a\sin(\phi))^2}$$

$$= R_s' - a\cos(\phi) - R_r'\sqrt{1 - \frac{a^2}{\left(R_r'\right)^2}\sin^2(\phi)} \qquad \text{(II-1.4)}$$

In most practical cases $R_r' >> a$, so

$$g(\phi) = g_0 - a\cos(\phi) \qquad \text{(II-1.5)}$$

where g_0 would be the length of the airgap at all points if the rotor were perfectly centered in the stator bore. Consequently, it follows for the normalized magnetic permeance of the air gap that

$$P = \frac{1}{g(\phi)} = g^{-1}(\phi) = \frac{1}{g_0 - a\cos(\phi)} = \frac{1}{g_0(1 - \delta_s\cos(\phi\}} \qquad \text{(II-1.6)}$$

where δ_s is the static eccentricity index in the machine.

With Fourier series analysis, magnetic permeance of the airgap length or inverse airgap length P is given approximately as

$$P = g^{-1}(\phi) = P_0 + P_1\cos(\phi) + ... \qquad \text{(II-1.7)}$$

In the presence of static eccentricity, the radial air gap length is a function of space only. Assuming a smooth stator and rotor, the permeance will be

$$P(\varphi) = \sum_{i=0}^{\infty} P_i \cos(i\phi) \qquad \text{(II-1.8)}$$

The magnitude of the harmonic permeance waves due to static eccentricity are found by Fourier analysis to be

$$P_i = 2\left[\frac{1}{g_0\sqrt{1-\delta_s^2}}\right]\left[\frac{1-\sqrt{1-\delta_s^2}}{\delta_s}\right]^i \qquad \text{(II-1.9)}$$

II-2: Derivation of expression for permeance for the machine having only dynamic eccentricity [Cameron et al.1986]

With dynamic eccentricity, C_r is the center of rotation. This type of eccentricity occurs when the center of the rotor is not at the center of rotation and the minimum airgap revolves with the rotor as shown in Figure II-2.1.

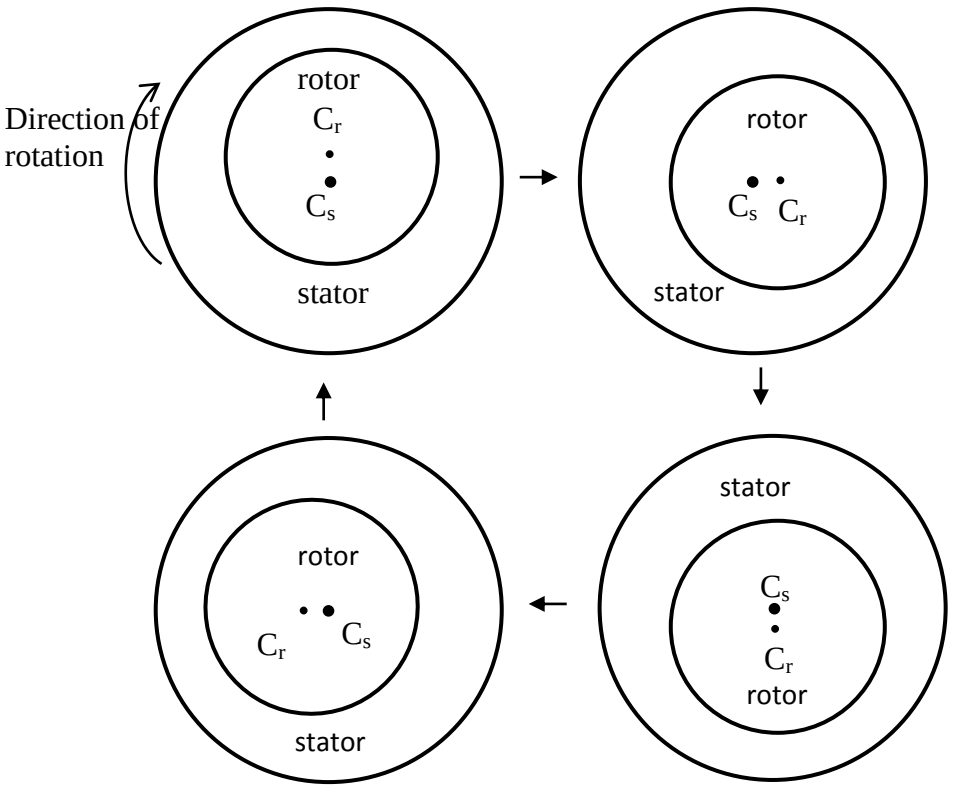

Figure II-2.1 Schematic diagram of the dynamically eccentric rotor

θ_r' denotes the periphery coordinate along the machine bore, referred to the rotor, then, if rotor rotates at an angular velocity ω_r the relation for Φ is then

$$\theta_r' = \phi - \omega_r t = \phi - \theta_r \qquad \text{(II - 2.1)}$$

where θ_r denotes the periphery coordinate referred to stator, and

$$\omega_r = (1-s)\frac{\omega}{p} \qquad \text{(II - 2.2)}$$

where ω is the supply angular frequency, s is the slip and p the number of the pole pairs of the machine.

The air gap function is defined as

$$g(\theta_r, \phi) = g_0(1 - \delta_d \cos(\phi - \theta_r)) \qquad \text{(II - 2.3)}$$

If θ_r' in Equation (II-2.1) is substituted into Equation (II-1.7), expression for the permeance P at the point θ_r at the instant of time t is given by,

$$P = g^{-1}(\theta_r, \phi) = P_0 + P_1 \cos(\phi - \theta_r) + ... \qquad \text{(II - 2.4)}$$

The radial air gap length in the presence of dynamic eccentricity is a function of space and time. The permeance can thus be represented as

$$P(\theta_r, \phi) = \sum_{j=0}^{\infty} P_j \cos[j(\phi - \theta_r)] \qquad \text{(II - 2.5)}$$

The magnitude of the harmonic permeance waves due to dynamic eccentricity are found by Fourier analysis to be

$$P_i = 2\left[\frac{1}{g_0\sqrt{1-\delta_d^2}}\right]\left[\frac{1-\sqrt{1-\delta_d^2}}{\delta_d}\right]^i \qquad \text{(II - 2.6)}$$

where δ_d is the dynamic eccentricity index.

II-3: Derivation of expression for permeance for the machine having mixed eccentricity [Cameron et al.1986]

Both static and dynamic eccentricities coexist. With mixed eccentricity, center of rotation can be anywhere between C_s and C_r.

In the presence of mixed eccentricity the air gap can be modeled as

$$g(\theta_r, \phi) = g_0(1 - \delta_s\cos(\phi) - \delta_d\cos(\phi - \theta_r)) \qquad \text{(II - 3.1)}$$

Then, the inverse air gap function P, can be written as

$$P(\theta_r, \phi) = g^{-1}(\theta_r, \phi) = \frac{1}{g_0(1 - \delta_s\cos(\phi) - \delta_d\cos(\phi - \theta_r))}$$

$$= P_0 + P_1\cos(\phi - \rho(\theta_r)) + P_2\cos(2\phi - 2\rho\rho(_r)) \ldots\ldots\ldots \qquad \text{(II - 3.2)}$$

The magnitude of the harmonic permeance waves due to dynamic eccentricity are found by Fourier analysis to be

$$P_i = 2\left[\frac{1}{g_0\sqrt{1-\delta^2}}\right]\left[\frac{1-\sqrt{1-\delta^2}}{\delta}\right]^i \qquad \text{(II - 3.3)}$$

where δ is the mixed eccentricity index

P is calculated by knowing the static and dynamic indices as shown in Figure II-3.1

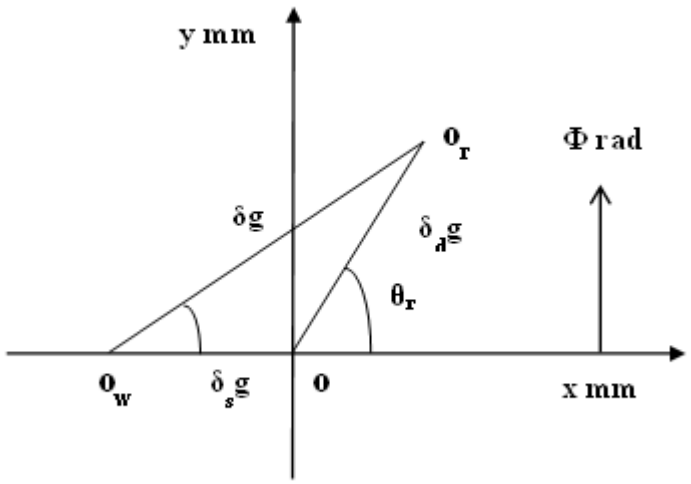

Figure II-3.1 Depiction of static and dynamic eccentricities in stator coordinates [Faiz et al. 2003]

From Figure II-3.1 for a given rotor angle θ_r,

$$\gamma(\theta_r) = \tan^{-1}\left(\frac{\delta_d \sin(\theta_r)}{\delta_s + \delta_d \sin(\theta_r)}\right) \qquad \text{(II - 3.4)}$$

$$\delta(\theta_r) = \sqrt{\delta_s^2 + \delta_d^2 + 2\delta_s\,\delta_d \cos(\theta_r)} \qquad \text{(II - 3.5)}$$

Appendix III

III-1:Overall Block diagram in SIMULINK

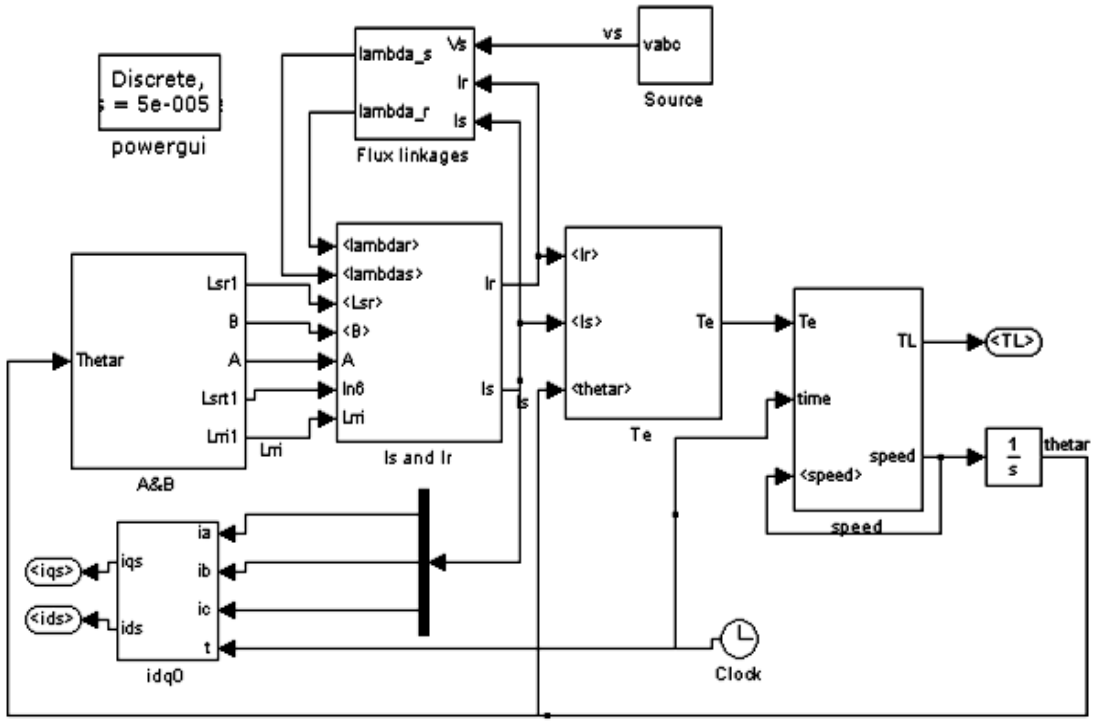

III-2: 3 Phase power supply block

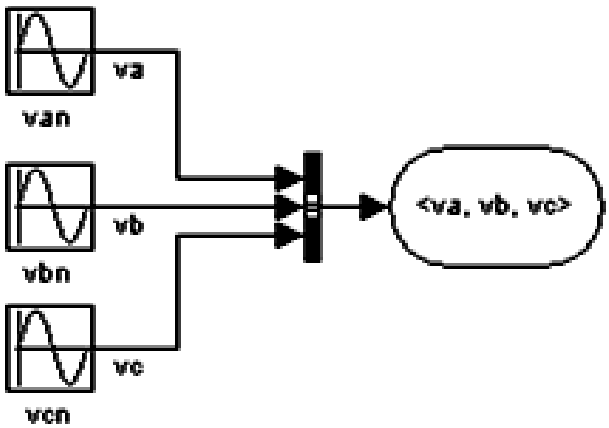

III-3: Flux linkage calculation block

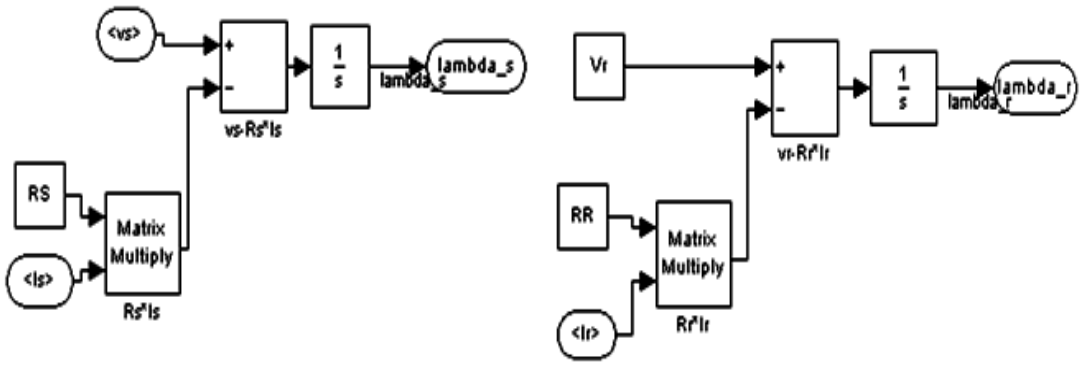

$$V_S = R_S I_S + \frac{d\lambda_S}{dt} \quad V_r = R_r I_r + \frac{d\lambda_S}{dt}$$

$$\lambda_S = L_{SS} I_S + L_{Sr} I_r \quad \lambda_r = L_{rS} I_S + L_{rr} I_r$$

III-4: Stator Current and rotor current calculation block

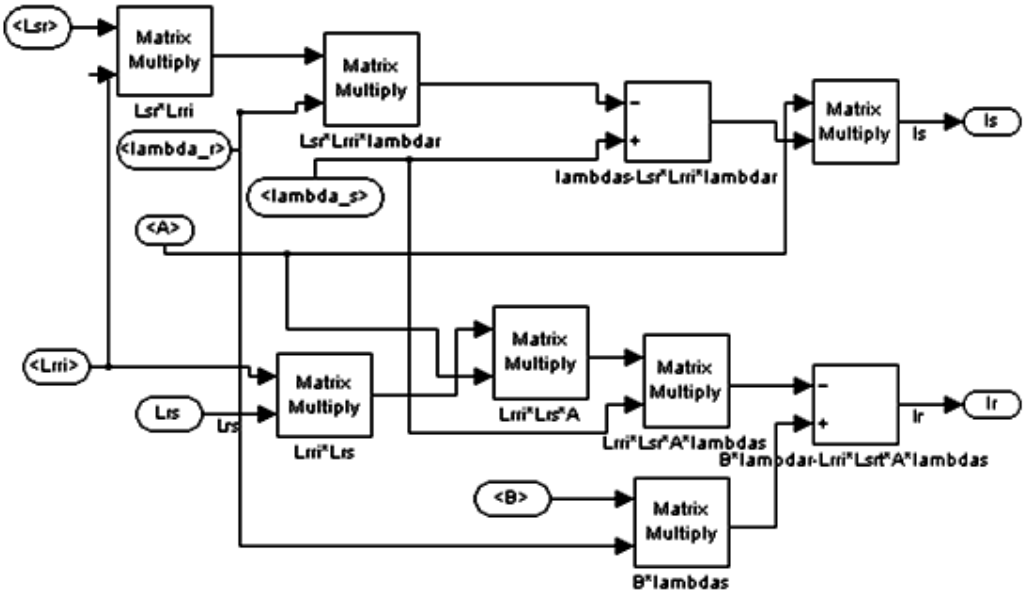

$$I_S = A\left[\lambda_S - L_{Sr} L_{rr}^{-1} \lambda_r\right] \quad I_r = B\lambda_r - L_{rr}^{-1} L_{rS} A \lambda_S$$

III-5: Constants A and B calculation block

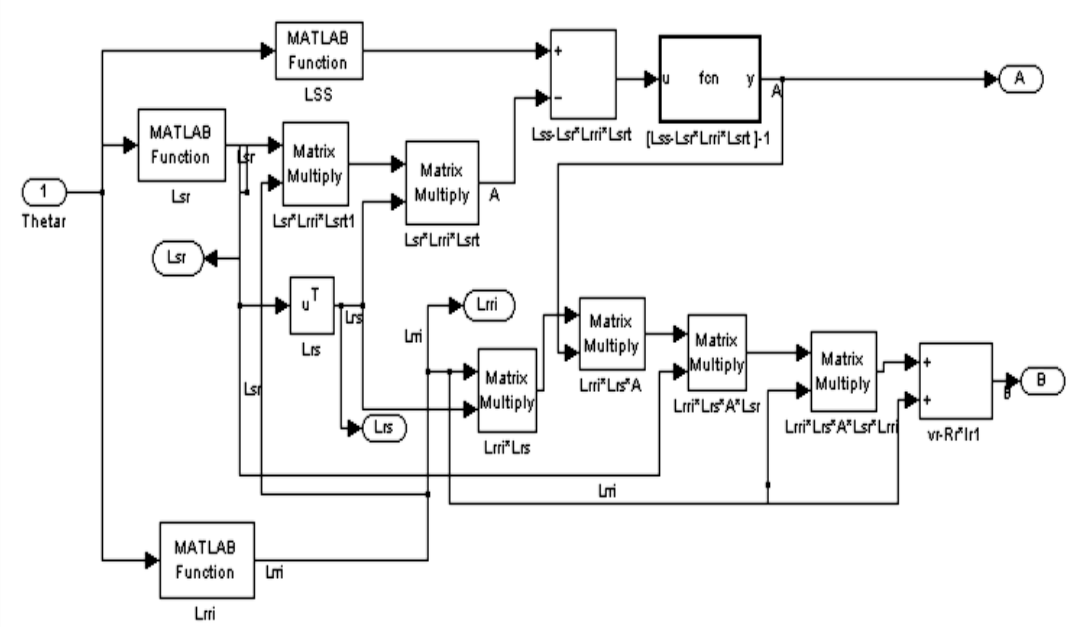

$$A = \left[L_{ss} - L_{sr} L_{rr}^{-1} L_{rs}\right]^{-1} \quad B = \left[L_{rr}^{-1} + L_{rr}^{-1} L_{rs}\, A\, L_{sr} L_{rr}^{-1}\right]$$

III-6: Dynamic Torque calculation block

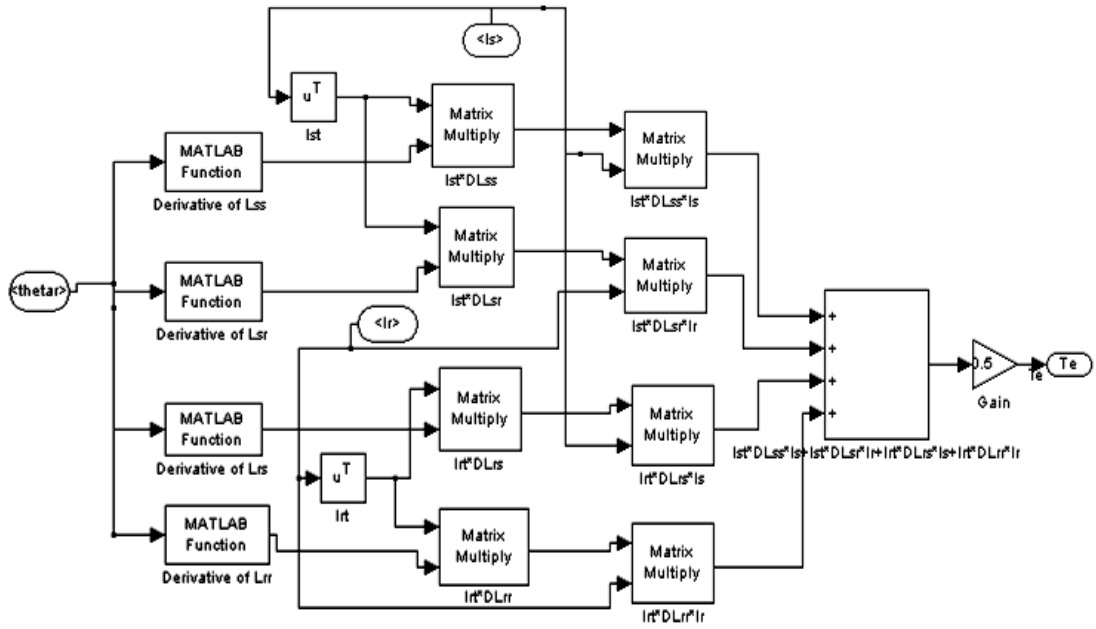

$$W_{co} = \frac{1}{2}\left[I_s^t L_{ss} I_s + I_s^t L_{sr} I_r + I_r^t L_{ss} I_s + I_r^t L_{rr} I_r\right] \quad T_e = \left[\frac{\partial W_{co}}{\partial \theta_m}\right] \ (I_s, I_r \text{ constant})$$

III-7: Extraction of dq components from stator currents

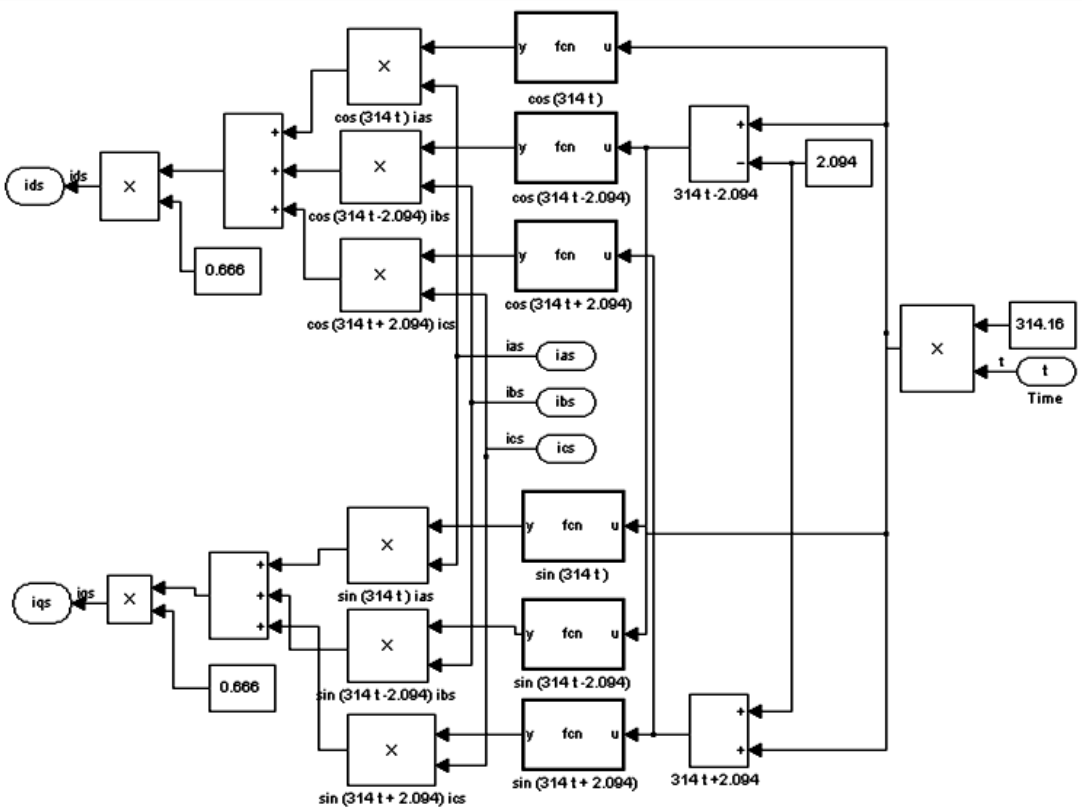

$$i_{qs} = 2/3\,[\cos(\omega_s t)\, i_{as} + \cos(\omega_s t - 2\pi/3)\, i_{bs} + \cos(\omega_s t + 2\pi/3)\, i_{cs}]$$

$$i_{ds} = 2/3\,[\sin(\omega_s t)\, i_{as} + \sin(\omega_s t - 2\pi/3)\, i_{bs} + \sin(\omega_s t + 2\pi/3)\, i_{cs}]$$

Appendix IV

IV-1: Sectional View of machine [courtesy Integrated Electric Co.Pvt.Ltd]

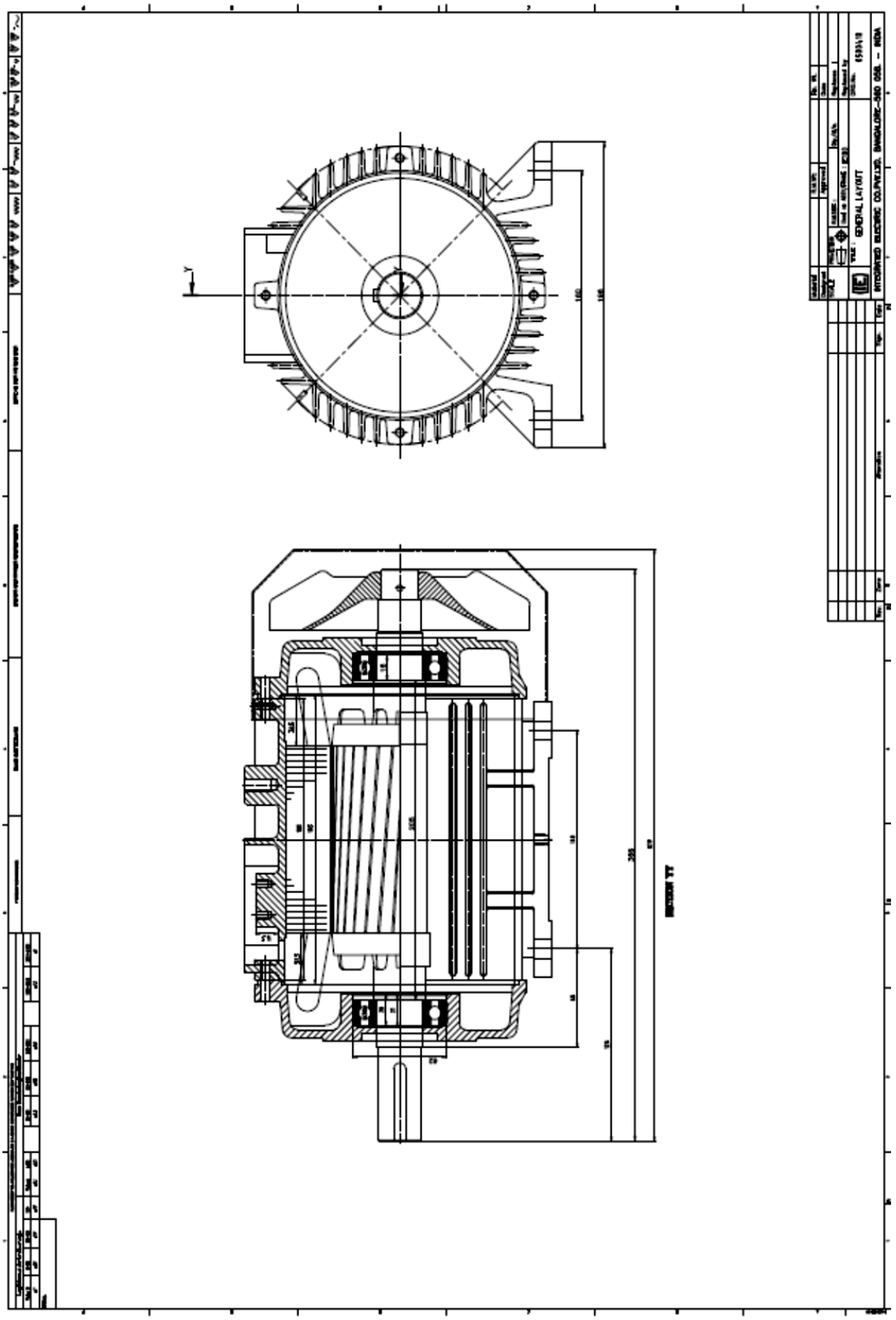

Appendix V

Data Sheets

V-1: Hall Effect transducer- LA 55-P

They have following features

- Current transducer, 50 A
- Operating Frequency Range: DC to 200kHz
- Accuracy: 0.9%
- Response Time:1µs
- Accuracy %:0.65%
- Current Consumption:10mA
- Current Range AC:± 70A
- Current Range DC:± 70
- Current Rating:50A
- Frequency Max:200kHz
- Frequency Min:0Hz
- Measuring Range:70A
- Operating Temperature Max:85°C
- Operating Temperature Min:-25°C
- Output Current:50mA
- Supply Current:50A
- Supply Voltage:15V
- Conversion ratio- 1:1000

V-2: NI SCXI 1338 current input, high-voltage Terminal block

Features:

- 249 Ohm precision resistor across each input
- Mounts to front of SCXI module
- Recommend for high-precision current measurements
- Recommend for use with SCXI-1120, SCXI-1120D, SCXI-1125 and SCXI-1126
- Shielded for quick, convenient signal connections

V-3: NI TBX-1316High-Voltage Attenuator Terminal Block

Features:

- Cabled terminal block for SCXI-1125.
- 600 V
- 200:1 attenuation (fixed)

- 8 differential input channels
- Lockable shielded metal enclosure

V-4: NI SCXI-1125 8-Channel Isolation Amplifier

Features:

- Programmable gain and filter settings
- Programmable offset calibration
- Signal inputs from ±2.5 mV to ±300 V
- 300 V isolation per channel
- NI-DAQmx measurement services software to simplify configuration and

Measurements

Gain/input range is a software-configurable setting that allows the user to choose the appropriate amplification to fully utilize the range of the DAQ device. It provides two filtering stages with an overall response of a four-pole Butterworth filter. Filter bandwidth is software configurable that allows the user to select a low pass filter cutoff frequency. The SCXI-1125 provides up to 300 V_{rms} working isolation per channel and has an input range of up to 1000 V DC when using an appropriate attenuator terminal block.

V-5:NI SCXI-1000 Chassis

Features:

- Rugged, compact 4-slot AC-powered chassis houses any SCXI modules
- Low-noise signal conditioning environment
- Rack-mount, panel mount, and portable options with forced air cooling
- 3 internal analog buses
- Timing circuitry for high-speed multiplexing
- NI-DAQ driver simplifies configuration and measurements

V-6: NI DAQ card 6024E

Some of the input and output characteristics are listed below.

Input Characteristics

Number of channels ..... 16 single-ended or 8 differential (software-selectable per channel)

Type of A/D converter (ADC)..... Successive approximation

Resolution ..... 12 bits, 1 in 4,096

Max sampling rate ..... 200 kS/s guaranteed

Output Characteristics

Number of channels ..... 2 voltage

Resolution ..... 12 bits, 1 in 4,096

Max update rate

DMA1 .....10 kHz, system dependent

Interrupts ..... 1 kHz, system dependent

Type of D/A converter (DAC).....Double-buffered, multiplying

Data transfers .....DMA1, interrupts, programmed I/O

For more details on NI hardware please refer http://www.ni.com.

VI Developed VI s

VI-1: Extraction of voltage and current data samples VI block

(i) Functional block diagram

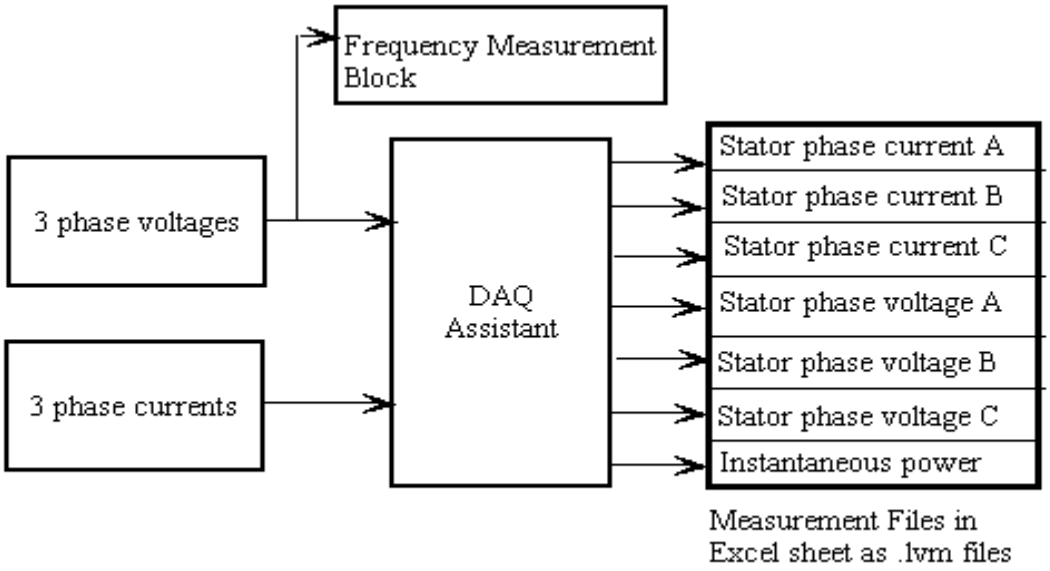

(ii) LabVIEW Implementation

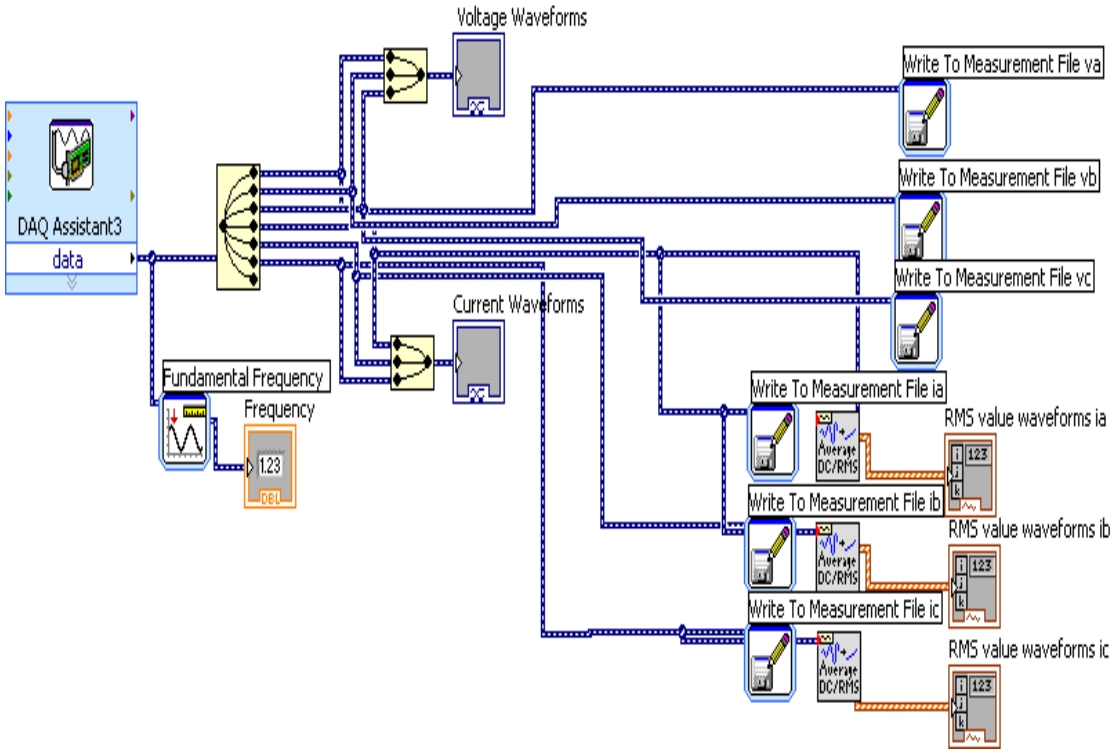

VI-2: Generation of dq components of stator currents VI

(i) Functional block diagram to produce dq components of currents and to perform PSD analysis on data samples

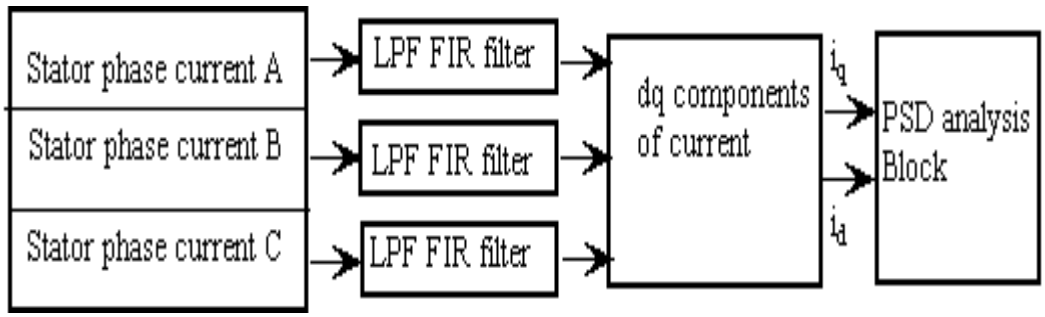

(ii) LabVIEW implementation

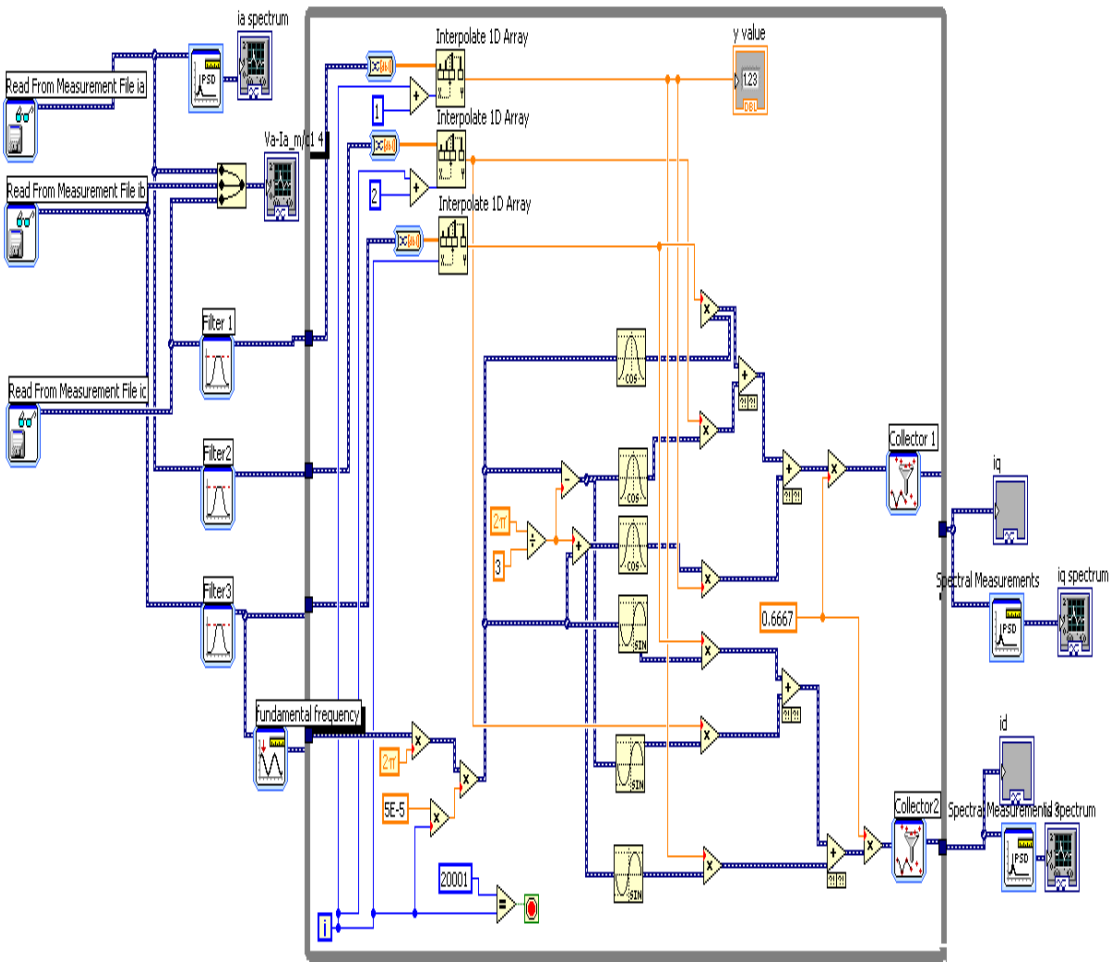

REFERENCES:

Ahmadian. K. and **Jalilian. A.** (2007). "A new method in modeling of rotor bar Skew effect in Induction Motor based on 2D-Modified Winding function Method." *Proc., of International Power Engineering Conference (IPEC),* 3-6 December 2007, Singapore, 630 – 635.

Antonino, J.D., Jover, P., Rieraa, M., Arkkiob, A. and **Roger, F.J.** (2007). "DWT analysis of numerical and experimental data for the diagnosis of dynamic eccentricities in induction motors." *Mechanical Systems and Signal Processing,* 21, 2575–2589.

Alfredo, R. M. and **Lipo, T.A.** (1999). "Complex vector model of the squirrel cage induction machine including instantaneous rotor bar currents." *IEEE Transactions on Industry Applications,* 35(6), 1332-1340.

Antonino, D. J., Riera-Guasp, M., Roger-Folch, J., Martínez, G.F. and **Peris, A**. (2006). "Application and optimization of the discrete wavelet transform for the detection of broken rotor bars in induction machines." *Applied and Computational Harmonic Analysis, Applied and Computational Harmonic Analysis, Elsevier,* 21**,** 268–279.

Cameron, J.R., Thomson, W.T. and **Dow, A.B.** (1986). "Vibration and current monitoring for detecting air gap eccentricity in large induction machines." *IEE Proceedings on Electric Power Applications,* 133 (3), 155-163.

Chetwani, S.H., Shah, M.K. and **Ramamoorthy, M.** (2005). "Online Condition Monitoring of Induction Motors through signal processing", *Proc., of 8th international conference on Electrical machines and systems,* Electrical Res. & Dev. Assoc., India, volume 3, 2175-2179.

Dorell, D. G., Thomson, W. T. and **Roach, S.** (1995). "Combined Effects Of Static And Dynamic Eccentricity On Air Gap Flux Waves And The Application Of Current Monitoring To Detect Dynamic Eccentricity In 3-Phase Induction Motors." *Proc., of 7th International Conference on Electrical machines and Drives*, Durham , UK., 412, 151-155.

Drif, M. and **Marques, A.J.** (2006). "Air gap Eccentricity Fault Diagnosis in Three Phase Induction Motors by the Instantaneous Power Signature Analysis." *Proc., of 3rd IET International Conference on Power Electronics, Machines and Drives*, Dublin, Ireland, 349-353.

Drif, M. and **Marques, A.J.** (2008). "Air gap Eccentricity Fault Diagnosis, in Three-Phase Induction Motors, Using the Instantaneous Power Factor Signature Analysis." *Proc., of 4th IET Conference on Power Electronics, Machines and Drive*, New York, 587 – 591.

Faiz, J and Iman, T.A. (2002). "Extension of Winding Function Theory for Non uniform Air Gap in Electric Machinery." *IEEE transactions on Magnetics*, 38(6), 3654-3657.

Faiz, J., Iman, T.A. and **Toliyat, H.A.** (2003). "An Evaluation of inductances of a squirrel cage induction motor under mixed eccentric conditions", *IEEE transactions on energy conversion*, 18(2), 252-258.

Faiz, J. and **Ebrahimpour, H.** (2005). "Precise derating of three phase induction motors with unbalanced voltages.", *Proc., of 40th IEEE/IAS Industy application annual meeting*, Kawloon, Hongkong , 485-491.

Faiz, J., Ebrahimi, B.M., Akin, B. and **Toliyat, H.A.** (2009). "Comprehensive Eccentricity Fault Diagnosis In Induction Motors Using Finite Element Method." *IEEE Transactions on Magnetics*, 45(3), 1764-1767.

Gang, N., Achmad, W., Jong-Duk, S., Bo-Suk, Y., Don-Ha, H. and **Dong-Sik, K.** (2008). "Decision-level fusion based on wavelet decomposition for induction motor fault diagnosis using transient current signal." *Science Direct- Expert Systems with Applications*, 35, 918-928.

Gojko, M.J., Durovic, M.D., Penman, J. and **Neil, A.** (2000). "Dynamic Simulation of Dynamic Eccentricity in Induction Machines- Winding Function Approach.", *IEEE Transactions on Energy Conversion*, 15(2), 143-148.

Ghoggal, A., Zouzou, S.E., Aboubou, A. and **Sahraoui, M.** (2005). "A 2D Model of Induction Machine Dedicated to faults Detection: Extension of the Modified Winding Function." *Journal of Electrical Systems 1-4*, 69-82.

Ghoggal, A., Aboubou, A., Zouzou, S.E., Sahraoui, M. and **Razik, H.** (2006). "Considerations about the modeling and simulation of air gap eccentricity in

induction motors." *Proc., of IEEE IECON 2006 Conf*erence, Paris, France, 4987-4992.

Guang-ming, X. and **Bi-qing, Z.** (2009). "An intelligent machinery fault diagnosis method based on wavelet packet analysis and hybrid support vector machine." *Expert Systems with applications: An International Journal,* 36(10), 12131-12136.

Guillermo, B., Angelo, C.D., Garcia, G., Solsona, J. and **Maria, I. V.** (2002) "A 2D Model of the Induction Motor:, An Extension of the Modified Winding Function Approach." *Proc., of 28th annual conference of the IEEE Industrial Electronics Society*, IECON2002, Sevilla, Spain, 62-67.

Guillermo, B., Cristian, D. A., Jorge, S., Guillermo, O. G. and **Marıa I. V.** (2006). "Application of an Additional Excitation in Inverter-Fed Induction Motors for Air-Gap Eccentricity Diagnosis." *IEEE Transactions on Energy Conversion*, 21(4), 839-847

Guillermo, B., Cristian, D. A., Jorge, S., Guillermo, O. G. and **Marıa I. V.** (2006). "Application of an Additional Excitation in Inverter-Fed Induction Motors for Air-Gap Eccentricity Diagnosis." *IEEE Transactions on Energy Conversion*, 21(4), 839-847

Guillermo, B., Cristian, D. A., Jorge, S., Guillermo, O. G. and **Marıa I. V.** (2006). "Application of an Additional Excitation in Inverter-Fed Induction Motors for Air-Gap Eccentricity Diagnosis." *IEEE Transactions on Energy Conversion*, 21(4), 839-847

Hamidi, H., Nasiri, A. R. and **Taringoo, F.** (2004). "Detection and Isolation of Mixed Eccentricity in Three Phase induction Motor Via Wavelet Packet decomposition." *Proc., of 5th Asian Control Conference,* Melbourne, Australia,1371-1375.

Hsu.John, S. (1998). "Instantaneous Power Factor Determined by Instantaneous Phasors.." *A document from the department of Energy's Information Bridge*: DOE Scientific and Technical information web site.

Jeffrey, C. R. and **Chee-Mun, O.** "Detecting Stator And Rotor Winding Faults In Three-Phase Induction Machines" *Electrical and Computer Engineering ECE Technical Reports,* Indiana, 1995.

Jong-Gyeum, K., Eun-Woong, L., Dong-Ju, L. and **Jong-Han, L.** (2005). "Comparison of voltage unbalance factor by line and phase voltage." *Proc., of 8th international Conference on Electrical Machines and Systems, 2005.* ICEMS 2005. Nanjing, 3, 1998 – 2001.

Joksimovic, M.G., Durovic, D.M. and **Obradovic, A.B.** (1999). "Skew and linear rise of MMF across slot modeling-Winding function approach." *IEEE transactions on Energy Conversions*, 14(3), 315-320.

Jordi, C., Luis, R., Juan, A. O., Javier A. R. and **Antonio, G.E.** (2008). "Fault detection in induction machines using power spectral density in wavelet decomposition." *IEEE Transactions on Industrial Electronics*, 55(2), 633-643.

Kral, C., Pirker, F. and **Pascoli, G.** (2001) "Rotor eccentricity detection of induction machines by means of torque estimation- Measurement results", *8th IEEE International Symposium on Diagnostic for Electric Machines, Power Electronics and Drives* , IEEE-SDEMPED, Bologna, Italy, 641– 644.

Krause, P. C. and **Thomas, C. H.** (1965). "Simulation of Symmetrical Induction Machinery", *IEEE Transactions on Power Apparatus and Systems*, 84 (11), 1038-1053.

Long, W., Bin, L., Xianghui, H., Thomas, G.H. and **Ronald, H.** (2005). "Improved online condition monitoring using static eccentricity induced negative sequence current information in induction machines." *Proc., of Industrial Electronics Society,* IECON 2005, 1737-1742.

Omar, T., Lahcene, N. Rachild, I. and **Maurice, F.** (2005). "Modeling of the Induction Machine for the Diagnosis of Rotor Defects. Part. I: An Approach of Magnetically Coupled Multiple Circuits" *Proc., of 31st Annual Conference of IEEE, Industrial Electronics Society*, IECON2005, Raleigh, NC, USA, 1580-1587.

Nabil, A. and **Toliyat, H.A.** (1998). "A Novel method for modeling Dynamic air gap eccentricity in synchronous machines based on modified winding function theory." *IEEE transactions on Energy Conversion*, 13(2), 156-162.

Nandi, S., Bharadwaj, R., Toliyat, H.A. and **Parlos, A.G.** (1998). "Performance analysis of a 3 phase induction motor under mixed eccentricity condition." *Proc., of IEEE Power Electronic Drives and Energy Systems for Industrial Growth, PEDES'98 Conference,* Perth, Australia, 123-128.

Nandi, S., Bharadwaj, R.M. and **Toliyat, H.A.** (2002). "Performance analysis of a three-phase induction motor under mixed eccentricity condition." *IEEE Transaction on energy conversion*, 17(3), .392-399.

Nandi, S., Bharadwaj, R.M. and **Toliyat, H.A.** (2002). "Mixed Eccentricity in Three Phase Induction Machines: Analysis, Simulation and Experiments." *Proc., of 37th industry Application Conference,* 4, 1525-1532.

Nandi, S. (2004). "Modeling of Induction Machines Including Stator and Rotor Slot Effects.", *IEEE Transactions on Industry Applications,* 40(4), 1058-1065.

Nandi, S., Toliyat, H.A. and **Xiaodong, Li.** (2005). "Condition Monitoring and Fault Diagnosis of Electrical Motors- A Review." *IEEE Transactions on Energy Conversion,* 20 (4), 719-729.

Nandi, S., Ilamparithi, T.C., Lee, S.B and **Hyun, D.** (2009). "Pole pair and slot number independent frequency domain based detection of eccentricity faults in induction machines using a semi on-line technique." *IEEE International Symposium on Diagnostic for Electric Machines, Power Electronics and Drives*, SDEMPED 2009, Cargèse (France), 1-7.

Nasiri, A., Poshtan, J., Kahaei,M.H. and **Taringoo F.** (2004). "A new scheme in model based fault detection in three phase induction motors." *Proc., of IEEE International Conference*, Mechatronics 2004, ICM '04 , 19-24.

Patton, R.J. and **Chen, J.** (1992). "On-line residual compensation in robust fault diagnosis of dynamic systems." *IFAC Symposium Artificial Intelligence in Real-Time Control*, Netherlands, 221-227.

Pillay, P. and **Manyage, M.** (2001). "Definitions of Voltage Unbalance." *IEEE Power Engineering Review,* .50-51.

Randy, S., Jason, G., Nesimi, E., **Wen, L.S.**, **Douglas, A. G.** and **Colin H.** (2006) "Investigation of Static Eccentricity Fault Frequencies using Multiple Sensors in Induction Motors and Effects of Loading." *Proc., of international IEEE conference on Industrial Electronics*, IECON 958-963.

Siddique, A., Yadava, G.S. and **Bhim, S.** (2005). "A Review of Stator Fault Monitoring Techniques of Induction Motors." *IEEE transactions on Energy Conversion,* 20 (1), 106-114.

Tan, S.C., Lim, C.P. and **Rao, M.V.C.** (2007) "A hybrid neural network model for rule generation and its application to process fault detection and diagnosis", *Science Direct-Engineering Applications of Artificial Intelligence*, 20, 203–213.

Tian, H., Bo-Suk, Y. and **Jong, M. L.** (2005). "A New Condition Monitoring and Fault Diagnosis System of Induction Motors using Artificial Intelligence Algorithms." *Proc., of IEEE International conference on Electric Machines and Drives,* San Antonio, TX, 1967-1974.

Thomas, V., Krishna, V. and **Jagadeesh, K. V.** (2003). "Online cage rotor fault detection using air-gap torque spectra." *IEEE Transactions on Energy Conversion*, 18(2), 265-270.

Thomson, W.T. and **Barbour, A.** (1998). "On-Line Current Monitoring and Application of a Finite Element Method to Predict the Level of Static Airgap Eccentricity in Three Phase Induction Motors." *IEEE Transactions on Energy Conversion*, 13 (4), 347-357.

Thomson, W.T. (2009). "On-Line Motor Current Signature Analysis Prevents Premature Failure of large Induction Motor Drives." Maintenance & asset management |ME|, 24 (3), 30-35.

Toliyat, H. A. and **Lipo, T. A.** (1995). "Transient Analysis of Cage Induction Machines Under Stator, Rotor Bar and End Ring Faults*." IEEE Transactions on Energy Conversion*, 10(2), 241-247.

Toliyat, H.A., Mohammed, S.A. and **Parlos, A.G**. (1996). "A Method for Dynamic Simulation of Air-gap Eccentricity in Induction Machines." *IEEE Transactions on Industry Applications*, 32(4), 910-918.

Xianghui, H., Habetler, T.G., Harley, R.G. and **Wiedenbrug, E.J.** (2007). "Using a Surge Tester to Detect Rotor Eccentricity Faults in Induction Motors." *IEEE Transactions on Industry Applications*, 43 (5), 1183-1190.

Xiaodong, Li., Qing, Wu. and **Nandi, S.** (2007). "Performance analysis of a three phase induction machine with inclined static eccentricity." *IEEE Transactions on Industry Applications*, 43 (2), 531-541.

Xiaogang, L., Yuefeng, L., Toliyat, H.A., Ahmed, E. and **Lipo, T.A.** (1995). "Multiple coupled circuit modelling of induction machines." *IEEE Transaction on Industry application*", 31(2), 311-318.

Yaguo, L., Zhengjia, H., Yanyang, Z. and **Qiao, H.** (2007). "Fault diagnosis of rotating machinery based on multiple ANFIS combination with GAS." *Mechanical Systems and Signal Processing*, 21(5), 2280–2294.

BIO-DATA:

Contact address: Rajalakshmi Samaga BL

w/o Dr. B.L Samaga MD, DNB

005, Mamatha Residency

Anegundi I cross, Bejai

Mangalore-4, D.K

Karnataka, India

Email id: rajisamaga@yahoo.com

Phone no: 9481268030

Qualification: BE in Electrical and Electronics Engineering

(SJCE, Mysore, Mysore University)

M. Tech in Power and Energy Systems

(KREC (NITK), Surathkal, Mangalore University).

PUBLICATIONS AND PRIZES WON OUT OF RESEARCH WORK

International journal publications:

1.Rajalakshmi Samaga and Dr.Vittal.K.P, (2010). "A Simplified Modeling Approach For Accounting Skewing Effect In Rotor Bars Of Squirrel Cage Induction Motor And Its Application In Motor Inductance Calculation", *Journal of Electrical Engineering*, Volume10/2010-Edition:4, Romania, Dec 2010, 178-183.

2.Rajalakshmi Samaga BL, K.P.Vittal, (2012). "Comprehensive Study of Mixed Eccentricity Fault Diagnosis in Induction Motors Using Signature Analysis*",* *International Journal of Electrical Power & Energy Systems* (IJPES), ELSEVIER Volume 35, February 2012, 180-185.

International conference publications

1.Sushma.P, Rajalakshmi Samaga.B.L and Dr.Vittal.K.P, (2010). "DQ Modeling Of Induction Motor For Virtual Flux Measurement", *Proc. of 9th IEEE International Power and Energy conference,*IPEC2010, Oct-27-29, Singapore, 903-908.

2.Rajalakshmi Samaga BL, Vittal K.P, (2011). "Investigations into effect of mixed air gap eccentricity on dq components of currents in Induction motor", *Proc. of IEEE 6th International Conference on Industrial and Information Systems*, ICIIS2011, 16th-19th August 2011, Kandy, Sri Lanka, pp.271-276.

3.Rajalakshmi Samaga BL, Dr.K.P.Vittal, (2011). "Air Gap Mixed Eccentricity Severity Detection in an Induction Motor", *Proc. of IEEE International Conference on Recent Advances in Intelligent Computational Systems, RAICS2011,* Sept 22-24, 2011, Trivandrum, 115-119.

4.Rajalakshmi Samaga BL, Panduranga Vittal and Vikas Kumar Jhunjhuwala, (2011). "Effect of unbalance in voltage supply on the detection of mixed air gap eccentricity

in an induction motor by Motor Current Signature Analysis", *Proc. of 2011 IEEE PES International Conference on Innovative Smart Grid Technologies –India, ISGT-India* 1-3 December 2011, Kollam, Kerala, 108-113.

National Conferences:

1.Rajalakshmi Samaga BL, Dr.K.P.Vittal, "Modeling Of Induction Motor For Mixed Eccentricity Condition", *Proc. of 4th national conference on Advances in Energy Conversion Technologies , AECT2011*,Feb 03 – 05, 2011, MIT, Manipal.

Awards won

1.Rajalakshmi Samaga BL, "Investigations into Asymmetrical Fault Detection by Motor Current Signature Analysis of Squirrel Cage Induction Motor", won **3rd prize** in the 7th annual national level technical paper contest under research category, VIMantra2010, Educator 2010**,** Conducted by National Instruments Corporation India**,** Dec13-14, Chennai.

2. Rajalakshmi Samaga BL, "Extraction of dq components of stator currents of an induction motor for mixed eccentricity fault detection", won **1st runner up** in the 8th annual national level technical paper contest under research category, VIMantra2011, Educator 2011**,** Conducted by National Instruments Corporation**,** Oct 12-13, Bangalore.